NAVAL POSTGRADUATE SCHOOL
Monterey, California

DISSERTATION

WAVELET ANALYSIS OF INSTANTANEOUS CORRELATIONS WITH APPLICATION TO FREQUENCY HOPPED SIGNALS

by

Nabil Hamdy Shaker Khalil

September 1997

Dissertation Advisor: Ralph D. Hippenstiel

REPORT DOCUMENTATION PAGE

Form Approved
OMB No. 0704-0188

1. AGENCY USE ONLY (Leave Blank)	2. REPORT DATE	3. REPORT TYPE AND DATES COVERED
	September 1997	Doctoral Dissertation

4. TITLE AND SUBTITLE
WAVELET ANALYSIS OF INSTANTANEOUS CORRELATIONS WITH APPLICATION TO FREQUENCY HOPPED SIGNALS

5. |

6. AUTHOR(S)
Nabil Hamdy Shaker Khalil

7. PERFORMING ORGANIZATION NAME(S) AND ADDRESS(ES)
Naval Postgraduate School
Monterey, CA 93943-5000

8. PERFORMING ORGANIZATION

9. SPONSORING/ MONITORING AGENCY NAME(S) AND ADDRESS(ES)

10. SPONSORING/ MONITORING AGENCY REPORT NUMBER

11. SUPPLEMENTARY NOTES
The views expressed in this dissertation are those of the author and do not reflect the official policy or position of the Department of Defense or the United States Government.

12a. DISTRIBUTION / AVAILABILITY STATEMENT
Approved for public release; distribution is unlimited.

12b. DISTRIBUTION CODE

13. ABSTRACT *(Maximum 200 words)*

Frequency hopped signals are widely used in various communication applications for their inherent security features. The demand, by civilian and governmental agencies, to intercept communication signals is increasing.

The interception task can be summarized by detecting the signal's presence in additive noise, classifying the modulation type, estimating the control parameters, decoding the data, and decrypting the information content. This work addresses the merging of wavelet and correlation concepts to detect, classify and estimate the parameters of frequency hopped signals.

We address the interception problem in two ways. The first approach is based on a visual inspection of the wavelet surfaces generated from the instantaneous correlation function of the communication signal and leads to hop start/stop times estimates. In the second approach, we apply an energy-based processing scheme to estimate the hop start and stop times, the hop-scale pattern, and the hop frequency.

Results show that frequency hopped signals can be identified at an SNR of 3 dB or 6 dB using visual inspection or an automated scheme, respectively.

14. SUBJECT TERMS	15. NUMBER OF PAGES
Wavelet analysis, time-varying correlation functions, instantaneous correlation functions, frequency hopped signals, interception, classification.	178
	16. PRICE CODE

17. SECURITY CLASSIFICATION OF REPORT	18. SECURITY CLASSIFICATION OF THIS PAGE	19. SECURITY CLASSIFICATION OF ABSTRACT	20. LIMITATION OF ABSTRACT
Unclassified	Unclassified	Unclassified	UL

Approved for public release; distribution is unlimited.

WAVELET ANALYSIS OF INSTANTANEOUS CORRELATIONS WITH APPLICATION TO FREQUENCY HOPPED SIGNALS

Nabil Hamdy Shaker Khalil
Colonel, Egyptian Army
B.S.E.E., Military Technical College, Egypt, 1978
M.S.E.E, Ain-Shams University, Egypt, 1990

Submitted in partial fulfillment of the
requirements for the degree of

DOCTOR OF PHILOSOPHY IN ELECTRICAL ENGINEERING

from the

NAVAL POSTGRADUATE SCHOOL
September 1997

Author: Nabil Khalil
Nabil Hamdy Shaker Khalil

Approved by:

Ralph D. Hippenstiel
Associate Professor of Electrical and Computer Engineering
Dissertation Advisor

Monique P. Fargues
Associate Professor of Electrical and Computer Engineering
Dissertation Co-advisor

Xiaoping Yun
Associate Professor of Electrical and Computer Engineering

G. M. Lundy
Associate Professor of Computer Science

Ching-Sang Chiu
Associate Professor of Oceanography

Approved by: Herschel H. Loomis, Jr.
Herschel H. Loomis, Jr., Chairman,
Department of Electrical and Computer Engineering

Approved by: Maurice D. Weir
Maurice D. Weir, Associate Provost for Instruction

ABSTRACT

Frequency hopped signals are widely used in various communication applications for their inherent security features. The demand, by civilian and governmental agencies, to intercept communication signals is increasing. The interception task can be summarized by detecting the signal's presence in additive noise, classifying the modulation type, estimating the control parameters, decoding the data, and decrypting the information content. This work addresses the merging of wavelet and correlation concepts to detect, classify and estimate the parameters of frequency hopped signals.

We address the interception problem in two ways. The first approach is based on a visual inspection of the wavelet surfaces generated from the instantaneous correlation function of the communication signal and leads to hop start/stop times estimates. In the second approach, we apply an energy-based processing scheme to estimate the hop start and stop times, the hop-scale pattern, and the hop frequency.

Results show that frequency hopped signals can be identified at an SNR of 3 dB or 6 dB using visual inspection or an automated scheme, respectively.

TABLE OF CONTENTS

LIST OF FIGURES

LIST OF SYMBOLS

- ACF Auto-correlation function
- AF Ambiguity function
- ASK Amplitude shift keying
- BPSK Binary phase shift keying
- BSK Binary shift keying
- CSIG Communication signal
- DFT Discrete Fourier transform
- DWT Discrete wavelet transform
- DWVD Discrete Wigner-Ville distribution
- FFT Fast Fourier transform
- FH Frequency hopping
- FSK Frequency shift keying
- FT Fourier transform.
- ICF Instantaneous correlation function
- MFSK M-ary frequency shift keying
- MWT Morlet wavelet transform
- OOK On-off keying
- PNG Pseudo-random number generator
- PSK Phase shift keying
- QAM Quadrature amplitude modulation
- QPSK Quadrature phase shift keying
- RBJ Repeat-back jammer
- SS Spread spectrum
- STFT Short time Fourier transform

- TFD Time-frequency distribution.
- WT Wavelet transform
- WVD Wigner-Ville distribution

ACKNOWLEDGMENTS

All gratitude is due to **ALLAH**, who made this success possible and affordable. I received much support during this endeavor which contributed to this success. First, I am indebted to my wife Seham for her unconditional support, love, patience and sacrifice. My appreciation to my daughters: Gehad, Nehal, Mennatalla, and Yara for their tolerance, care and patience.

Second, I wish to express my deepest gratitude and sincere thanks to my patient mentor, Professor Ralph Hippenstiel, whose support, guidence, knowledge and enthusiasm have been a constant inspiration to me. I am also deeply indebted to Professor Monique Fargues for her sincere support, invaluable advice and helpful comments during the research.

Third, I would like to thank the remaining members of my committee: Professors G.M. Lundy, Roberto Christi, Xiaoping Yun and Ching-Sang Chiu, for their invaluable discussions and comments.

Finally, I would like to thank faculty, staff, and fellow students in the Electrical and Computer Engineering Department at Naval Postgraduate School for their support during this endeavor.

I. INTRODUCTION

A. PROBLEM STATEMENT AND OVERVIEW

The demand to be able to intercept communication signals is increasing, as interception is a basic investigation tool for civilian, intelligence and military authorities. The task of intercepting a communication signal can be summarized by detecting the signal's presence in additive noise, classifying the modulation type, estimating the control parameters required for reception, decoding the data, and decrypting the information content. Sometimes, the procedure is stopped at the detection (identification) step such as in geo-location or spectrum monitoring. Intelligence applications aim at the final step which is to extract the information content.

Communication signals can utilize a great diversity of digital modulation techniques. Among the digital techniques, the spread spectrum signal (SS) is widely used. Frequency hopping signals (FH) are a subset of SS, and are used primarily in this dissertation. In the open literature, many signal processing tools are available for the interception task, and among those are the correlation analysis and wavelet analysis. Each of these tools has been used independently in the signal processing and communication area. In this work we will address the merging of the wavelet and correlation concept to detect, classify and estimate signal parameters.

The FH signal is a non-stationary process. Hence a specific type of two-dimensional correlation function, called the instantaneous correlation function, is selected, as it accommodates the time-varying nature of the signal of interest. Application of wavelet analysis to correlation functions is a new area and is still in the exploratory stage. The automation of the interception and exploitation of digital communication signals is the final goal. This work addresses the interception, identification, classification, and parameter extraction of FH signals.

We start by investigating the wavelet transform of different types of the correlation functions. Then, we select the instantaneous correlation function (ICF) as

the candidate correlation representation. We derive the instantaneous correlation function of the FH signal and analyze its wavelet transform obtained by using the Morlet wavelet. The wavelet transform of the instantaneous correlation function is a 3-dimensional (3-D) surface. We partition the 3-D surface into a number of 2-D surfaces, where each corresponds to one wavelet scale (called the wavelet surface).

We address the interception problem in two approaches. First, we visually inspect the 2-D wavelet surfaces to identify and classify the structure of the FH signal and obtain an estimate for the hop time interval. Second, we apply a proposed processing scheme to estimate the hop start/stop time, the hop-scale pattern, and the hop frequency. The extraction of the hop start/stop time is addressed using an edge detection approach by applying a compass operator, a technique which is well known in the image processing area. The hop-scale pattern is obtained by applying an energy analysis. The energy analysis assigns a scale index (called the proper scale) to each hop. The proper scale of each hop is that scale which has the greatest energy content. The sequence of proper scales, representing the hop sequence, is called the hop-scale pattern. The frequency of each hop can be extracted from the wavelet surface at the proper scale. Thus, the identification and classification of the FH signal may be accomplished as follows:

1. Based on the hop-scale pattern:
   If two or more wavelet scales are applied, the hop-scale pattern of the FH signal will be different from the hop-scale patterns of other digital modulation signals.

2. Based on the frequency diversity:
   If all hop frequencies reside in one scale then the FH signal will have different frequency components as a function of the hop intervals.

This dissertation is organized into eight chapters. In Chapter I, we introduce the problem and review related work with a focus on the interception of FH signals. In Chapter II, we introduce the most significant signal analysis tools. In Chapter III, we derive the wavelet response to correlation functions. In Chapter IV, we derive the

ICF for the FH signal. In Chapter V, we perform the wavelet analysis of the ICF of the FH signal. In Chapter VI, we analyze the processing scheme. In Chapter VII, we provide the simulation results. Finally, Chapter VIII contains conclusions and recommendations for future work.

B. INTERCEPTION OF DIGITAL COMMUNICATION SIGNALS

1. Introduction

Interception of communication signals is of interest to a wide range of applications in surveillance, intelligence, reconnaissance, geo-location, spectral monitoring and jamming [Ref. 1].

Digital communication systems can use a large diversity of modulation techniques. Examples of these techniques are: ASK, BPSK, BFSK, QAM, MPSK and MFSK. Interception of digital communication signals consists of detection (identification), classification (feature extraction), parameter estimation, decoding, and decrypting. Through out this dissertation we will use the following definitions:

1. Detection or identification is the process of discriminating between noise and a digitally modulated signal.
2. Classification (feature extraction) is the process of discriminating between different modulation types, by obtaining significant parameters or signal constellation which uniquely specify the modulation type.
3. Parameter estimation is the process of extracting the control parameters of the signal.
4. Decoding is the process of detecting and correcting the errors of the communication channel.
5. Decrypting is the process of restoring the original information content of the transmitted messages.

2. Interception Tools

A large number of open-literature publications address the interception of digital communication signals. The different signal processing tools used for signal interception may be categorized as follows:

1. Basic tools: Spectral analysis, correlation analysis, and parametric modeling.
2. Linear tools: Linear transforms including the wavelet transform.
3. Non-linear tools: Higher-order spectra, spectral correlation, and cyclic-feature processing.
4. Other tools: Eigen-analysis, singular-value decomposition, and stochastic resonance.

There are two different approaches to address the interception. The first approach addresses the interception as a decision-making problem applied to a set of alternative hypotheses. This requires statistical decision theory and hence a statistical description of the alternatives. The second approach handles the interception as a statistical pattern-recognition problem.

3. Digital Signal Modulation

Different tools can be used for intercepting digital modulations. For ASK, QAM, BPSK, QPSK, and FSK, applications are addressed in references [Ref. 2] to [Ref. 14], [Ref. 17] and [Ref. 32]. Since the FSK modulation is related to the FH signal, the interception tools for FSK are briefly introduced as follows:
Spectral correlation and visual inspection is applied for identification of FSK signals in [Ref. 2]. Higher-order moments are applied for FSK signals in [Ref. 3]. Wavelet analysis of the FSK signal is applied for timing extraction in [Ref. 5, 17] where it is shown that the frequency transitions of the FSK signal are related to inflection points contained in the scalogram.

4. Spread Spectrum Signals

Interception of spread spectrum signals is addressed in [Ref. 18] to [Ref. 35]. There are five conventional techniques to intercept frequency hopped (FH) signals [Ref. 18, 19]. These are:

1. Wideband energy detectors (wide band radiometer),
2. Optimum-multichannel FH pulse-matched filters,
3. Maximum-channel filter-bank combiners,
4. Optimum partial-band FH pulse-matched detectors, and
5. Partial-band filter-bank combiners.

These techniques differ mainly in two points. The first difference is in the bandwidth of the interception filter(s) relative to the bandwidth of the FH signal. The second difference is in the number of parallel channels relative to the number of hopping frequencies. Consequently, they differ in the required minimum signal-to-noise ratio (SNR) for acceptable performance.

Time or frequency uncertainty can be minimized by using overlapping techniques [Ref. 20]. A likelihood-ratio-test detector and a channelized receiver are widely accepted as the optimum system for detecting FH signals [Ref. 20] to [Ref. 24]. The maximum-likelihood detector (ML), using a bank of correlators, is addressed in [Ref. 22]. It assumes prior knowledge of the hopping times and frequencies, and one correlator is designated to each primary frequency region. Results show that the coherent ML scheme gives a probability of detection of 0.5 at an SNR of 4.5 dB for a probability of false alarm of 10^{-9}. For the noncoherent ML scheme, this performance requires an SNR of about 5.9 dB.

A generalized likelihood ratio test for a multiple hop observation interval is addressed in [Ref. 23]. It assumes prior knowledge of hop frequencies, hop rate, and hop times. Using an observation interval of 10^3 hops and a probability of false alarm of 10^{-3}, a probability of miss of 10^{-5} is achieved at an SNR of 8 dB. The same performance requires an SNR of 5 dB using an observation interval of 10^5 hops.

Applying wavelet analysis to the interception of FH signals is addressed in [Ref. 35]. FH classification is based on locating transition spikes due to frequency transitions. The authors suggest using the STFT for the hop frequency estimation instead of the wavelet transform because wavelets have varying frequency resolution and the FH signal has a wide bandwidth.

II. FOURIER ANALYSIS AND WAVELETS

Signal analysis (expansion, decomposition, or transformation) is a method used to represent time signals as a linear combination of elementary building blocks (or elementary basis functions). This representation is vital to the area of signal processing. Each expansion is defined by its basis functions, or equivalently, its basic building blocks. There are numerous linear expansion methods. Well-known examples are the Shannon expansion, the Karhunen-Loeve expansion, the Gram-Schmidt expansion, the eigen-analysis, and the most popular, the Fourier analysis. In this chapter, we summarize the evolution of the analysis tools in three steps. First, we introduce the Fourier analysis as used for stationary signals. Then, we introduce time-frequency distributions, which can be used to represent time-varying signals. Finally, we introduce the concept of the wavelet analysis to represent time-varying signals over a time-scale plane.

A. FOURIER ANALYSIS

The major reference for this section is [Ref. 36]. The Fourier transform (FT), also called Fourier analysis, is the most popular signal decomposition (expansion). The Fourier transform is used to represent a stationary process by decomposing it into sinusoidal or complex exponential components. Here, a stationary process is defined as a process whose spectrum is not varying with time. Hence, Fourier techniques work well and allow successful frequency localization of the spectral components. When a non-stationary process is present, its time-varying spectrum requires an additional dimension (i.e., time). The major problem with the classical Fourier analysis is that it uses an infinitely long sinusoidal or complex exponential basis of functions. This makes time localization impossible.

By classical Fourier analysis we mean the Fourier series (FS), the continuous-time Fourier transform (FT), the discrete-time Fourier series (DFS), and the discrete-

time Fourier transform (DTFT).

The discrete Fourier transform (DFT), or its fast implementation, the fast Fourier transform (FFT), uses finite integration time. The Fourier transform cannot give a time resolution better than the integration interval. To cope with the requirement of tracking time evolution and to provide time localization, the short-time Fourier transform (STFT) was introduced. The STFT uses a window function which affects the time resolution; that is, the longer the window interval the worse is the time resolution.

1. Fourier Series

Given a periodic continuous time signal $x(t)$, with period T, the Fourier series (FS) expansion is given by :

$$x(t) = \sum_{k=-\infty}^{\infty} C(k) e^{j2\pi f_o kt}, \tag{II.1}$$

where

$$C(k) = \frac{1}{T} \int_T x(t) e^{-j2\pi f_o kt} dt \tag{II.2}$$

and $f_o = \frac{1}{T}$.

Note that the expansion coefficients $C(k)$ are evaluated at integer values of k. Parseval's relation for this power signal (recall that power signals have finite average power and infinite energy) is given by :

$$P_x = \frac{1}{T} \int_T |x(t)|^2 dt = \sum_{k=-\infty}^{\infty} |C(k)|^2, \tag{II.3}$$

where P_x is the average power of the signal. The signal has to satisfy the Dirichlet conditions to have a valid Fourier series expansion. These conditions can be summarized as: the signal has a finite number of discontinuities, a finite number of maxima and minima, and it is absolutely integrable (over one period).

2. Fourier Transform

A non-periodic continuous time signal, x(t), can be represented as

$$x(t) = \int_{-\infty}^{\infty} X(f) e^{j2\pi ft} df, \tag{II.4}$$

where

$$X(f) = \int_{-\infty}^{\infty} x(t) e^{-j2\pi ft} dt. \tag{II.5}$$

Note that both the signal and the transform are continuous functions of time and frequency, respectively.

The Dirichlet conditions have to be met by the non-periodic signal with one modification; that is, the time support of the signal is considered instead of the period in the above-addressed Dirichlet conditions.

Parseval's relation is given by

$$E_x = \int_{-\infty}^{\infty} |x(t)|^2 dt = \int_{-\infty}^{\infty} |X(f)|^2 df \tag{II.6}$$

where E_x is the total energy of the signal.

Short-Time Fourier Transform. Because of the lack of time localization, non-stationary signals have time-varying spectra which cannot be represented by the classical Fourier transform. The time evolution of the time-varying spectra needs to be considered. Hence, there is a need for an expansion in time and frequency such as the short-time Fourier transform (STFT). This transform windows the signal around a certain time instant, performs the frequency domain analysis, and repeats the process at other time instants. Note that it is assumed that the windowed signal will have a non-time-varying spectrum (local stationarity) within the time window. Therefore, the STFT for a continuous signal x(t) is given by

$$X(\omega, l) = \int_{-\infty}^{\infty} x(t) g^*(t - l) e^{-j\omega t} dt, \tag{II.7}$$

where $g(t)$ is the window function. $X(\omega, l)$ is the spectral description of $x(t)$ when the window is centered at the time l. When the window $g(t)$ has a Gaussian shape, the

STFT is called the Gabor transform. The STFT depends on a window function with a fixed width (in time). Recall that the time localization and frequency localization of the STFT are controlled by the window width. Consequently, the STFT offers a fixed-time resolution and a related fixed-frequency resolution, which results in a uniform tiling in the time-frequency plane.

The time and frequency resolution are governed by the uncertainty principle, which will be addressed shortly. For details, see [Ref. 38]. The STFT for discrete time signals is defined as

$$X(k,n) = \sum_{m=\infty}^{\infty} g(m-n)x(m)e^{-j2\pi k\frac{m}{M}}, \tag{II.8}$$

where $k = 0, 1, \ldots, M-1$.

3. Discrete-Time Fourier Series

The discrete-time Fourier series (DTFS) for a periodic discrete signal $x(n)$ with period N is given by

$$x(n) = \sum_{k=0}^{N-1} C(k)e^{j2\pi k\frac{n}{N}}, \tag{II.9}$$

and

$$C(k) = \frac{1}{N}\sum_{n=0}^{N-1} x(n)e^{-j2\pi k\frac{n}{N}}, \tag{II.10}$$

where $C(k)$ represents the expansion coefficient at the discrete frequency $w_k = 2\pi k\frac{n}{N}$. Parseval's relation is given by

$$P_x = \sum_{k=0}^{N-1} |C(k)|^2 = \frac{1}{N}\sum_{n=0}^{N-1} |x(n)|^2 \tag{II.11}$$

where P_x is the average power of the infinite energy periodic signal $x(n)$. The Dirichlet conditions must be met by $x(n)$.

4. Discrete-Time Fourier Transform

The discrete-time Fourier transform (DTFT) for finite length non-periodic discrete signals is given by

$$x(n) = \frac{1}{2\pi}\int_{2\pi} X(\omega)e^{j\omega n}d\omega, \tag{II.12}$$

where

$$X(\omega) = \sum_{k=-\infty}^{\infty} x(n)e^{-j\omega n}. \tag{II.13}$$

Note that the discrete frequency ω ranges from $-\pi$ to π. Parseval's relation is given by

$$E_x = \sum_{n=-\infty}^{\infty} |x(n)|^2 = \frac{1}{2\pi}\int |X(\omega)|^2 d\omega, \tag{II.14}$$

where E_x is the total energy of the signal.

Discrete Fourier Transform. A finite-length non-periodic discrete signal has a continuous-frequency-domain representation $X(\omega)$. For digital signal processing it is easier to represent $X(\omega)$ by its discrete-frequency samples. This leads to the discrete Fourier transform (DFT). The DFT is given by

$$x(n) = \frac{1}{N}\sum_{k=0}^{N-1} X(k)W_N^{-kn}, \tag{II.15}$$

and

$$X(k) = \sum_{n=0}^{N-1} x(n)W_N^{kn}, \tag{II.16}$$

where $W_N = e^{\frac{-j2\pi}{N}}$ and $n, k = 0, 1, \cdots, N-1$. The DFT requires N^2 complex multiplication operations and $N(N-1)$ complex addition operations. The fast Fourier transform (FFT) implements the DFT with fewer multiplications. The FFT has computation complexity (number of multiplications) $\frac{N}{2}log_2 N$ if N is power of 2.

B. TIME-FREQUENCY DISTRIBUTIONS

1. Introduction

A time-frequency distribution (TFD) describes non-stationary signals by displaying the energy density over time and frequency simultaneously. Let the signal and its Fourier transform be denoted by $s(t)$ and $S(\omega)$, respectively. The following terms and definitions [Ref. 38] are useful in TFD discussions:

- Energy density or instantaneous power is given by

$$|s(t)|^2. \tag{II.17}$$

- Total energy of the signal is given by

$$\int |s(t)|^2 \, dt. \tag{II.18}$$

- Mean time is given by

$$\langle t \rangle = \int t \, |s(t)|^2 \, dt. \tag{II.19}$$

- Time variance is given by

$$\sigma_t^2 = \int (t - \langle t \rangle)^2 \, |s(t)|^2 \, dt, \tag{II.20}$$

  where σ_t^2 is an indication of the duration of the signal.

- Energy density spectrum is given by

$$|S(\omega)|^2 . \tag{II.21}$$

  It is the intensity per Hertz near the frequency ω.

- Parseval's theorem states that

$$\int |S(\omega)|^2 \, d\omega = \int |s(t)|^2 \, dt. \tag{II.22}$$

- Mean frequency is given by

$$\langle \omega \rangle = \int \omega \, |S(\omega)|^2 \, d\omega . \tag{II.23}$$

- Frequency variance is given by

$$\sigma_\omega^2 = \int (\omega - \langle \omega \rangle)^2 \, |S(\omega)|^2 \, d\omega, \tag{II.24}$$

  where σ_ω^2 is an indication of the rms bandwidth.

- The uncertainty principle:

  It is a fundamental statement regarding the Fourier transform pairs. It governs the relationship between the spread of any signal in the time domain and in the frequency domain. This relationship is given by $\sigma_t \sigma_\omega \geq 1/2$. This means that there is a trade-off time localization and frequency localization.

2. Fundamental Properties of Time-Frequency Distributions

The major reference for these properties is [Ref. 38]. Let $p(t,\omega)$ be the intensity of the signal $s(t)$ at time t and frequency ω. Then $p(t,\omega)\Delta t\Delta\omega$ is the fractional energy in the cell $\Delta t\Delta\omega$ at time t and frequency ω. Basic properties of the TFD are given by:

- Marginal property: Summing up the energy distribution for all frequencies at a particular time gives the instantaneous energy. Summing over all times at a particular frequency gives the energy density spectrum, i.e.,

$$\int p(t,\omega)d\omega = |s(t)|^2 \tag{II.25}$$

and

$$\int p(t,\omega)dt = |S(\omega)|^2 . \tag{II.26}$$

Note: Any joint distribution that yields the correct marginal property is consistent with the uncertainty principle.

- Total energy property: The total energy of the distribution should be equal to the total energy of the signal.

$$E = \int\int p(t,\omega)d\omega\, dt = \int |s(t)|^2\, dt = \int |S(\omega)|^2\, d\omega \tag{II.27}$$

Note: If the distribution satisfies the marginal property then the total energy property is automatically satisfied.

- Time-shift-invariance: The shifted signal $s(t-t_0)$ will have the distribution $p(t-t_0,\omega)$.

- Frequency-shift-invariance: The modulated signal $s(t)e^{j\xi t}$ will have $p(t,\omega-\xi)$ as its distribution.

- Time and frequency shift invariance: The signal $s(t-t_0)e^{j\xi t}$ will have $p(t-t_0,\omega-\xi)$ as its distribution.

- Linear scaling property: The signal $s_{sc}(t) = \sqrt{a}s(at)$ will have the distribution $p_{sc}(t,\omega) = p(at,\omega/a)$, which will satisfy the marginal property of the scaled signal $s_{sc}(t)$.

- Weak finite-support property: If $s(t)$ has zero value outside the time interval (t_1,t_2) or outside the frequency range (ω_1,ω_2), so does the distribution $p(t,\omega)$.

- Strong finite-support property: If $s(t)$ has zero value at any time t_0 or at any frequency ω_0, then $p(t,\omega)$ will be zero for any time t_0 or frequency ω_0.

  Note: It is impossible for the signal $f(t)$ to be both time and frequency limited. Therefore, if a distribution satisfies the weak finite-support property, it cannot be limited to a finite region of time-frequency plane.

3. Wigner-Ville Distribution

The major reference of this topic is [Ref. 38, 39]. The reason the Wigner-Ville distribution (WVD) is discussed in detail is that we relate the WVD and the wavelet transform of the instantaneous correlation function. Another reason is that the WVD is typically used to represent a non-stationary process.

The WVD, in terms of the signal $s(t)$ or its spectrum $S(\omega)$, is defined by:

$$W(t,\omega) = \left[\frac{1}{2\pi}\right] \int_{-\infty}^{\infty} s^* \left(\frac{t-\tau}{2}\right) s \left(\frac{t+\tau}{2}\right) e^{-j\omega\tau} d\tau, \tag{II.28}$$

and

$$W(t,\omega) = \left[\frac{1}{2\pi}\right] \int_{-\infty}^{\infty} S^* \left(\frac{\omega+\theta}{2}\right) S \left(\frac{\omega-\theta}{2}\right) e^{-jt\theta} d\theta. \tag{II.29}$$

4. Properties of the Wigner-Ville Distribution

The WVD has the following properties:

- The WVD is always real, even if $s(t)$ is a complex signal. This is because $W(t,\omega) = W^*(t,\omega)$.
- The WVD satisfies the following symmetry relations:

  $$W(t,\omega) = W(t,-\omega) \quad \text{if} \quad s(t) \quad \text{is real, i.e., if} \quad S(\omega) = S(-\omega),$$

  and

  $$W(t,\omega) = W(-t,\omega) \quad \text{if} \quad S(\omega) \quad \text{is real, i.e., if} \quad s(t) = s(-t).$$

- The marginal property is satisfied in both time and frequency. Hence the total energy property is also satisfied.
- The time and frequency shift invariance properties are satisfied.

- For $s(t) = A(t)e^{j\phi(t)}$ the conditional spread in frequency is given by

$$\sigma^2_{\omega/t} = \langle\omega^2\rangle_t - [\langle\omega\rangle_t]^2 = 0.5\left\{\left[\frac{A'(t)}{A(t)}\right]^2 - \left[\frac{A''(t)}{A(t)}\right]\right\}, \qquad \text{(II.30)}$$

  where "$'$" denotes the time derivative. Since Equation II-30 may result in negative values, it cannot be properly used as a measure of bandwidth. Therefore, while WVD can be used to compute a reliable mean frequency, it cannot be used to obtain reliable values for the spread of those frequencies.

- WVD of sum of two signals: If $s(t) = s_1(t) + s_2(t)$, then the WVD is given by

$$W(t,\omega) = W_{11}(t,\omega) + W_{22}(t,\omega) + W_{12}(t,\omega) + W_{21}(t,\omega), \qquad \text{(II.31)}$$

  where

$$W_{i,j}(t,\omega) = \left[\frac{1}{2\pi}\right]\int_{-\infty}^{\infty} s_i^*\left(\frac{t-\tau}{2}\right) s_j\left(\frac{t+\tau}{2}\right) e^{-j\omega\tau} d\tau \qquad \text{(II.32)}$$

  is the cross WVD. The cross WVD is complex-valued, but $W_{12} = W_{21}^*$. Hence, $W_{12}(t,\omega) + W_{21}(t,\omega)$ is real and we can express $W(t,\omega)$ as:

$$W(t,\omega) = W_{11}(t,\omega) + W_{22}(t,\omega) + 2\text{Re}\ [W_{12}(t,\omega)]\,. \qquad \text{(II.33)}$$

The additional term $2\text{Re}\,[W_{12}(t,\omega)]$ is often called the cross term or the interference term.

Note: The signal is said to be composed of more than one signal (i.e., multicomponent signal) if it can be segmented into separate regions in the time-frequency plane.

Note: The WVD at time t depends on the values of the signal at the time moments $(t - \tau/2)$ and $(t + \tau/2)$. Even if there is no noise at time t, the WVD will reflect the noise component existing at those time moments $(t - \tau/2)$ and $(t + \tau/2)$. There are other types of TFDs, all forming one class, called the general Cohen's class. Cohen's class incorporates different kinds of TFDs which differ only in the definition of the window function. Window functions may be chosen to optimize the TFD according to certain criteria. One example of this criteria might be to minimize cross terms.

C. WAVELET ANALYSIS

Wavelet analysis is a new trend for representing non-stationary signals. It is widely applied for many areas of signal processing. In the following discussion we introduce the basic concepts of wavelet analysis.

1. Frames

A basis for a vector space V is a set S of vectors in V such that S is linearly independent and S spans V [Ref. 41]. Therefore, a basis can express any vector in the space V by a linear expansion. The resultant set of expansion coefficients is unique. Completeness and uniqueness of the expansion coefficients are directly related to the exact reconstruction of the original vector from the expansion coefficients. This property is required in signal processing applications which use the expansion algorithm to reconstruct the original signals. For simple computation of the expansion coefficients, the vectors of S are required to be orthogonal. Orthogonality will make it possible to compute the expansion coefficients (analysis) using simple inner products with the basis vectors. Reconstruction (synthesis) and decomposition (analysis) are done using the same set of basis vectors.

Orthogonality of the basis vectors (or basis functions) is defined as follows: the set of basis vectors $v_k(t)$ is said to be orthogonal if

$$\langle v_k(t), v_m(t) \rangle = a_{k,m}\delta(k-m), \tag{II.34}$$

where k, m are integers, $a_{k,m}$ is a constant and δ is the Kronecker delta function. The delta function $\delta(k-m)$ will be zero everywhere except where $m = k$ it will be one. Since the orthogonality is not a condition for having a set of basis vectors, we may find a set of non-orthogonal basis vectors. For any orthogonal set of basis vectors $v_k(t)$ the finite energy time signal $f(t)$ can be expanded using the set of basis functions $v_k(t)$ as:

$$f(t) = \sum_k \frac{a_k v_k(t)}{||v_k(t)||}, \tag{II.35}$$

where

$$a_k = \langle f(t), v_k(t) \rangle,$$

and $||v_k(t)||$ is the L^2 norm of the vector $v_k(t)$. Further, if we assume unit L^2 norm for the vectors $v_k(t)$, the vectors become an orthonormal set, and the expansion formula will be

$$f(t) = \sum_k a_k v_k(t), \tag{II.36}$$

where

$$a_k = \langle f(t), v_k(t) \rangle.$$

It is worth mentioning here that due to orthogonality (or orthonormality) both the analysis and synthesis of the expansion are carried out using the same set of basis vectors.

For a biorthogonal basis, we need two different sets of basis vectors, the original set $v_k(t)$ (the basis) for the expansion and a dual set $\tilde{v}_k(t)$ (dual basis) for reconstruction (or synthesis). The sets of the basis and the dual basis are not orthogonal, but each vector and its dual are orthogonal. The expansion is given by

$$f(t) = \sum_k a_k v_k(t), \tag{II.37}$$

where

$$a_k = \langle f(t), \tilde{v}_k(t) \rangle.$$

If the set S of the expansion vectors does not satisfy the linear independence condition stated above, then the set is called a "frame." Expansion with frames does not maintain uniqueness of expansion coefficients [Ref. 37]. Also, the exactness of the reconstruction will be replaced with an approximate representation. For more details about the theory of frames see [Ref. 42, 43]. Frames do not satisfy the Parseval's theorem of energy, which states that the energy in the original function will be distributed among the expansion coefficients without loss or gain. For frames, the total energy in the expansion coefficients will have two bounds A and B such

that:

$$A||f||^2 \leq \sum_k |\langle f(t), v_k(t)\rangle|^2 \leq B||f||^2 \tag{II.38}$$

where $0 \leq A, B < \infty$. Note that if $A = B$, then the frame is called a tight frame and

$$A||f||^2 = \sum_k |\langle f(t), v_k(t)\rangle|^2. \tag{II.39}$$

If $A = B = 1$, then the frame becomes an orthonormal set and

$$||f||^2 = \sum_k |\langle f(t), v_k(t)\rangle|^2, \tag{II.40}$$

which is the the Parseval's theorem.

There are different categories of wavelets, orthogonal wavelets, non-orthogonal, and biorthogonal wavelets. The Daubechies family, Symmlet, Coiflet, and Meyer wavelets are examples of orthogonal wavelets, while the Morlet wavelet is an example of a non-orthogonal wavelet. As mentioned earlier, not all applications of signal expansions require perfect reconstruction. Applications such as signal identification and classification are examples of this type. Therefore, unless the orthogonality is required to meet another criteria, we can exploit non-orthogonal wavelet transforms.

2. Continuous Wavelet Transform

The continuous wavelet transform (CWT) forms the mathematical basis for wavelet analysis. The concept behind wavelet analysis is that all basis functions can be generated from a single function called the mother wavelet, usually denoted by $\psi(t)$. Other wavelets can be generated using two distinct operations; scaling and translation. Scaling means expanding (dilating) or compressing the wavelet function according to a specific scaling value. The scale will be denoted by s. The translation allows shifting of the (scaled) wavelet to a desired position in time. This shift will be denoted by k. The scaled and translated wavelet is denoted by

$$\psi_{s,k}(t) = \frac{1}{\sqrt{s}}\psi\left(\frac{t-k}{s}\right), \tag{II.41}$$

where $\sqrt{s}$ is a normalization factor to maintain the L^2 norm of $\psi_{s,k}(t)$ to be constant at any scale s .

The integral form of CWT of the finite energy signal $f(t)$ with respect to the wavelet function $\psi(t)$ is given by [Ref. 42, 46]

$$W_f(s,k) = \int_{-\infty}^{\infty} f(t)\psi_{s,k}(t)dt, \tag{II.42}$$

or

$$W_f(s,k) = \frac{1}{\sqrt{s}}\int_{-\infty}^{\infty} f(t)\psi\left(\frac{t-k}{s}\right)dt. \tag{II.43}$$

The wavelet analysis is carried out by computing inner products (projections) between the signal and the wavelet functions. We can also interpret the wavelet analysis as a linear operation which transforms the signal using modified kernel functions, where the kernel of the transform is the mother wavelet, and the modifications are the scaling and the translation operation [Ref. 44]. If the wavelet function satisfies the admissibility condition, we can apply the rule of the resolution of identity to recover the signal from its wavelet transform. The admissibility condition is given by [Ref. 44]

$$C_\psi = \int_{-\infty}^{\infty} \frac{|\Psi(\omega)|^2}{|\omega|}d\omega < \infty, \tag{II.44}$$

where $\Psi(\omega)$ is the Fourier transform of $\psi(t)$. This condition will be true if $\Psi(0) = 0$ or equivalently

$$\int_{-\infty}^{\infty} \psi(t)dt = 0. \tag{II.45}$$

The admissibility condition implies that the wavelet has a zero mean (i.e., DC component is zero). Therefore, it can be interpreted as a bandpass function. This implies that the wavelet must be an oscillatory function. The recovery (synthesis) formula, extracted from the resolution of identity rule, is given by

$$f(t) = \int_{\infty}^{\infty}\int_{\infty}^{\infty} W_f(s,k)\psi_{s,k}(t)dsdk. \tag{II.46}$$

3. Properties of Continuous Wavelet Transform

The following properties of the wavelet ransform are given below without proof. More details can be found in [Ref. 45].

1. Linearity: The wavelet transform is a linear operation on the analyzed signal. If the signal $f(t)$ is given as:

$$f(t) = f_1(t) + f_2(t), \tag{II.47}$$

then the wavelet transform of $f(t)$ is given by

$$W_f(s,k) = W_{f_1}(s,k) + W_{f_2}(s,k). \tag{II.48}$$

2. Shift-invariance: The CWT is shift invariant. If $g(t) = f(t - t_o)$, then it has a CWT given by

$$W_g(s,k) = W_f(s, k - t_o). \tag{II.49}$$

3. Time-scaling-invariance: If $g(t) = \frac{1}{\sqrt{a}} f(\frac{t}{a})$, then it has a CWT given by

$$W_g(s,k) = W_f\left(\frac{s}{a}, \frac{k}{a}\right). \tag{II.50}$$

4. Parseval's relation for the CWT becomes:

$$\int_\infty^\infty ||f(t)||^2 dt = \frac{1}{C_\psi} \int_\infty^\infty \int_\infty^\infty ||W_f(s,k)||^2 \frac{dsdk}{s^2} \tag{II.51}$$

implying that the CWT conserves the signal energy.

5. Time localization: From the definition of CWT and by the sifting property of the Dirac delta function, the CWT of an impulse at time t_o will be [Ref. 47] $\frac{1}{\sqrt{s}} \psi(\frac{t_o - k}{s})$. This means that the response of the CWT, at any scale s, will be a scaled and time reversed replica of the mother wavelet centered at location t_o on the shift axis (k). Therefore, the ability to define the location t_o will depend on the width of the scale wavelet. And since, a smaller scale value will result in a shorter wavelet, the time localization will be more precise.

6. Frequency localization: In fact, the uncertainty principle controls the time and frequency resolution of the wavelet transform at any scale, as the smaller the scale is the shorter the wavelet and the wider its frequency representation are. Consequently, the shorter wavelet has worse frequency localization than the original wavelet. Generally, the time localization is better at smaller scale values while the frequency localization is better at larger scale values.

4. Scalogram

Using a scalogram, the finite energy signal $f(t)$ is represented by the distribution of $|W_f(s,k)|^2$ over the time-scale plane. From Parseval's theorem for the wavelet

transform, Equation II-51, integration of $|W_f(s,k)|^2$ with respect to the differential $\frac{dsdk}{s^2}$ provides the total energy. By the definition of the scaled wavelet function in Equation II.41, the scale value s is inversely proportional to the frequency. Hence, the differential $\frac{ds}{s^2}$ is proportional to the differential of the frequency. Therefore, the quantity $|W_f(s,k)|^2$ may be viewed as a spectral density in units of power per Hertz [Ref. 44]. Consequently, the scalogram represents the power spectral density of the signal over the time-scale plane. Finally, we have the quantity

$$\frac{1}{C_\psi}\int_\infty^\infty ||W_f(s,k)||^2\frac{ds}{s^2} \tag{II.52}$$

which represents the signal instantaneous power, while the quantity

$$\frac{1}{C_\psi s^2}\int_\infty^\infty\int_\infty^\infty ||W_f(s,k)||^2 dk \tag{II.53}$$

represents the portion of the signal energy contained within the scale s. This fact is exploited in identifying the scale of each hop. In summary, the CWT is a linear, time-shift-invariant, time-scaling-invariant, and frequency-scaling-invariant operator.

5. Discrete Wavelet Transform

The CWT is defined by an integral transform over continuous variables in the scale s and the time shift k. Hence, performing the CWT requires expensive computations. Therefore, in practice a discrete grid for s and k is used. A widely accepted discretization is to specify $s = s_o^m$ and $k = nk_o s_o^m$, where m and n are integers, and $s_o > 1$, and $k_o > 0$ [Ref. 45]. Furthermore, if we select $s_o = 2$ and $k_o = 1$ we obtain the well-known dyadic wavelet sampling (tiling) grid. Hence the scaled and translated wavelet indexed by m and n is given by

$$\psi_{m,n}(t) = 2^{\frac{-m}{2}}\psi(2^{-m}t - n). \tag{II.54}$$

Figure 1 shows the time-frequency tiling of the STFT while Figure 2 shows the time-scale tiling of the wavelet transform.

In digital signal processing there are two related concepts that help understanding the wavelet transforms: the multiresolution analysis and the filter-bank theory. These concepts are discussed next.

6. Multi-Resolution Concepts in Discrete Wavelet Transforms

Introduction. We will briefly introduce the WT from the perspective of the multiresolution analysis (MR). The signal (or the time function) $f(t)$ is expanded in terms of the wavelet functions. These wavelets have a frequency bandpass shape, so they result in a set of successive details of the signal. For the approximation we need a special basis, called the scaling function $\phi(t)$, which is not a wavelet. It has a low pass frequency behavior and performs averaging. The discrete wavelet transform is given by

$$f(t) = \sum_{k=-\infty}^{\infty} c(k)\phi_k(t) + \sum_{j=0}^{\infty}\sum_{k=-\infty}^{\infty} d(j,k)\psi(j,k)(t), \tag{II.55}$$

where j and k are integers, the coefficient $c(k)$ constitutes the coefficients of the approximation, while $d(j,k)$ constitutes the coefficients of the added details or equivalently the fine resolutions [Ref. 47]. If the wavelets and the associated scaling functions form an orthonormal set of basis functions the coefficients are given by

$$c(k) = \langle f(t), \phi_k(t) \rangle, \tag{II.56}$$

and

$$d(j,k) = \langle f(t), \psi_{j,k}(t) \rangle. \tag{II.57}$$

The expansion form of the DWT is related to the subspace representation. Let us define the following subspaces: V_j is the scaling space at the j^{th} level, and W_j is the wavelet space at the j^{th} level. Let $V_{j+1} = V_j + W_j$. This means that the approximation at the $(j+1)^{st}$ level (or scale) can be represented by a coarser approximation V_j and a coarser detail W_j, both at the j^{th} level. Note that the subspaces V_j are spanned by the scaling functions $\phi_k(t)$ and the subspaces W_j are spanned by the wavelet functions $\psi_{k,j}(t)$.

Subspaces have to satisfy a set of conditions to become an MR representation. These conditions are [Ref. 46]:

1. Orthogonality and completeness:

$$\begin{aligned} V_j \cap W_j &= \{0\}. \\ V_j \oplus W_j &= V_{j+1}. \\ V_j \oplus \sum_{j=0}^{\infty} W_j &= L^2. \end{aligned} \tag{II.58}$$

2. Scale-invariance: If $f(t) \in V_j$ then $f(2t) \in V_{j+1}$.
3. Shift-invariance: If $f(t) \in V_j$ then $f(t-k_o) \in V_j$ for a given constant k_o .

Scaling and Wavelet Equations. The MR subspace representation leads to a method to formulate two equations in terms of the unknown scaling and wavelet functions. From the orthogonality and completeness property we deduce that $V_0 \subset V_1$. This means any function living in V_o, e.g., $\phi_0(t)$, can be expressed as a linear combination of functions living in V_1, e.g., $\phi_1(t)$. Hence, by substitution we get

$$\phi(t) = \sqrt{2} \sum_k h_0(k) \phi(2t-k), \tag{II.59}$$

where $\phi_0(t) = \phi(t)$ and $\phi_1(t) = \phi(2t)$. This equation includes two different scales of the scaling function and is known by many names: the scaling equation, the dilation equation, the refinement equation, or the multiresolution-analysis equation. The coefficients $h_o(n)$ are called the scaling filter coefficients. Using the condition, $V_0 \oplus W_0 = V_1$, which implies that $W_0 \subset V_1$, we have

$$\psi(t) = \sqrt{2} \sum_k h_1(k) \phi(2t-k) \tag{II.60}$$

also is called the wavelet equation. The coefficients $h_1(n)$ are called the wavelet filter coefficients.

In summary, an MR approach leads to a complete orthonormal set of the scaling and wavelet functions. Moreover, if the scaling function has compact support,

the wavelet function will be built up of a finite number of the scaling multipliers. Therefore, the scaling and the wavelet functions can be realized by finite-impulse-response (FIR) filters. For more details about wavelet and scaling equations see [Ref. 47, 42].

For discrete data the filter-bank concept leads to a simple method for computing the wavelet coefficients. The wavelet function is replaced by the coefficients of the wavelet filter $h_1(n)$ and the scaling function is replaced by the coefficients of the scaling filter $h_0(n)$. In [Ref. 46, 47, 42], the following two recursive equations are obtained:

$$\begin{aligned} c(j,k) &= \sum_m h_0(m-2k)c(j+1,m) \\ d(j,k) &= \sum_m h_1(m-2k)c(j+1,m). \end{aligned} \tag{II.61}$$

These two recursive equations enable us to compute the j^{th} scale wavelet transform from the $(j+1)^{st}$ scale using $h_0(m)$ and $h_1(m)$. The factor 2 in front of the parameter k decimates the output wavelet coefficients by 2. Figure 3 shows the realization of the recursive equations. This realization is equivalent to the well-known 2-band analysis bank of filter implementation. The implementation of the discrete wavelet transform using the recursive procedure is known as Mallat's algorithm. Figure 4 shows a multi-stage wavelet analysis bank and the corresponding ideal subspace designation (or spectral decomposition).

7. Daubechies Wavelet Family

The Daubechies wavelet family is a compactly supported orthonormal set of wavelet functions [Ref. 42]. The Daubechies wavelet are generated by solving the scaling and wavelet equations. An additional set of constraints is applied to satisfy the maximum number of vanishing moments for each wavelet. Each Daubechies wavelet is assigned a number related to the number of vanishing moments, hence, each wavelet is denoted as Daub-N. There are two conventions in assigning the number N; the first one is to let N refer to the number of vanishing moments; the second one is to let N

refer to the length of the wavelet filter (i.e., the number of wavelet coefficients). We will adopt the first designation since it is adopted by the MATLAB Wavelet Toolbox, where each Daubechies wavelet is expressed by the coefficients of its scaling filter. The coefficients of the wavelet filters are the interpolated high pass versions of the scaling filter. The Daubechies wavelet of order N has $2N$ coefficients, and has finite support over $[0, 2N-1]$. The number of vanishing moments is an indication of the smoothness of the the wavelet filter, since the number of vanishing moments will imply the number of zeros of $\Psi(\omega)$ at $\omega = \pi$. The higher the order the longer and smoother is the Daubechies filter.

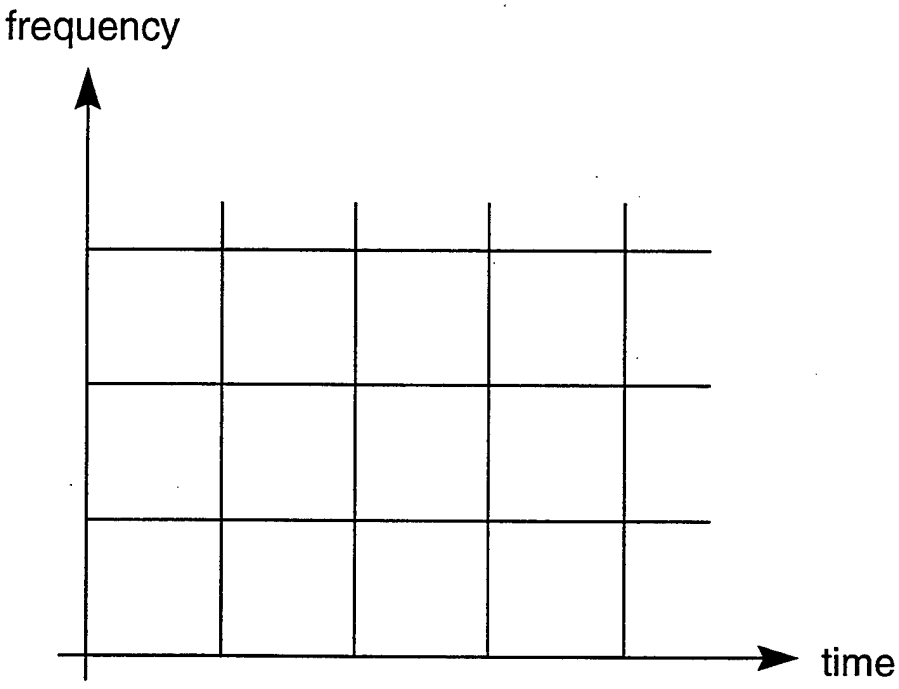

Figure 1. Time-Frequency tiling of the STFT.

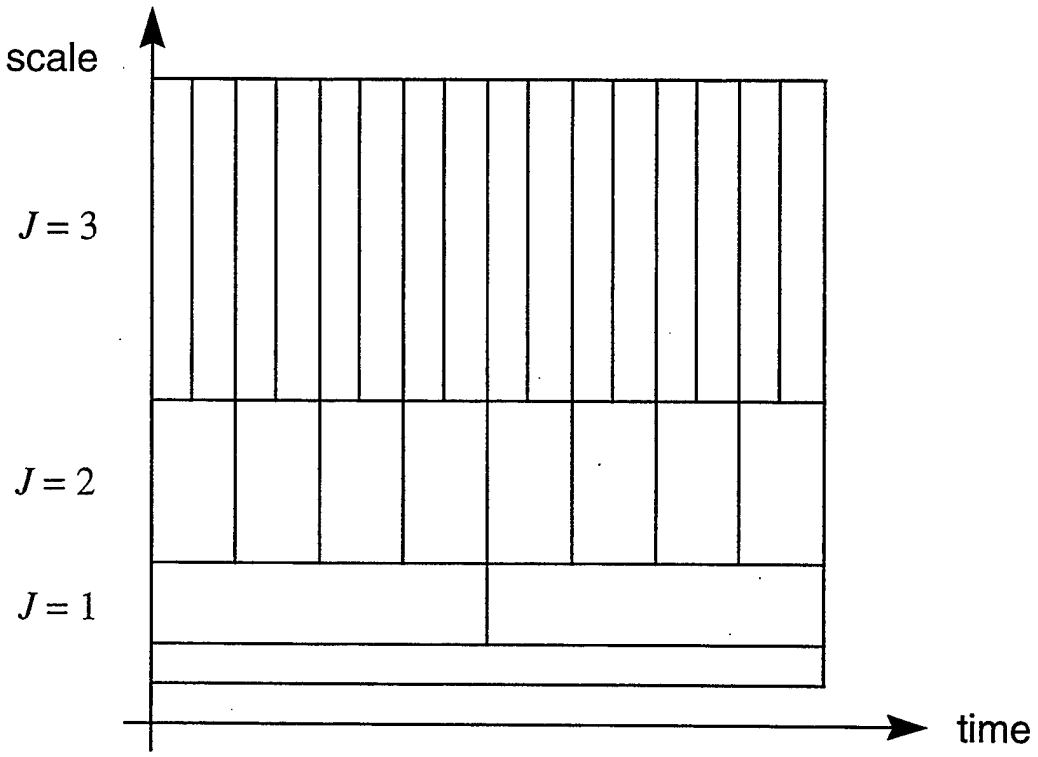

Figure 2. Time-Scale tiling of the wavelet transform.

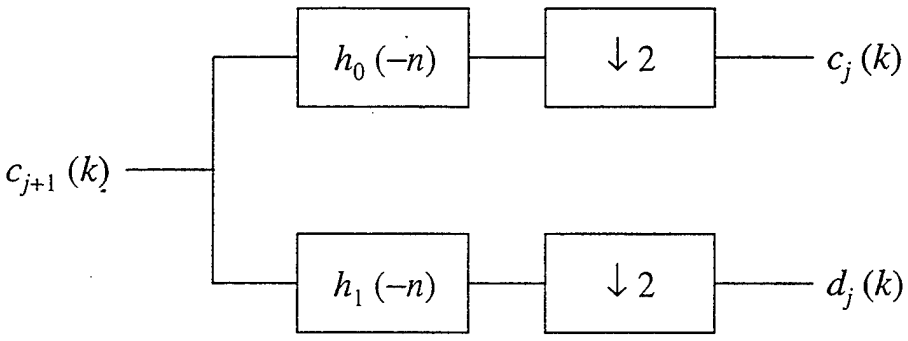

Figure 3. Recursive computation of wavelet coefficients.

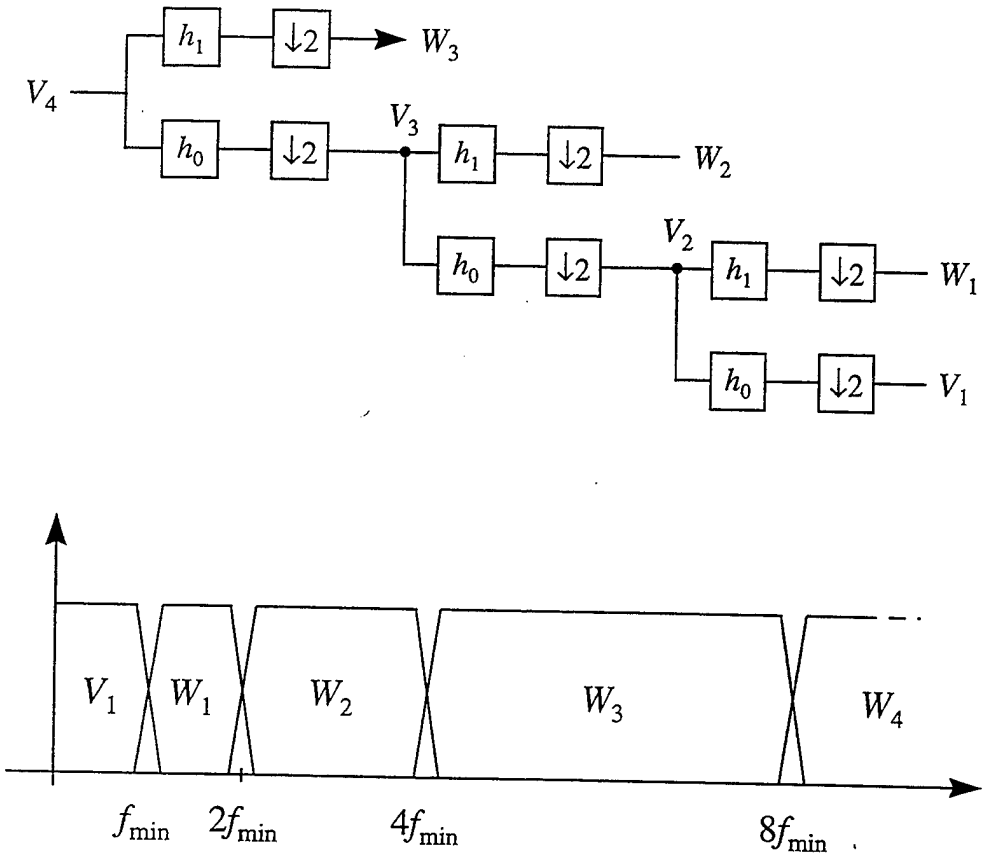

Figure 4. Multiple-Stage wavelet analysis bank and its subspace designation.

III. WAVELET TRANSFORMS AND CORRELATION FUNCTIONS

Correlating two functions results in a measure of similarity between them and is accomplished by evaluating an inner product. Correlation analysis has been used extensively in the signal processing and communication area, e.g., in spectral estimation, system modeling, signal detection and parameter estimation.

The Wiener-Khinchin theorem relates the signal's auto-correlation function and power spectral density for a stationary stochastic process, through a Fourier transform. Due to their time-varying spectra, FH signals are non-stationary and can be represented using time-frequency distributions. Traditionally, Fourier kernels are used in the time-frequency distributions.

Wavelet decomposition can be used to represent non-stationary signals over the time-scale plane. Therefore, we will consider the wavelet transform of the correlation function as an alternative for non-stationary signal representation.

In this chapter, we will introduce different choices for the correlation function and derive the corresponding wavelet transform response. In the derivation of the wavelet transform we will use the analytic definition of the correlation function and the wavelet function without specifying a functional form.

A. CORRELATION FUNCTIONS

1. Definitions of Auto-Correlation Functions

Depending on the underlying process, various definitions are given to the auto-correlation function (ACF). The process may be deterministic, stochastic, finite-energy, infinite-energy, non-time-varying (stationary) or time-varying (non-stationary). Next, we will introduce the different definitions of the ACF. The main reference for this topic is [Ref. 51].

1. Deterministic ACF: The ACF is defined for deterministic, infinite-energy, and

non-time-varying signals by

$$R(\tau) = \lim_{T\to\infty} \frac{1}{2T} \int_{-T}^{T} x(t)x^*(t+\tau)dt\,, \tag{III.1}$$

where "T" is the observation interval and "τ" is the time lag or the time delay. For finite energy signals the ACF is defined as:

$$R(\tau) = \int_{-\infty}^{\infty} x(t)x^*(t+\tau)dt\,. \tag{III.2}$$

For stationary signals or processes (i.e., wide-sense stationary) $R(t,\tau)$ is a function of the time delay only, hence, it is denoted by $R(\tau)$. For a non-stationary signal, $R(t,\tau)$ will be represented by a 2-D surface over the time "t" and the time delay "τ".

2. Stochastic ACF: The ACF of a stochastic process is the correlation between two samples of the process taken at t_1 and t_2, and is defined as:

$$R(t_1,t_2) = E\{x(t_1)x^*(t_2)\}\,, \tag{III.3}$$

where E is the expectation operator and "$*$" stands for the complex conjugation. For a stationary (or wide-sense stationary) process, $R(t_1,t_2)$ depends only on the time lag $\tau = t_2 - t_1$, resulting in a stationary spectrum. For a non-stationary process, $R(t_1,t_2)$ depends on the time instants t_1 and t_2, resulting in a time-varying spectrum.

2. Properties of Auto-Correlation Functions

We will briefly introduce the significant properties of the ACF for finite-energy signals. For more details see [Ref. 36, 52].

1. Conjugate symmetry:

$$R(t,\tau) = R(t,-\tau)^*, \tag{III.4}$$

i.e., the real part of $R(t,\tau)$ is an even function with respect to the lag τ while the imaginary part is an odd function.

2. Mean-squared value:

$$R(t,\tau)|_{\tau=0} = E\{|x(t)|^2\}. \tag{III.5}$$

3. Positive definiteness: The ACF, denoted by $R(t_1,t_2)$, is said to be positive definite if

$$\sum_{i,j} a_i a_j^* R(t_i,t_j) \geq 0 \tag{III.6}$$

for any $a_i, a_j \neq 0$. Positive definite property of the ACF guarantees that the spectrum of the signal is non-negative.

4. Wiener-Khinchin theorem:

$$S_{xx}(f) = \int_{-\infty}^{\infty} R(\tau) e^{-j2\pi f\tau} d\tau. \tag{III.7}$$

The power spectral density function $S_{xx}(f)$ of the stationary signal is obtained by Fourier transforming its (positive definite) ACF. Note that the non-stationary signals have time-varying spectra, therefore, no power spectral density is defined.

3. The Instantaneous Correlation Function

The ACF of deterministic and stochastic processes are computed using time domain averaging and the expectation operator, respectively. This means that a smoothing process has to be applied to compute the correlation functions.

The instantaneous correlation function (ICF) does not use an averaging operation (integration nor expectation). The instantaneous correlation function is defined as the product of two samples of the process. These two samples are drawn at two time instants centered about time t. The instantaneous correlation function $R^i(t,\tau)$ is defined as:

$$R^i(t,\tau) = x\left(t+\frac{\tau}{2}\right) x^*\left(t-\frac{\tau}{2}\right), \tag{III.8}$$

where "i" stands for the instantaneous nature of the correlation function.

$R^i(t,\tau)$ satisfies the following properties:

1. Conjugate symmetry, i.e.,

$$R^i(t,\tau) = R^{i*}(t,-\tau). \tag{III.9}$$

2. Squared value,

$$R^i(t,\tau)|_{\tau=0} = |x(t)|^2, \tag{III.10}$$

i.e., at $\tau = 0$, $R^i(t,\tau)$ will represent the instantaneous power of the signal at time "t".

If $x(t)$ is a sinusoidal signal then multiplication of the instantaneous values of $x(t)$ in the sense of Equation III-8 will generate cross terms in the ICF. For example, the real-valued sinusoidal signal $x(t) = A\cos(\omega t)$ has an ACF given by:

$$R(\tau) = \frac{A^2}{2}\cos(\omega\tau), \tag{III.11}$$

while the ICF is given by:

$$R^i(t,\tau) = \frac{A^2}{2}\left[\cos(2\omega t) + \cos(\omega\tau)\right]. \tag{III.12}$$

The ACF of a single sinusoidal signal has only one component and no cross term, while the ICF has cross terms. If the signal $x(t)$ is represented by its analytic form, say $x(t) = A\exp j\omega t$, then its ICF is given by:

$$R^i(t,\tau) = A^2\exp(j\omega\tau). \tag{III.13}$$

That is, the ICF of a single complex exponential signal has no cross term. Therefore, to minimize cross terms it is recommended to use the analytic form of the input process in the computation of the Time-Frequency Distributions [Ref. 49]. In this dissertation, we will focus on the analytic form of the signals. Therefore, the first step of the processing scheme will be transforming the intercepted (real) signal using the Hilbert transform technique.

Another point worth mentioning is the exploitation of the conjugate-symmetry property of the ICF. In computing the surface of the ICF we need to compute only half the ICF surface, corresponding to positive (or negative) time lag "τ". The other half can be generated by the conjugate-symmetry property. This implies that the second half of the surface of the ICF carries no additional information. Therefore, the processing scheme may be applied to only one half of the ICF surface which will save computational cost and storage.

B. WAVELET TRANSFORMS OF CORRELATION FUNCTIONS

In Chapter II, we discussed the linearity property of the wavelet transform which allows the application of linear system theory to the wavelet transform. In this section, we will investigate the wavelet transform for the different definitions of the correlation function.

1. The Wavelet Transform of the Auto-Correlation Function

The wavelet transform of the stochastic ACF of a stationary process is addressed in [Ref. 48], similarly, we will address the ACF for a deterministic signal. Wavelet transform of the ACF will have similar results. For a deterministic, finite-energy, stationary signal, the (time-averaged) ACF is given by:

$$R(\tau) = \int_{-\infty}^{\infty} x(t)x^*(t+\tau)dt\,. \tag{III.14}$$

From the Wiener-Khinchin theorem we get

$$S_{xx}(f) = \int_{-\infty}^{\infty} R(\tau)e^{-j2\pi f\tau}d\tau. \tag{III.15}$$

Let $W_{xx}(s,\ell)$ denote the Wavelet transform of $R(\tau)$. Note, the subscript "xx" in $W_{xx}(s,\ell)$ stands for the wavelet transform of the ACF of $x(t)$ (in contrast to $W_x(s,\ell)$ which denotes the wavelet transform of $x(t)$). The wavelet basis function is denoted by $g(\tau)$. The wavelet transformation will be carried over the time lag variable "τ" to the wavelet shift variable "ℓ" and the wavelet scale "s". $W_{xx}(s,\ell)$ is then given by:

$$W_{xx}(s,\ell) = \frac{1}{\sqrt{s}}\int_{-\infty}^{\infty} R(\tau)g^*\left(\frac{\tau-\ell}{s}\right)d\tau\,. \tag{III.16}$$

Let $G(f)$ denote the FT of $g(\tau)$, then

$$FT\{g\left(\frac{\tau-\ell}{s}\right)\} = |s|\;G(sf)e^{-j2\pi f\ell}\,. \tag{III.17}$$

For positive scale values ,"s", $g\left(\frac{\tau-\ell}{s}\right)$ is given by:

$$g\left(\frac{\tau-\ell}{s}\right) = \int_{-\infty}^{\infty} sG(sf)e^{-j2\pi f\ell}e^{j2\pi f\tau}df\,. \tag{III.18}$$

We can write $W_{xx}(s,\ell)$ as:

$$W_{xx}(s,\ell) = \sqrt{s}\int_{-\infty}^{\infty}\int_{-\infty}^{\infty} R(\tau)e^{-j2\pi f\tau}d\tau G^*(sf)e^{j2\pi f\tau}df, \tag{III.19}$$

or

$$W_{xx}(s,\ell) = \sqrt{s}\int_{-\infty}^{\infty} S_{xx}(f)G^*(sf)e^{j2\pi f\ell}df\,. \tag{III.20}$$

Equation III.20 has the form of an inverse FT from the variable f back to the variable ℓ. Therefore, we can write

$$W_{xx}(s,\ell) = FT^{-1}\{\left(\sqrt{s}S_{xx}(f)G^*(sf)\right)\}. \qquad \text{(III.21)}$$

From Equation III.21 we deduce the following:

1. The wavelet transform, of a finite-energy signal, at any wavelet scale $s \neq 0$, represents a linear filtering operation using a band pass filter whose impulse response is the (time-reversed) wavelet function at the scale s. Equivalently, the filter has a frequency response given by the FT of the scaled wavelet.

2. The wavelet transform of the ACF, $R(\tau)$, of the stationary finite-energy signal $x(t)$, gives a band pass filtered version of the power spectral density $S_{xx}(f)$ of this signal (up to a constant, $\sqrt{s}$), the used band pass filter is dependent on both the chosen wavelet function and the chosen wavelet scale.

2. The Wavelet Transform of the Instantaneous Correlation Function

The Wigner-Ville Distribution (WVD) is used to represent non-stationary processes since they are characterized by their time-varying spectra. The WVD applies a one-dimensional Fourier transformation to the ICF. The Fourier transform is carried out taking the time delay τ to the frequency f, keeping the global time t unchanged. This allows for displaying the time evolution of the spectrum of the signal. For one-dimensional time signals, the one-dimensional wavelet transform carries out a transformation from one global time variable "t" to the two wavelet variables, the shift ℓ and the scale s. Consequently, the signal is represented by a time-scale distribution in the wavelet domain. The wavelet domain is called the time-scale domain. For the two-dimensional surface, indexed by time "t" and the delay "τ", we carry out the wavelet transformation along the time delay. This permits a display as a function of time. In this section, we will derive the relation between the time-frequency representation of the signal $x(t)$ using the WVD and the time-scale representation of the same signal using the wavelet transform of the ICF.

Let $V_x(t,f)$ denote the WVD of the signal $x(t)$,

$$V_x(t,f) = \int_{-\infty}^{\infty} x(\left(t-\frac{\tau}{2}\right) x^* \left(t+\frac{\tau}{2}\right) e^{-j2\pi f\tau} d\tau. \qquad \text{(III.22)}$$

Since the ICF of the signal $x(t)$ is defined as:

$$R_x^i(t,\tau) = x\left(t-\frac{\tau}{2}\right) x^*\left(t+\frac{\tau}{2}\right), \qquad \text{(III.23)}$$

where τ is time shift (or time delay) relative to time t. The WVD may be defined as:

$$V_x(t,f) = \int_{-\infty}^{\infty} R_x^i(t,\tau) e^{-j2\pi f\tau} d\tau\,. \qquad \text{(III.24)}$$

The wavelet function $g(\tau)$, has been scaled by s and shifted by ℓ along the τ axis, to form $g_{s,\ell}(\tau)$ which is given by:

$$g_{s,\ell}(\tau) = \frac{1}{\sqrt{s}} g\left(\frac{\tau-\ell}{s}\right), \qquad for\, s>0\,. \qquad \text{(III.25)}$$

Let $G(f)$ denote the FT of $g(\tau)$, thus

$$FT\{g\left(\frac{\tau-\ell}{s}\right)\} = s\; G(sf) e^{-j2\pi f\ell}\,. \qquad \text{(III.26)}$$

Then

$$g\left(\frac{\tau-\ell}{s}\right) = \int_{-\infty}^{\infty} sG(sf) e^{-j2\pi f\ell} e^{j2\pi f\tau} df\,. \qquad \text{(III.27)}$$

Let $W_{xx}^i(t;s,\ell)$ be the wavelet transform of the ICF $R_x^i(t,\tau)$. Note that the superscript "i" indicates the instantaneous feature of the ICF. $W_{xx}^i(t;s,\ell)$ is given by:

$$W_{xx}^i(t;s,\ell) = \frac{1}{\sqrt{s}} \int_{-\infty}^{\infty} R_x(t,\tau) g^*\left(\frac{\tau-\ell}{s}\right) d\tau\,. \qquad \text{(III.28)}$$

Substituting $g^*\left(\frac{\tau-\ell}{s}\right)$ from Equation III.27 into Equation III.28 and exchanging the integration operations we get

$$W_{xx}^i(t,s,\ell) = \sqrt{s} \int_{-\infty}^{\infty} G^*(sf) \left[\int_{-\infty}^{\infty} R_x^i(t,\tau) e^{-j2\pi f\tau} d\tau\right] e^{j2\pi f\ell} df\,. \qquad \text{(III.29)}$$

Substituting Equation III.24 into Equation III.29 we have

$$W_{xx}^i(t;s,\ell) = \sqrt{s} \int_{-\infty}^{\infty} G^*(sf) V_x(t,f) e^{j2\pi f\ell} df\,. \qquad \text{(III.30)}$$

Equation III.30 is in the form of an inverse Fourier transform. Therefore, $W^i_{xx}(t;s,\ell)$ and $\sqrt{s}G^*(sf)V_x(t,f)$ are a Fourier transform pair with respect to the variable "ℓ", i.e., "ℓ". This relation suggests that we can obtain a filtered version of the WVD by Fourier transforming the $W^i_{xx}(t;s,\ell)$.

IV. FREQUENCY HOPPED SIGNALS AND THEIR CORRELATION FUNCTIONS

Communication systems can utilize a large number of digital modulation techniques. Among those, spread spectrum modulation is widely used. Spread spectrum refers to any modulation scheme that produces a transmitted bandwidth much larger than the information bandwidth [Ref. 50]. We will briefly address the different digital modulation schemes and focus on frequency hopping.

A. DIGITAL MODULATION SCHEMES

For comparison, digital communication schemes are briefly presented. Digital modulation techniques use the binary and the M-ary schemes. Binary schemes consist of the on-off keying (OOK), also called ASK, binary phase shift keying (BPSK), and frequency shift keying (FSK). M-ary schemes are generalizations of the binary schemes for transmitting M symbols, e.g., M-ary PSK or M-ary FSK.

1. Binary schemes

The major reference of this topic is [Ref. 51].

- OOK: The OOK signal is represented by:

$$s(t) = A_c\, m(t) \cos w_c t, \tag{IV.1}$$

where A_c is the carrier signal amplitude, $m(t)$ is the transmitted binary data over the bit duration T_b. For unipolar representation it has either "1" or "0". Therefore, over an observation time T_b the signal is zero (i.e., $m(t) = 0$) or it is a single sinusoid at frequency ω_c (i.e., $m(t) = 1$).

- BPSK: The BPSK signal is represented by:

$$s(t) = A_c \cos\left[w_c t + \Delta\theta m(t)\right], \tag{IV.2}$$

where $m(t)$ is the bi-polar message signal. Over the bit interval T_b the signal has the value ± 1 depending on whether the bit information is 1 or 0. $\Delta\theta$ is

the corresponding phase shift. Usually, $\Delta\theta$ is chosen as $\pi/2$. Therefore, the BPSK signal has either one of the two forms:

$$s(t) = \pm A_c \sin w_c t \; ; \quad \text{for} \quad m(t) = \pm 1 \, . \tag{IV.3}$$

Therefore, under any value of $m(t)$ the BPSK signal will be a sinusoid with a fixed frequency component but with a phase of zero or π.

- FSK: The continuous phase FSK signal is given by:

$$s(t) = A_c \cos\left[w_c t + \theta(t)\right], \tag{IV.4}$$

and

$$\theta(t) = D_f \int_{-\infty}^{t} m(\ell) d\ell \, , \tag{IV.5}$$

where D_f is a modulation index. For binary messages $m(t)$ the resultant FSK signal is called the binary FSK scheme. The FSK signal has one of two frequencies without phase discontinuities at the transition points.

2. M-ary Schemes

For an M-ary schemes a message $m(t)$ has M symbols. Consequently, the transmitted signal will have M different states.

- M-ary ASK: The M-ary scheme of the OOK (or ASK) may be implemented for different values of M. An example is QAM (*i.e.*, $M = 4$). All of the QAM states have the same single frequency components but differ in amplitude.
- M-ary PSK (MPSK): The M-ary PSK is generated similar to BPSK with the exception that the value of $\Delta\theta$ is chosen according to the number M. Thus, all the MPSK states have the same frequency component but differ in phase.
- M-ary FSK (MFSK): The M-ary scheme is similar to BFSK. But, instead of two symbols (states), it has a set of M symbols. Consequently, M different frequencies are transmitted. Thus, the MFSK signal can be expressed as $s(t) = A_c \cos(w_i t + \theta_i)$ where ω_i and θ_i are the i^{th} frequency and phase corresponding to the i^{th} symbol of the message $m(t)$.

In summary, digital modulation techniques are characterized by their signaling mode which consists of a single fixed frequency component over the duration of a given bit.

B. SPREAD SPECTRUM COMMUNICATION SIGNALS

The major reference for this section is [Ref. 19, 50]. Spread spectrum (SS) communication signals are characterized by a wide transmission bandwidth, and a low power spectral density. SS signals have two main advantages:

1) The message has a low probability of being intercepted (LPI) as a result of the wide frequency band, and the low power spectral density of the signals.

2) SS systems can reject jamming signals and allow many users to share the same frequency band as a result of the spreading gain [Ref. 19, 50].

Among the different possible SS modulation formats, the following are prevalent:

1) Frequency Hopping (FH): The complex baseband signal, $c(t)$, with basic pulse shape $p(t)$,is given by

$$c(t) = \sum \exp\ [j(2\pi f_n t + \phi_n]\, p[t - nT_h], \tag{IV.6}$$

where T_h is the pulse duration, better known as the hop interval. The pseudo-randomly generated sequence of frequencies $\{f_n\}$ will drive the modulator to generate a modulated version of $p(t)$. $\{\phi_n\}$ is an associated phase shift at each carrier frequency f_n.

2) Direct Sequence (DS) Modulation: The complex baseband signal, $c(t)$, of DS is given by

$$c(t) = \sum_n c_n p(t - nT_c), \tag{IV.7}$$

where $\{c_n\}$ is a pseudorandom sequence which modulates a sequence of pulses over a duration T_c, known as the chip interval.

3) Time Hopping (TH): The pulse waveform is given a fraction of duration T_s, i.e., T_s/M. A typical time hopping waveform might be

$$c(t) = \sum_n p\left(t - \left(n + \frac{a_n}{M}\right) T_s\right), \tag{IV.8}$$

which means the pulse will be controlled by the pseudo-random number (a_n) to appear at any of the M time segments within the duration T_s.

4) Hybrid Modulations: A blend of the above techniques may satisfy better performance according to some requirements.

Figure 5 shows a typical SS system. The SS spectrum uses two types of modulation. The first type, the baseband data modulation, is also called the primary modulation. The second type, the actual SS modulation, is also called the secondary modulation. For simple SS system realizations, certain combinations of primary and secondary modulations are usually employed. For DS, the binary phase shift keying (BPSK) is used as the primary data modulation scheme. For FH, the M-ary frequency shift keying (MFSK) is used. The FH system which implements MFSK data modulation is known as the pure FH scheme, and is the most popular and widely applied FH scheme. Another advantage for the pure FH scheme is its resistance against Repeat-back jammers (RBJ) which estimate the FH signal frequency and consequently send a proper jamming waveform. Thus, pure FH schemes minimize the hostile activity of RBJ as each hop frequency carries one symbol of the transmitted message only.

C. THE FREQUENCY HOPPED SIGNAL

The FH of the BFSK signal is given by

$$x(t) = \sqrt{2P}\sin\left[(\omega_0 + \omega_n + d_n\Delta\omega)t\right], \tag{IV.9}$$

where P is the signal power. The frequencies ω_0 and $\Delta\omega$ are constants, and ω_n is the frequency for the n^{th} symbol d_n whose value is ± 1.

During any hop, only one frequency component will be at the transmitter output when the hopping interval equals the symbol interval. The range of variation of $\omega_c = (\omega_n + \omega_0 \pm \Delta\omega)$ is known as the hopping bandwidth. Two types of FH systems exist depending on the hop interval T_h and the symbol interval T_s: fast-frequency hopping (FFH) and slow frequency hopping (SFH) which differ in their hopping speed. The number of hops within one symbol duration is the measure of the speed of the hopping rate. For pure FH signals with BFSK, the SFH requires $T_h \geq T_s$ while FFH requires $T_h < T_s$. The SFH contains one or more symbols during the hop interval while the FFH has one or more hops over one symbol interval. Figure

6 shows a typical pure FH system using the BFSK as a primary modulation. Figure 7 illustrates a typical time-frequency behavior of the BFSK pure FH scheme.

D. THE INSTANTANEOUS CORRELATION FUNCTION OF FREQUENCY HOPPED SIGNALS

Spread spectrum studies have usually considered the FH signal as a stationary process [Ref. 19, 50] even though the spectrum of the FH signal varies with each hop interval. Therefore, the correlation representation, using time averaging, is not suitable for this nonstationary process.

One way to identify the FH signal is to monitor the time evolution of the signal. Hence, we need to keep the time dependency in the correlation representation. In this work we resort to the time-varying correlation definition for characterizing the FH signals. Therefore, we select the instantaneous correlation function (ICF) as the candidate correlation representation. In this section, we will address the structure of the ICF of the pure FH signals.

The pure FH signal may be represented as successive intervals (i.e., hops) with single complex exponentials. The frequency within each interval (i.e., the hop frequency) is controlled by a randomly generated sequence of numbers, therefore, we can assume the following about the used frequencies:

(1) The number of the different hopping frequencies is much larger than the number of observed hops.

(2) The selection of discrete hopping frequencies (hopping pattern) is determined by a pseudo-random number generator (PNG), i.e., all hopping frequencies are equi-probable.

(3) The observation interval is much smaller than the period of PNG. The period of PNG is the number of generated hops times the hop interval.

As a result, we can deduce that any two successive hops will have two different frequencies. The difference in the frequency of adjacent hops will generate

the structure of the instantaneous correlation functions. Recall that we define the instantaneous correlation function as:

$$R(t,\tau) = s\left(t+\frac{\tau}{2}\right)s^*\left(t-\frac{\tau}{2}\right), \tag{IV.10}$$

where t is time and τ is time lag. Over the two-dimensional plane of time and time lag (i.e., $t-\tau$ plane) we compute the ICF for the time lag $|\tau| \leq T_h$, which will allow correlating adjacent hops only. If the values of $(t+\frac{\tau}{2})$ and $(t-\frac{\tau}{2})$ are both confined within the L^{th} hop then the ICF will be given by:

$$\begin{aligned} R(t,\tau) &= e^{j\omega_L(t+\tau/2)}\left(e^{j\omega_L(t-\tau/2)}\right)^* \\ &= e^{j\omega_L\tau}, \end{aligned} \tag{IV.11}$$

which is a function of τ and ω_L only. Note that the values of $(t+\frac{\tau}{2})$ and $(t-\frac{\tau}{2})$ are both confined within the same L^{th} hop if they satisfy,

$$(L-1)T_h \leq (t+\frac{\tau}{2})\ and\ (t-\frac{\tau}{2}) \leq LT_h. \tag{IV.12}$$

This inequality forms the boundaries of the diamond cellular shape for different values of L. This cellular structure is shown in Figure 8. Inside each diamond D_L, the ICF results from correlating signals belonging to the same hop, while outside the diamond the ICF results from correlating signals belonging to two consecutive hops.

A detailed derivation of the ICF is given in Appendix A, which leads to the doubly indexed correlation function $R_{\text{m,n}}(t,\tau)$ given by:

$$R_{\text{m,n}}(t,\tau) = \exp j\left\{(\omega_m-\omega_n)t + (\omega_m+\omega_n)\frac{\tau}{2}\right\}. \tag{IV.13}$$

where m and n are the indices of the two adjacent hops. Note that:

1) Within the main diamond of the n^{th} hop, i.e., $m=n$, the ICF is given by

$$R_{n,n}(t,\tau) = \exp\{j(\omega_n\tau)\}. \tag{IV.14}$$

2) Outside the main diamond in the upper triangle between hop numbers (n) and $(n+1)$, the ICF is given by

$$R_{n+1,n}(t,\tau) = \exp\left\{j(\omega_{n+1}-\omega_n)t + (\omega_{n+1}+\omega_n)\frac{\tau}{2}\right\}. \qquad \text{(IV.15)}$$

In conclusion, the instantaneous correlation function of a pure FH signal has a cellular or diamond structure. Inside the L^{th} diamond it has a single complex exponential component along the delay axis representing the L^{th} hop frequency. Outside the diamond, $R(t,\tau)$ is a product of two terms, $e^{j(\omega_n-\omega_m)t}$ and $e^{j(\omega_n+\omega_m)\tau/2}$, where ω_n and ω_m are two consecutive hop frequencies.

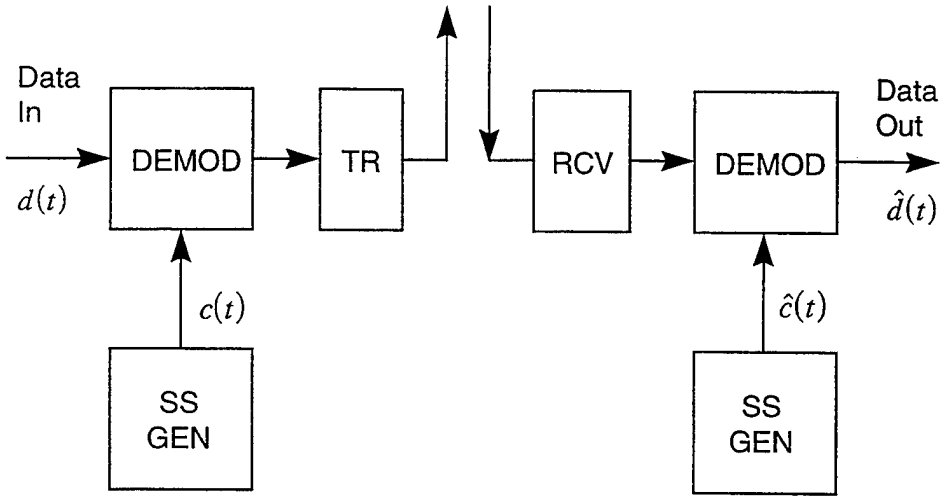

Figure 5. Modern SS system.

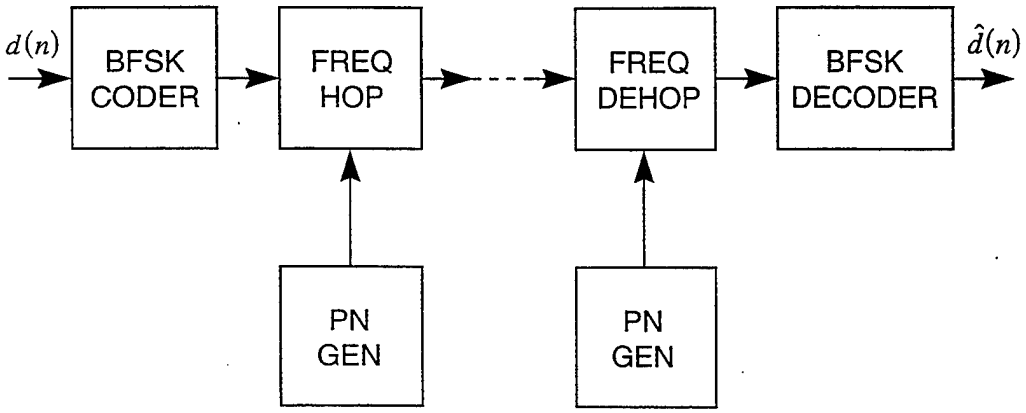

Figure 6. BFSK-FH system.

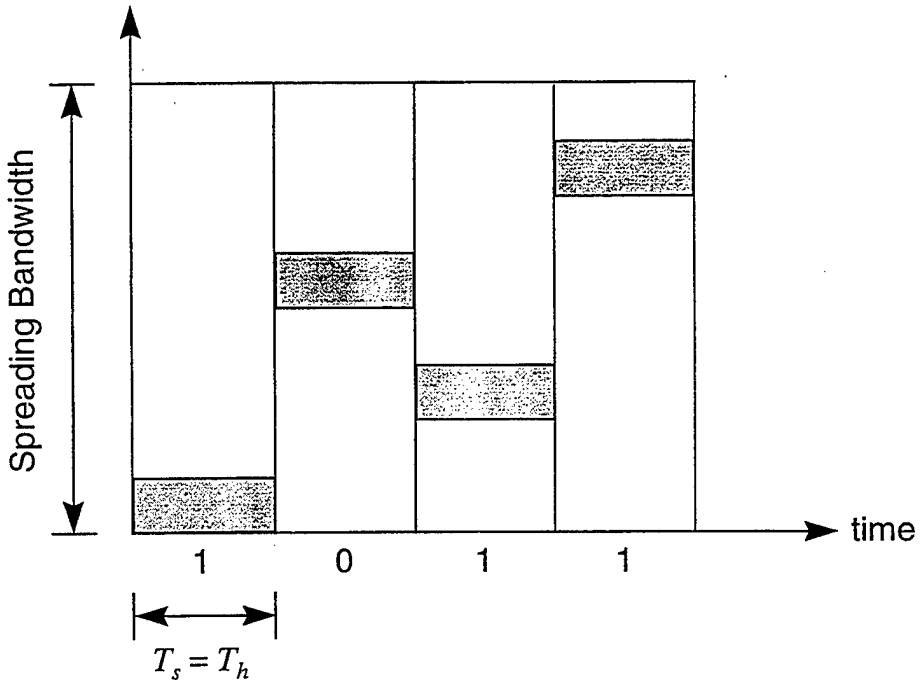

Figure 7. Time-Frequency behavior of BFSK-FH signal.

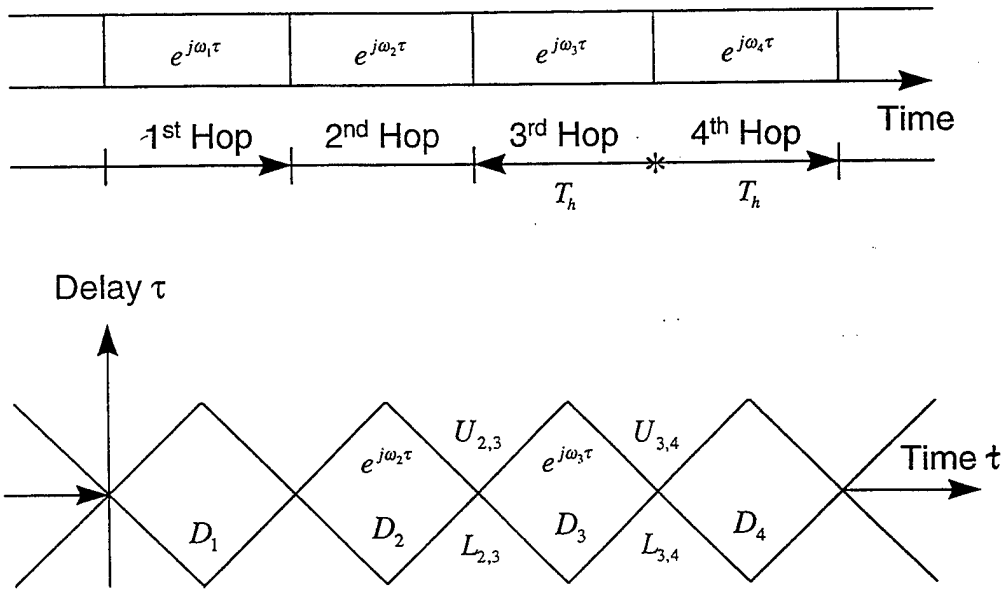

Figure 8. FH signal and the cellular (diamond) structure of its ICF.

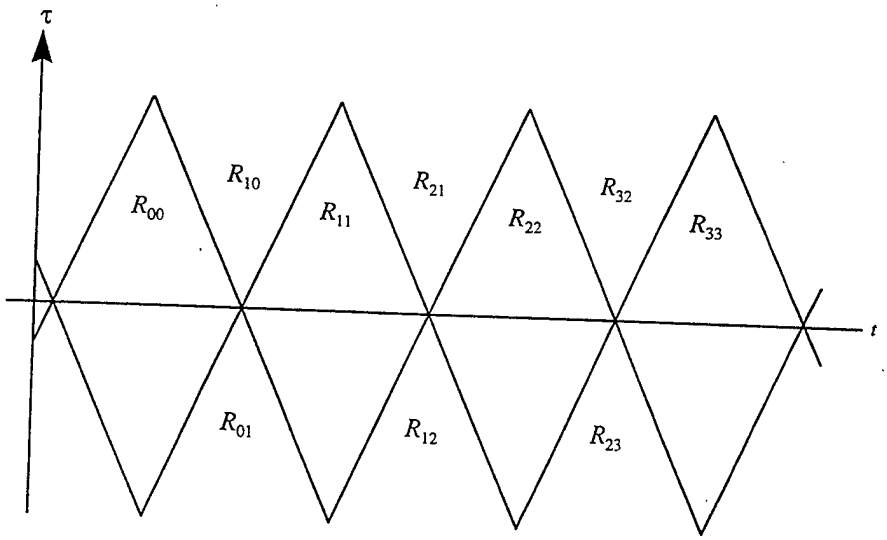

Figure 9. Areas and indices of the doubly indexed function $R_{\mathrm{m,n}}(t, \tau)$.

V. ANALYSIS USING MORLET WAVELETS

We studied the structure of the ICF surface obtained for complex FH signal in chapter IV, and showed that it consists of complex sinusoidal components. In this chapter, we will analyze the Morlet wavelet transform of the ICF. We will use the Morlet basis function for two reasons. First, the Morlet wavelet is a complex sinusoid, modulated by a Gaussian window, and is inherently best suited for filtering sinusoidal signals. Second, the Morlet wavelet has a mathematical formulation which makes the analysis and derivations tractable.

Recall that the mother Morlet wavelet $g(t)$ is given by:

$$g(t) = e^{jkt}e^{-t^2/2\sigma^2}, \quad for -\infty < t < +\infty, \tag{V.1}$$

where k is a constant that represents the modulation frequency, and σ^2 is inversely proportional to the roll-off factor of the Gaussian window. The Fourier transform is given by:

$$G(\omega) = e^{-\frac{1}{2}(\omega-k)^2}. \tag{V.2}$$

The Morlet wavelet does not satisfy the admissibility nor the orthogonality condition as it exists over an infinite time interval, but for practical applications it is truncated when it is sufficiently attenuated. If the wavelet has finite support (non-zero only over finite interval), then the scaled and shifted wavelet, $g_{s,\ell}(t)$, will be non-zero over the interval $[\ell - n\sigma s, \ell + n\sigma s]$, where s is the scale and ℓ is the shift. Here, n is a preselected number which ensures sufficient decay. The functional dependence of $g_{s,\ell}(t)$ is as described in Equation II.41. Usually, n is chosen ≥ 4 [Ref. 46].

A. TRANSFORM OF A TIME-LIMITED COMPLEX EXPONENTIAL

We showed in Chapter IV that the ICF of the FH signal consists of complex exponential components with frequencies that differ from region to region. Therefore,

we need to address the response of the wavelet transform to complex exponential signals. Let the signal $f(t)$ be a complex exponential $Ae^{j\omega_L t}$ defined over the interval $t \in [LT, (L+1)T]$, where T is the hop interval, and L stands for the L^{th} hop. When $\sigma = 1$, the Morlet wavelet transform (MWT) is given by:

$$W(s,\ell) = A\frac{1}{\sqrt{s}}\int_{\ell-ns}^{\ell+ns} e^{j\omega_L t}e^{-jk((t-\ell)/s)}e^{-((t-\ell)^2/2s)}dt\,, \tag{V.3}$$

where ℓ is confined to the interval $[LT+ns, (L+1)T-ns]$. This interval guarantees that the wavelet will be confined over the same hop without crossing the border to another hop. Later on we will compute the wavelet transform when the signal runs over the border between two adjacent hops. The exponent in Equation V.3 can be written as:

$$-\frac{1}{2}\frac{t^2}{s^2} + \left(j\omega_L - j\frac{k}{s} + \frac{\ell}{s^2}\right)t + j\frac{k\ell}{s} - \frac{1}{2}\frac{\ell^2}{s^2}\,. \tag{V.4}$$

Substituting $\omega_L - k/s = \omega$ we obtain

$$W(s,\ell) = A\frac{1}{\sqrt{s}}e^{-(\ell^2/2s^2)+j(k\ell/s)}\int_{\ell-ns}^{\ell+ns}\exp\left[-\frac{1}{2s^2}t^2 + \left(j\omega + \frac{\ell}{s^2}\right)t\right]dt\,. \tag{V.5}$$

This equation can be reduced to

$$W(s,\ell) = A\sqrt{\frac{\pi s}{2}}\exp\left[-\frac{s^2\omega_L^2}{2} - \frac{k^2}{2} + j\omega_L k + j\omega_L\ell\right](EF)\,, \tag{V.6}$$

where EF is given by:

$$EF = erf\left[\frac{1}{\sqrt{2}}(n + j(\omega_L s - k))\right] + erf\left[\frac{1}{\sqrt{2}}(n - j(\omega_L s - k))\right]\,, \tag{V.7}$$

for $\ell \in [LT+sn, (L+1)T-sn]$.

We note that the magnitude of $W(s,\ell)$ is independent of the wavelet shift variable ℓ.

The term EF defined above can be approximated using the following formula for the complex error function [Ref. 54] with

$$
\begin{aligned}
erf(x+jy) &= erf(x) + \frac{e^{-x^2}}{2\pi x}\left[1-\cos 2xy + j\sin 2xy\right] \\
&\quad + \frac{2}{\pi}e^{-x^2}\sum_{m=1}^{\infty}\frac{e^{-(1/4)m^2}}{m^2+4x^2}\left[f_m(x,y)+jg_m(x,y)\right] \\
&\quad + \varepsilon(x,y), \qquad \text{(V.8)}
\end{aligned}
$$

where

$$
\begin{aligned}
f_m(x,y) &= 2x - 2x\cosh(my)\cos(2xy) + m\sinh(my)\sin(2xy) \\
g_m(x,y) &= 2x\cosh(my)\sin(2xy) + m\sinh(my)\cos(2xy)\ ,
\end{aligned}
$$

and $|\varepsilon(x,y)| \approx 10^{-16}|erf(x,y)|$.

Since EF is of the form

$$
EF(x,y) \equiv erf(x+jy) + erf(x-jy),
$$

we need to determine $erf(x-jy)$. Recall that $\sin(x)$ and $\sinh(x)$ are odd functions while $\cos(x)$ and $\cosh(x)$ are even functions. Thus we can express

$$
\begin{aligned}
erf(x-jy) &= erf(x) + \frac{e^{-x^2}}{2\pi x}\left[(1-\cos 2xy) - j\sin 2xy\right] \\
&\quad + \frac{2}{\pi}e^{-x^2}\sum_{m=1}^{\infty}\frac{e^{-(1/4)m^2}}{m^2+4x^2}\left(f_m(x,-y)+jg_m(x,-y)\right), \qquad \text{(V.9)}
\end{aligned}
$$

where

$$
\begin{aligned}
f_m(x,-y) &= 2x - 2x\cosh(my)\cos(2xy) + m\sinh(my)\sin(2xy), \\
g_m(x,-y) &= -2x\cosh(my)\sin(2xy) - m\sinh(my)\cos(2xy)\,.
\end{aligned}
$$

Or, equivalently,

$$
\begin{aligned}
f_m(x,-y) &= f_m(x,y), \\
g_m(x,-y) &= -g_m(x,y).
\end{aligned}
$$

Using

$$erf(x - jy) = erf^*(x + jy), \tag{V.10}$$

and

$$erf(x + jy) + erf(x - jy) = 2Re\{erf(x + jy)\}, \tag{V.11}$$

where $Re\{\cdot\}$ denotes the real part, we can express $W(s, \ell)$ as:

$$\begin{aligned} W(s,\ell) &= A\sqrt{2\pi s}\exp\left[-\frac{s^2\omega_L^2}{2} - \frac{k^2}{2} + s\omega_L k + j\omega_L \ell\right] \\ &\quad \cdot Re\left\{erf\left(\frac{1}{\sqrt{2}}[n + j(\omega_L s - k)]\right)\right\}, \end{aligned} \tag{V.12}$$

for $l \in [LT + ns, (L+1)T - ns]$.

Equation V.12 shows that the transform has a linear phase response, $\Phi(\omega)$, independent of the scale s, which is given by:

$$\Phi(\omega) = \omega_L \ell. \tag{V.13}$$

Note that if the complex exponential signal has an initial phase shift, θ_L, the phase of the output of the transform will change to

$$\Phi(\omega) = (\omega_L \ell + \theta_L). \tag{V.14}$$

The amplitude may be expressed as $AB(s, \omega)$, where $B(s, \omega)$ is the wavelet gain given by:

$$B(s,\omega) = \sqrt{2\pi s}\exp\left[-\frac{s^2\omega_L^2}{2} - \frac{k^2}{2} + s\omega_L k\right] Re\left\{erf\left(\frac{1}{\sqrt{2}}[n + j(\omega_L s - k)]\right)\right\}. \tag{V.15}$$

The gain of the Morlet wavelet transform $B(s, \omega)$ is plotted in Figure 10 as a function of scale and frequency.

The spectral response of the wavelet is plotted for values of $s = 0.5, 1$, and 2. Over this dyadic grid the spectral response contains some regions of low response due to the narrow bandwidth of the Morlet wavelet filters. In many applications, discrete-scale wavelets are preferred. Note that, the scale grid needs to be sampled

linearly (i.e., $s = 1, 2, 3, 4, \ldots$) or the roll-off factor (σ^2) of Equation V.1 has to be decreased when applying Morlet wavelets for full spectral coverage.

Complex error function. The error function used in $W(s, \ell)$ has a complex argument and we use a computational method given in [Ref. 54, 56] to compute it.

The error function is defined as

$$erf(z) = \frac{2}{\sqrt{\pi}} \int_0^z e^{-u^2} du, \tag{V.16}$$

while the complementary error function is defined as:

$$erfc(z) = 1 - erf(z). \tag{V.17}$$

Let $w(z)$ be defined as:

$$w(z) = e^{-z^2} erfc(-jz). \tag{V.18}$$

Then, for a complex argument z, the error function is expressed as:

$$erf(z) = 1 - e^{-z^2} w(jz). \tag{V.19}$$

The function $w(z)$ is tabulated for some values of z in [Ref. 54] and may be computed using the algorithm described in [Ref. 56].

B. ANALYSIS OF THE TRANSITION REGION

The transition region is defined as that where the FH signal $f(t)$ changes from one to another hop at time t_r. Thus, the wavelet transform involves two different signal frequency components in the transition region. The transition region between interval L and interval $L+1$ will be defined as $\ell \in [(L+1)T - ns, (L+1)T + ns]$, where the Morlet wavelet support interval is $2ns$.

Hence, the Morlet wavelet transform is given by:

$$W(s, \ell) = \frac{A}{\sqrt{s}} \int_{\ell - ns}^{t_r} e^{j\omega_L t} g^* \left(\frac{t - \ell}{s} \right) dt + \frac{A}{\sqrt{s}} \int_{t_r}^{\ell + ns} e^{j\omega_{L+1} t} g^* \left(\frac{t - \ell}{s} \right) dt, \tag{V.20}$$

where $t_r - ns < \ell < t_r + ns$.

The two parts of Equation V.20 can be solved similarly to Equation V.3, which leads to

$$
\begin{aligned}
W(s,\ell) \;=\; & \sqrt{\frac{\pi s}{2}}\exp\left[-\frac{s^2\omega_L^2}{2}-\frac{k^2}{2}+s\omega_L k+j\omega_L\ell\right] \\
& \left\{erf\left(\frac{1}{\sqrt{2}}\left[\frac{t_r-\ell}{s}-j(\omega_L s-k)\right]\right)+erf\left(\frac{1}{\sqrt{s}}[n+j(\omega_L s-k)]\right)\right\} \\
& +\sqrt{\frac{\pi s}{2}}\exp\left[-\frac{s^2\omega_{L+1}^2}{2}-\frac{k^2}{2}+s\omega_{L+1}k+j\omega_{L+1}\ell\right] \\
& \left\{erf\left(\frac{1}{\sqrt{2}}[n-j(\omega_{L+1}s-k)]\right)\right. \\
& \left.-erf\left(\frac{1}{\sqrt{2}}\left[\frac{t_r-\ell}{s}-j(\omega_{L+1}s-k)\right]\right)\right\}. \qquad \text{(V.21)}
\end{aligned}
$$

Over the length of the transition region the magnitude of MWT depends on ℓ.

Figures 11 and 12 show an example of the magnitude and the phase of the wavelet transform over a transition region. Two frequencies are used (4 and 7 rad/sec) and the magnitude and the phase of the wavelet transform are plotted for scale $s = 1$. The magnitude of the wavelet coefficients, for the signal with the first frequency (i.e., f=4), is larger than the magnitude of the wavelet coefficients of the signal with the second frequency (i.e., f=7). The magnitude and the phase of the wavelet transform for scale $s = 0.5$ is plotted in Figure 12. The magnitude of the wavelet coefficients, for the signal with the first frequency (i.e., f=4), is smaller than the magnitude of the wavelet coefficients of the signal with the second frequency (i.e., f=7). Note also that there is a gradual transition between the two magnitudes according to Equation V.21. This indicates that the Morlet wavelet transform does not produce spikes at the transition points between frequency hops.

C. ANALYSIS OF IDEAL WHITE GAUSSIAN NOISE

We investigate the response of the Morlet wavelet to ideal white Gaussian noise. The WT is given by:

$$W_n(s,\ell) = \int_{-\infty}^{\infty} \frac{1}{\sqrt{s}} n(t) g^*(\frac{t-\ell}{s}) dt. \tag{V.22}$$

For white Gaussian noise $n(t)$ and due to the linearity of the wavelet transform, the output $W_n(s,\ell)$ has a Gaussian distribution. Since $n(t)$ is assumed having zero mean and variance σ_n^2, then the mean value of $W_n(s,\ell)$ is

$$\begin{aligned} E\{W_n(s,\ell)\} &= E\left(\int_{-\infty}^{\infty} \frac{1}{\sqrt{s}} n(t) e^{-jk((t-\ell)/s)} e^{-(1/2)((t-\ell)/s)^2} dt\right) \\ &= 0. \end{aligned} \tag{V.23}$$

Since $W_n(s,\ell)$ is zero mean, its variance is given by:

$$\begin{aligned} \sigma_w^2 &= E\left\{|W(s,\ell)|^2\right\} = E\{W(s,\ell)W^*(s,\ell)\} \\ &= \frac{1}{s}\int_{-\infty}^{\infty}\int_{-\infty}^{\infty} dt_1 dt_2 E\left\{[n(t_1)n^*(t_2)] g\left(\frac{t_1-\ell}{s}\right) g^*\left(\frac{t_2-\ell}{s}\right)\right\}. \end{aligned} \tag{V.24}$$

When two samples $n(t_1)$ and $n(t_2)$ are assumed independent identically distributed Gaussian (i.i.d.) random variables, the term $E\{[n(t_1)n^*(t_2)\}$ is equal to zero except when $t_1 = t_2$. Hence we have

$$\begin{aligned} \sigma_w^2 &= \frac{\sigma_n^2}{s}\int_{-\infty}^{\infty} \left| g\left(\frac{t-\ell}{s}\right)\right|^2 dt \\ &= \sigma_n^2\sqrt{\pi}. \end{aligned} \tag{V.25}$$

Consequently, the Morlet wavelet transform of white Gaussian noise, with zero mean and σ_n^2 variance, is Gaussian with zero mean and a variance of $\sigma_n^2\sqrt{\pi}$ at any wavelet scale s. Note that we assumed an infinite support for the Morlet wavelet in the above derivation. If we carry out the same procedure for the finite support wavelet,

we will have a different expression for the variance of $W_n(s,\ell)$ due to integrating the term $\left|g\left(\frac{t-\ell}{s}\right)\right|^2$ over a finite interval. In such a case, the variance becomes

$$\sigma_w^2 = \frac{\sigma_n^2}{s}\int_{-ns}^{ns}\left|g\left(\frac{t-\ell}{s}\right)\right|^2 dt, \tag{V.26}$$

which results in

$$\sigma_w^2(s,\ell) = \sigma_n^2\sqrt{\pi}\, erf(ns)\,. \tag{V.27}$$

We note that for $ns >> 1$, $erf(ns)$ is well approximated by 1. Thus, we conclude that the variance of the wavelet transform will be essentially independent of the wavelet scale and can be approximated by $\sigma_n^2\sqrt{\pi}$.

Actual Noise of the Wavelet Surfaces. Application of the wavelet transform to the ICF surface will result in a number of wavelet surfaces corresponding to the number of wavelet scales used. Since, we exploit the wavelet surfaces for identifying the FH signal, we need to investigate the noise distribution over these surfaces. The noise of the wavelet surfaces is approximated as Gaussian noise. The following considerations assist in making this decision:

1) The noise background is assumed to be additive white Gaussian noise. The FH sinusoidal components and the noise are assumed to be independent. Noise realizations at two different time instants are assumed to be uncorrelated and independent.

2) The ICF surface consists of noise components which result from the product of two independent Gaussian random variables. This resulting noise surface has a K-distribution shape shown in Figure 13, where r is the correlation coefficient of the two Gaussian random variables [Ref. 57].

3) The wavelet transform of the ICF surface is a weighted sum of the ICF samples.

According to the central limit theory, usually, the sum of number of identically distributed random variables tends to a Normal (Gaussian) distribution. Since we take the wavelet transform of the ICF surface in the time delay direction, the samples of the wavelet surfaces, in the time delay direction, may be approximated as having a Gaussian distribution. Simulation results show that the noise distribution over

the wavelet surfaces, taken in direction of time delay, has approximately a Gaussian distribution. The Gaussian assumption was tested using a chi-square test. The main central part of the noise distribution (excluding the tails) was found to be Gaussian with confidence level $\geq 90\%$.

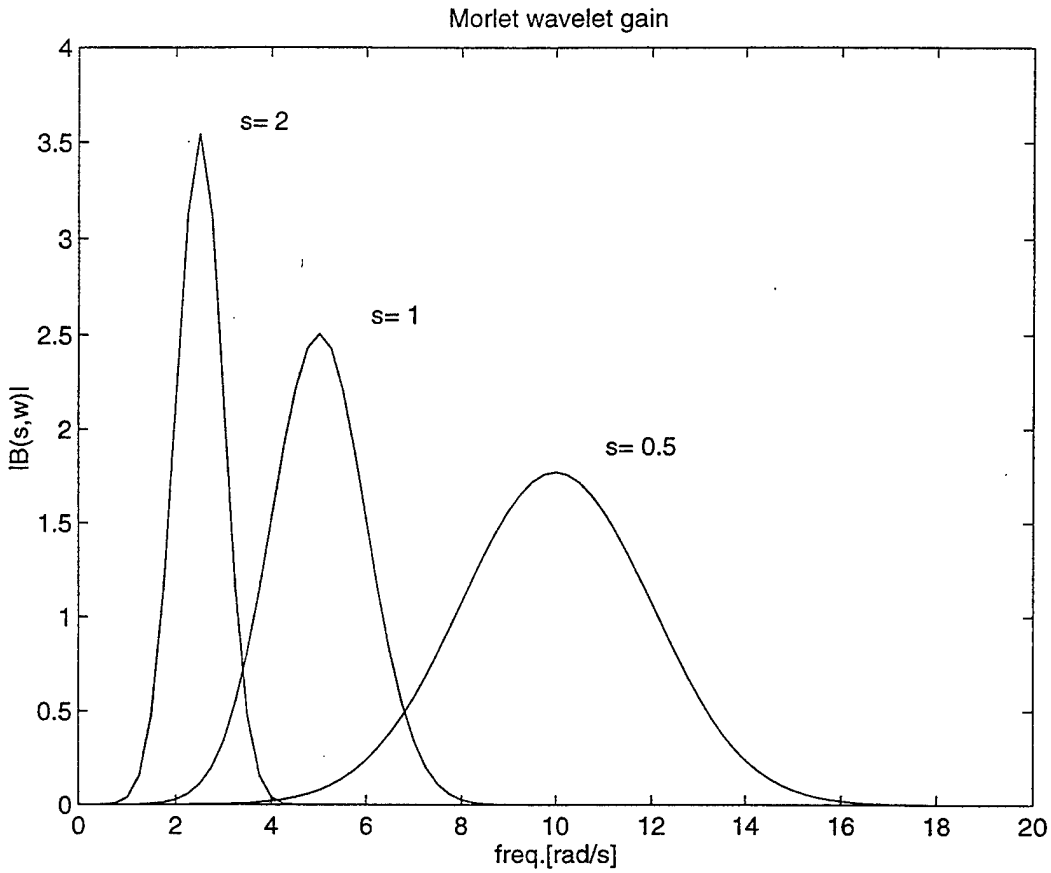

Figure 10. Morlet wavelet gain.

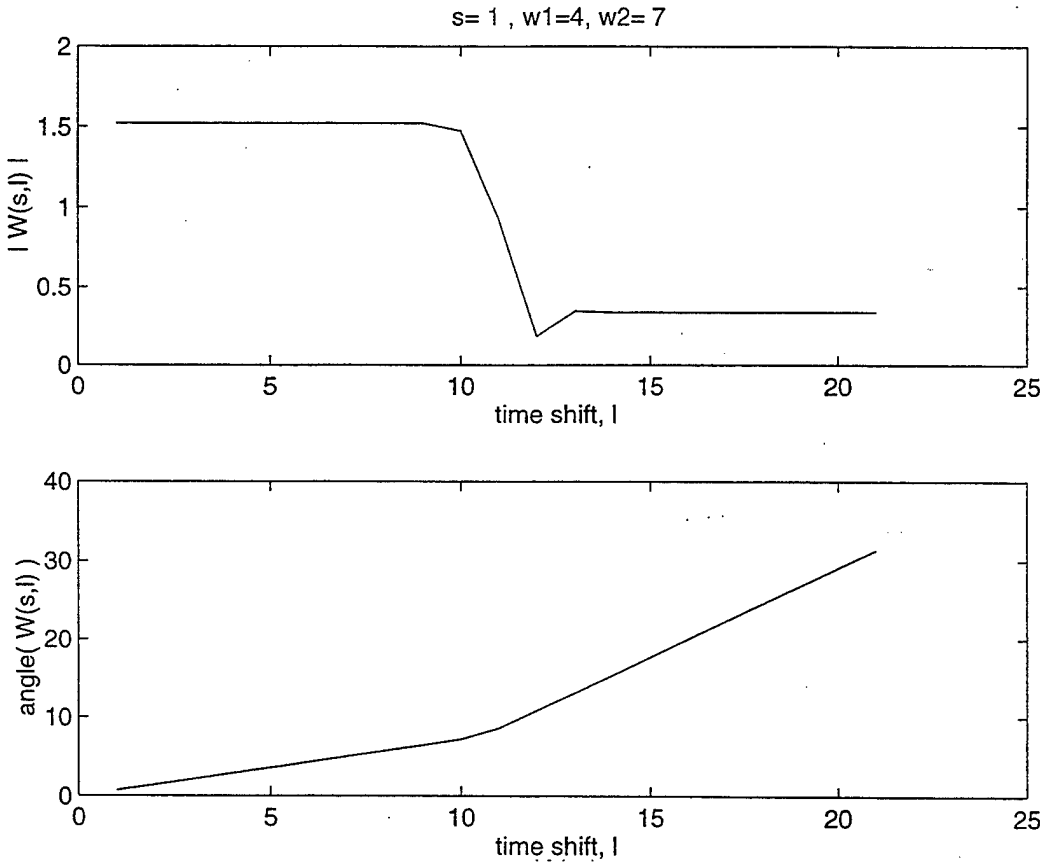

Figure 11. Morlet wavelet gain and phase over the transition region (s=1).

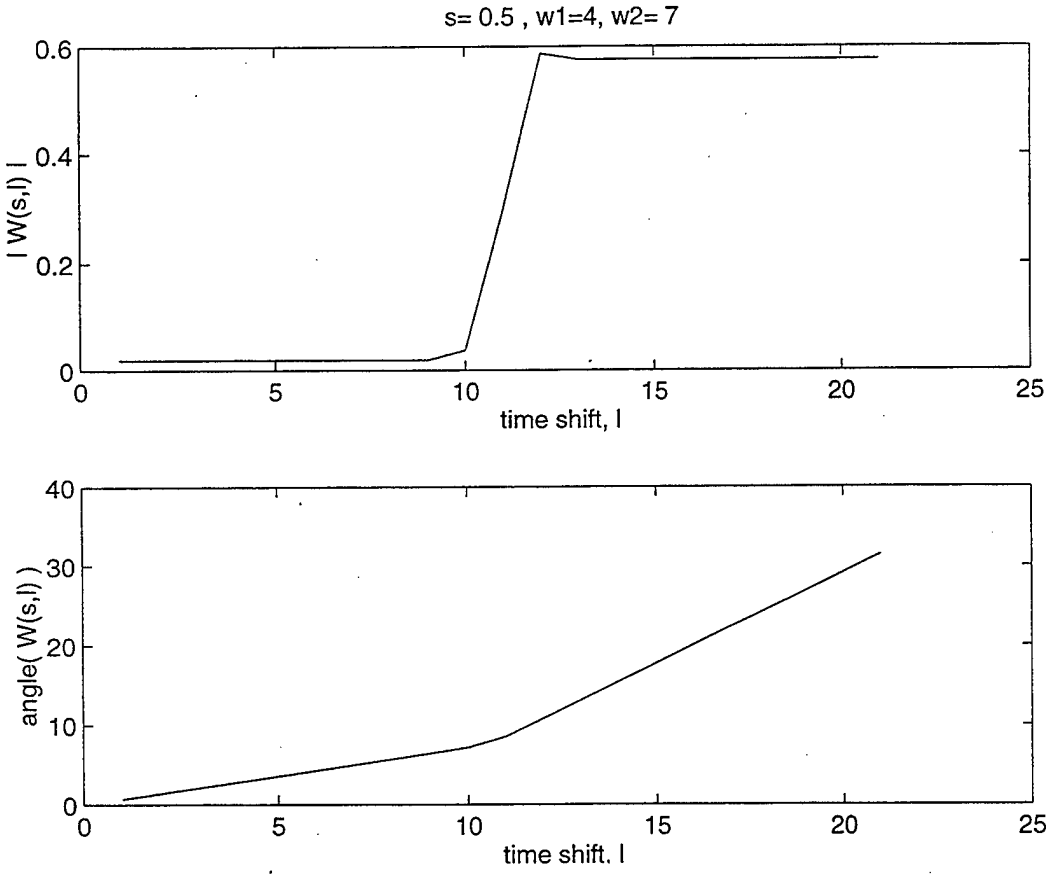

Figure 12. Morlet wavelet gain and phase over the transition region (s=0.5).

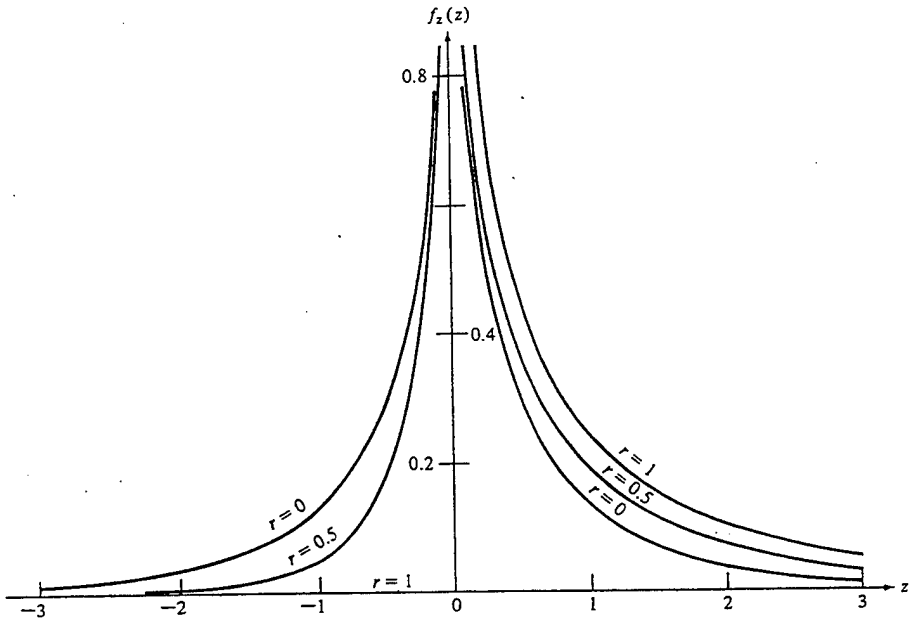

Figure 13. The K-distribution.

VI. ANALYSIS OF THE PROCESSING SCHEME

A. INTRODUCTION

Our goal is to exploit the wavelet transform of the ICF surface in order to identify FH modulation schemes. The wavelet transform results in a set of wavelet surfaces, one for each scale. We address the interception problem using two approaches, either of them can be used independently, but they differ in performance as will be shown later. In the first approach, we visually inspect the 2-D wavelet surfaces to identify and classify the structure of the FH signal and obtain an estimate for the hop time interval. In the second approach, we apply a proposed processing scheme to estimate the hop start/stop times, the hop-scale pattern, and the hop frequency. The extraction of the hop start/stop times is addressed using an edge detection approach by applying a compass operator which is well known in the image processing area. The hop-scale pattern is obtained by applying an energy analysis. The energy analysis assigns a scale index (called the proper scale) to each hop. The proper scale, for each hop, is that scale which has the greatest energy content. The sequence of proper scales, representing the hop sequence, is called the hop-scale pattern. The frequency of each hop can be extracted from the wavelet surface at the proper scale.

The identification of the FH signal may be accomplished based on:

(1) The hop-scale pattern: If two or more wavelet scales are applied, the hop-scale pattern of the FH signal will be different from the hop-scale patterns of other digital modulation signals.

(2) The frequency diversity: If all frequencies reside in one scale, then, an FH signal will have different frequency components as a function of the hop intervals.

Recall that, the ICF of the FH signal has a cellular structure which comprises of a tiling of diamonds. Each hop results in a diamond with a width equal to the hop interval. Thus, the diamond boundaries point to the hop start/stop times. All wavelet

surfaces at all scales emphasize the signals and hence the diamonds which belong to that scale. Other signals are attenuated. In this chapter, we address aspects of the discrete implementation, the proposed processing scheme, the measured parameters, and performance measures. In section VI.B, we address the discrete form of the ICF and its output expression to a white noise input. In section VI.C, we address the visual inspection and FH identification from the wavelet surfaces and obtain an estimate for hop time intervals. Then we compare the FH wavelet surfaces with wavelet surfaces from other digital modulation schemes. In section VI.D, we consider an energy analysis for identifying the scale of each frequency hop. We also investigate the performance of scale identification and evaluation measures. In section VI.E, we address the equalization of the spectral shape of the ICF and its impacts on the performance of scale identification. In section VI.F, we address the hop frequency extraction from the wavelet surfaces at the proper scale and from the original time signal. We also investigate the performance of frequency extraction and evaluation measures. Finally, we address the extraction of the hop start/stop times in section VI.G.

B. PROCESSING SCHEME

The interception problem usually assumes some prior knowledge about the signal of interest. In our case, we assume the signal hopping bandwidth is approximately known and the data is properly heterodyned and sampled.

1. Processing Sequence

The input data parameters to our processing scheme are the parameters of the FH signal (i.e., sampling frequency and the range of possible frequencies) while the outputs are:

(a) The wavelet transform of the ICF surface, i.e., the wavelet surfaces.

(b) The scale of each hop.

(c) The frequency of each hop.

(d) The hop interval start/stop times.

The data (input) process generates FH signals according to some predetermined input parameters (i.e., number of hops, hop interval, hop frequencies, sampling frequency and SNR). The analysis process generates the ICF surface and computes its wavelet transform at the predetermined wavelet scales. The measurement process extracts the outputs (the scale of each hop, the frequency of each hop, and the hop interval start/stop times).

Figure 14 shows the functional description of the processing scheme where the Input stands for the input process. The Hilbert Transform generates the analytic form of the signal. The Instantaneous Correlation Function generates the (discrete time) ICF surface. The Wavelet Transform computes the (discrete time) wavelet transform of the ICF surface (i.e., wavelet surfaces). The Scale Identifier identifies the hop scale. The Hop Frequency extracts the hop frequency from the wavelet surfaces. The Hop Timing extracts the hop start/stop times and the hop interval.

2. Discrete-Time Implementation of the Instantaneous Correlation Function

For discrete implementations, let $R(n,u)$ define the ICF of the discrete-time signal $x(n)$,

$$R(n,u) = x\left(n+\frac{u}{2}\right)x^*\left(n-\frac{u}{2}\right), \tag{VI.1}$$

where n is time and u is the time delay. Note that, the normalized sampling interval is 1 for the discrete implementation. In addition, the combined index $n \pm \frac{u}{2}$ should assume only integer values. Therefore, there will be two choices:

- Zero-inserted ICF: If we let u assume only even integer values, then $R(n,u)$, for odd u, must be set to zero.
- Frequency-doubled ICF: If we let $u = 2m$ then $R(n,m)$ will be defined as

$$R(n,m) = x(n+m)x^*(n-m)\,. \tag{VI.2}$$

Zero-inserted ICF. The effect of zero insertion to the ICF will result in doubling the number of wavelet coefficient over the resultant surfaces, implying more computation and storage load. Each hop will reside within its scale according to its associated signal frequency.

Frequency-doubled ICF. The frequency-doubled discrete ICF has the following characteristics in contrast to the zero-inserted ICF:

- Due to doubling the frequency, the minimum sampling frequency of the monitored signal will be twice the Nyquist rate.
- We obtain half the number of coefficients at the ICF surface and consequently at the wavelet surfaces.
- Over the wavelet surfaces, each hop will be located at a lower scale index than its associated signal frequency (lower scale index indicates higher frequency according to the MATLAB designation, see VI.A.3).

Since we usually pick a sampling frequency which is a multiple of the Nyquist rate, the choice of the frequency doubled ICF is advantageous because of a fewer number of coefficients, hence, saving in computation and storage. On the other hand, the loss of processing gain, due to pushing each hop to a lower scale index, can be overcome by chosing higher sampling frequency. For these reasons we adopted the definition of the frequency-doubled ICF in the processing scheme.

3. MATLAB Discrete Wavelet Transform

The MATLAB Wavelet Toolbox is used to implement the discrete wavelet analysis of the ICF surface. The wavelet transformation is carried out using the one-dimensional wavelet transform in the direction of the time delay u for each time element of the correlation function (as previously addressed in Chapter III). MATLAB uses a scale index designation and a corresponding multi-level decomposition tree as shown in Figure 15. S_j denotes the output of the wavelet transform at the j^{th} wavelet scale (i.e., the wavelet coefficients or the details at the j^{th} level). A_j denotes the approximation at the j^{th} level. H_0 is the scaling filter (low pass filter) and H_1 is

the wavelet filter (high pass filter) [Ref. 59]. MATLAB uses the Daub-N designation where N indicates the wavelet order and the number of vanishing moments, while the actual filter length is $2N$ [Ref. 59].

C. VISUAL IDENTIFICATION

In this section, we address the visual inspection of the wavelet surfaces in order to identify the FH modulation scheme. We investigate different approaches to represent these surfaces and considered real and complex valued wavelet functions.

1. Real and Complex-Valued Wavelets

According to Daubechies [Ref. 42], there is no symmetric or anti-symmetric real compactly-supported orthonormal wavelet. Symmetry property can be achieved only for complex-valued wavelets. Symmetry of a wavelet implies that the FIR filter representation has a linear phase response [Ref. 36]. It is an important feature in some wavelet applications, such as numerical resolution of partial differential equations with boundary conditions [Ref. 60]. A complex-valued Daubechies wavelet of order 3 is given in [Ref. 60] and has been used for comparison with the MATLAB real Daubechies wavelet of the same order. The Daub-3 complex wavelet has the following scaling coefficients:

$$\begin{aligned} h_0(1) = h_0(6) &= \frac{3 + j\sqrt{15}}{64}, \\ h_0(2) = h_0(5) &= \frac{5 - j\sqrt{15}}{64}, \\ h_0(3) = h_0(4) &= \frac{15 + j\sqrt{15}}{64}. \end{aligned} \tag{VI.3}$$

2. Surface Representation

Structure of the FH signal can be identified and classified by visually inspecting the wavelet surfaces. We can also obtain an estimate for the hop start/stop times. The next automated step is achieved by applying a proposed processing scheme to estimate the hop start/stop times, the hop-scale pattern, and the hop frequency. Using the

analytic form of the FH signal, the ICF surface will be a complex-valued function. Therefore, for any real or complex wavelet function the resultant two-dimensional wavelet surfaces are complex-valued. Hence, we consider the real part, the imaginary part, the magnitude, or the phase (angle) of the complex-valued surface.

An opinion test was carried out to assess the quality of identification from the wavelet surfaces using different representations. The Morlet wavelet and Daubechies wavelet of order 3 were both used in their real and complex form. Four different representations were investigated: real part, imaginary part, magnitude (absolute value), and phase. The objective of the opinion test is to identify the cellular structure over the wavelet surface and to identify the diamond boundaries as an indication of the hop start/stop times.

Figures 16 to 19 present the real part of the WT obtained with the real-valued Daubechies wavelet of order 3, at an input SNR values of 10 and 3 dB. In Figures 16 and 17 we note that we can not identify the FH structure over the surface of the ICF denoted by "CF". For wavelet surfaces, labeled "S1r", "S2r",..., "S5r", we can identify diamond patterns at the hops number 1, 2,..., 5 , respecively. Same findings can be observed in Figures 18 and 19 about wavelet surfaces. These results show that we can identify the FH structure from the wavelet surfaces, while it is not possible to do so from the ICF surface.

D. ENERGY ANALYSIS AND SCALE IDENTIFICATION

Energy analysis is performed over the wavelet surfaces at all scales considered. For the energy analysis we assume correct hop timing. The hop interval and hop start/stop times are estimated by visual inspection (and later on from the processing scheme). Thus, we can point to each hop over the wavelet surface and compute the energy contained. The energy contained at all scales are compared to identify the proper scale of each hop.

1. Energy and Energy per Sample

Parseval's theorem for the complete orthogonal filter bank (over L partitions) is applied to the discrete time wavelet analysis [Ref. 45]. It is given by:

$$||x(n)||^2 = \sum_{k \in Z} \left(|C(L, 2k)|^2 + \sum_{j=1}^{L} |d(j, 2k+1)|^2 \right), \tag{VI.4}$$

where, in the sense of wavelet analysis, $C(L, 2k)$ are the scaling coefficients at the scale L, $d(j, 2k+1)$ are the wavelet coefficients at scale j, and k is the wavelet shift variable.

Therefore, the quantity

$$E(j) = \sum_{k=-\infty}^{\infty} |d(j, k)|^2 \tag{VI.5}$$

represents the portion of the signal's energy over the j^{th} scale. For narrowband signals which reside within one scale, the signal energy will belong to that scale. However, some portions of the signal energy will be leaking to other scales. To identify the proper scale one can consider the maximum value due to the following quantities:

1) Wavelet coefficient.

2) Total energy.

3) Energy per sample.

Energy per sample is defined as:

$$A(j) = \frac{E(j)}{N(j)}, \tag{VI.6}$$

where j is the scale index, $E(j)$ is the total energy at the j^{th} scale, and $N(j)$ is the number of wavelet coefficients at this scale (i.e., the number of surface coefficients). According to the scale designation of the MATLAB Wavelet Toolbox,

$$N(j) = \frac{1}{2} N(j+1). \tag{VI.7}$$

If the signal $x(t)$ resides within the scale j or resides within the scale $(j+1)$, with the same total energy, we have

$$A(j+1) = 2A(j)\,. \tag{VI.8}$$

Thus, there will be a 3 dB gain in the energy per sample per each increment in the scale index.

Table 1 summarizes the energy distribution obtained with wavelet analysis using Daubechies wavelet of order 2 (Daub-2) and order 10 (Daub-10). There are three input vectors with 64 samples each, the first vector has a frequency of $3/8F_s$, the second has $3/16F_s$, and the third has $3/32F_s$, where F_s is the sampling frequency. This means that the first input vector resides within the first scale, the second vector resides within the second scale, and the third vector resides within the third scale. We conclude the following:

- The total energy of the input signals is distributed among the scales. The sum of the total energies over the scales is slightly less than the input signal total energy since we disregard contribution from the low pass section.
- The proper scale (where the signal resides) has the greatest share of the total energy. This share is greater (percentage wise) if a longer wavelet (e.g., Daub-10) is used than for a shorter wavelet (e.g., Daub-2).
- Energy per sample at the proper scale is larger if the signal resides at a higher scale. The gain factor in energy per sample (if the signal resides within scale 2 rather than scale 1) is approximately 1.41 and 1.64 for Daub-2 and Daub-10, respectively. We note that ideally, the gain factor in energy per sample should be 2 per scale index.

Table 1: Energy Distribution of Daub-2 and Daub-10 Wavelets

Measure	Wavelet	Scale	Signal with $f = (3/8)F_s$	Signal with $f = (3/16)F_s$	Signal with $f = (3/32)F_s$
Max Coefficient	Daub-2	1	1.3365	0.6574	0.4349
		2	0.5753	1.6998	1.0356
		3	0.3743	0.3594	1.8480
	Daub-10	1	1.2524	0.3818	0.3284
		2	0.3968	2.0331	0.5504
		3	0.1854	0.3859	2.8296
Total Energy	Daub-2	1	29.7687	7.2565	0.8486
		2	1.1313	23.3282	8.2775
		3	1.0495	0.9492	21.2601
	Daub-10	1	31.4508	1.6228	0.4040
		2	0.3980	29.9017	1.9671
		3	0.0875	0.3900	29.0447
Sample Energy (average per sample)	Daub-2	1	0.9201	0.2199	0.0257
		2	0.0628	1.2960	0.4599
		3	0.1049	0.0949	2.1260
	Daub-10	1	0.7671	0.0396	0.0099
		2	0.0133	0.9967	0.0656
		3	0.0036	0.0163	1.2102

2. Scale Identification in an Ideal Noise Environment

In this particular simulation, the correlation surface is approximated by sinusoidal signals embedded in ideal white Gaussian noise. The maximum coefficient, total energy, and energy per sample are tested. The signal-to-noise ratio is expressed as:

$$SNR = \frac{\text{input signal power}}{\text{input noise variance}}.$$

Three different input vectors at $3F_s/8$, $3F_s/16$, and $3F_s/32$, each with 2048 samples, are analyzed using Daub-2 and Daub-10 wavelets. SNR values are 10, 5, 2.5, 0, -2.5, -5, -10, and -15 dB. Each SNR level was used in 20 trials. Results are shown in Table 2 where the tabulated SNR is the smallest SNR at which each measure correctly designates the proper scale 100% of the time.

Table 2: Noisy Observation

Measure Wavelet Type	Greatest Coefficient	Total Energy	Sample Energy
	Smallest SNR [dB]		
Daub-2	2.5	0	-10
Daub-10	0	-2.5	-10

These results show that the energy per sample achieves the lowest SNR value compared to the other two measures. Consequently, this measure is considered the most reliable one for proper scale identification.

3. Hop-Scale Pattern

We recall that scale identification means assigning a scale index to each hop of the observed signal. The hop is assigned the scale whose energy per sample is the greatest among the values of the other scales; hence, it is called the proper scale. Therefore, a sequence of hops will have a sequence of proper scales, also called the hop-scale pattern.

Properly selecting a heterodyne and a sampling frequency will result in proper choice of the wavelet scales. The number of scales is defined by the number of octaves in the heterodyned signal. The designation of the scales (scale indices) is controlled by the selected sampling frequency, as each scale index is defined in terms of fractions of the sampling frequency as shown in Figure 15. As an example, assume we have an FH signal with hopping bandwidth of 30-90 MHz. If the signal is heterodyned to 10-70 MHz and sampled at 280 MHz, then the proper wavelet scales are S2, S3, and S4. If the FH signal is heterodyned to 2-62 MHz and sampled at 280 MHz, then the proper wavelet scales are S2, S3, S4, S5, and S6.

To distinguish the FH signal from other modulation types, the number of scales used must be at least two. The hop-scale pattern will then be comprised of two symbols (i.e., two scale numbers). For other modulations the hop-scale pattern will be comprised of one symbol (i.e., one scale number). For the MFSK scheme with a carrier frequency in the above mentioned band, the bandwidth of the modulated signal is typically 25 KHz (i.e., the channel separation for the wireless sets). Thus, the MFSK signal bandwidth can not span an octave except when we heterodyne to a very low frequency (i.e., less than 25 KHz). Hop-scale patterns are also useful for hop frequency extraction from wavelet surfaces, since they point to the proper scale where most of the signal energy is concentrated. Therefore, frequency extraction, if done on that wavelet surface, will provide correct values.

4. Success Rate

Performance of scale identification is evaluated as the success rate, P_{id}. We generate known hop-scale patterns and obtain the percentage of the correctly identified hop-scales. Therefore, P_{id} is defined as:

$$P_{id} = \frac{\text{number of correct hop-scales}}{\text{total number of hops}}. \tag{VI.9}$$

The probability of error, given by $P_e = 1 - P_{id}$, is the error in identifying the correct scale. The quality of scale identification depends on the height of the greatest energy

per sample relative to the other sample energies from other scales. Therefore, a suggested measure, d_h, of the quality of scale identification is defined as:

$$d_h = \frac{\max(\{A(j)\}) - \text{mean}(\{A(j)\})}{\sqrt{\text{var}(\{A(j)\})}}, \tag{VI.10}$$

where $\max(\cdot)$ is the maximum value, mean $(\cdot)$ is the mean value, and $\text{var}(\cdot)$ is the variance. The term d_h measures the distance between the height of the energy per sample at the proper scale to its average values over all scales, and is expressed in terms of the standard deviation of the energy per sample.

E. EQUALIZATION OF THE SPECTRAL SHAPE OF THE INSTANTANEOUS CORRELATION FUNCTION

Simulations show that the ICF of white noise (data set) has a triangular type spectrum in the direction of the time delay. Figure 20 shows theoretical and experimental frequency spectra taken in direction of the time delay (i.e., transforming the time delay to frequency). Thus, the energy per sample for all wavelet scales need to be compensated since the spectrum is colored.

Figure 20 shows that the slope of the ICF spectrum is 1, thus, its height, $q(j)$, at the middle of the j^{th} scale is:

$$q(j) = 1 + \frac{3(N-1)}{2^{j+1}},$$

where N is the number of ICF data points in the direction of the time delay. Note that the ICF of white noise is created by multiplying samples of the white noise in the time domain. Therefore, the resultant FT of the ICF is the convolution of two FT of the white noise, consequently, we obtain the triangular spectral (FT) shape. As a result, we will apply an equalizer, whose values are the reciprocal of $q(j)$, to compensate the magnitude distortion at all scales.

The performance of the scale identification is evaluated and a new success rate P_{id} is computed. Results are presented Chapter VII.

F. FREQUENCY ESTIMATION

In Chapter III, we related the WVD of the signal $x(t)$ to the wavelet transform of its ICF. The relation is stated in Equation III.33 and it is repeated here for convenience:

$$W_{xx}^{i}(t;s,\ell) = \sqrt{s}\int_{-\infty}^{\infty} G^{*}(sf)V_{x}(t,f)e^{j2\pi f\ell}dt,$$

where $W_{xx}^{i}(t;s,\ell)$ is the wavelet transform of the ICF of $x(t)$, $V_x(t,f)$ is the WVD of $x(t)$. In Chapter 2, we discussed the properties of WVD and concluded that the WVD provides the means to estimate the signal frequencies. The FT of the wavelet surface gives a bandpass filtered version of the WVD of the FH signal. Thus, the hop frequency can be extracted from a Fourier transform of the wavelet surface, in the delay direction, over the main diagonal of the proper diamond.

1. Frequency Resolution

The Fourier transform of the wavelet coefficients can be used for spectral estimation at any scale. Consequently, the frequency resolution will be dependent on the Fourier transformation. The frequency resolution (i.e., the minimum spacing between two resolved narrow band components) of the DFT is approximately equal to $\Delta f = F_s/N$. Thus, at any given scale k, the number of data points $N(k)$ will be related to the number of input data points N by:

$$N(k) = N\frac{1}{2^k}.$$

The sampling frequency at which the data points are taken is scale dependent, i.e., $F_s(k) = F_s/2^k$, where F_s is the input sampling frequency.

At the k^{th} scale, both the number of data points (wavelet coefficients) and the sampling frequency have been reduced by the same factor. Consequently, the FT of the $N(k)$ data points has a frequency resolution given by:

$$\Delta f(k) = \frac{F_s(k)}{N(k)} = \frac{F_s}{N} \equiv \Delta f\,. \tag{VI.11}$$

This means the frequency resolution of the Fourier transform is constant, independent of the wavelet scale.

2. Success Rate

Performance of the frequency estimation procedure is evaluated in terms of the success rate, P_f. The hop frequency is considered correctly estimated if the spectral peak is at the true spectral bin. P_f is defined as:

$$P_f = \frac{\text{number of correct hop frequencies}}{\text{total number of hops}}. \tag{VI.12}$$

The probability of error in estimating the correct hop frequency is denoted by P_e, where $P_e = 1 - P_f$. The hop frequency is estimated as the bin number corresponding to the peak of the FT over a specified region of the wavelet surface. Therefore, the quality of the frequency estimation depends on the spectral height of the peak relative to the average background. A measure of the quality of the frequency estimation is given by:

$$d_f = \frac{\max\left(|X(f)|\right) - \text{mean}\left(|X(f)|\right)}{\sqrt{\text{var}\left(|X(f)|\right)}}, \tag{VI.13}$$

where $X(f)$ is the FT over the wavelet surface, max $(\cdot)$ is the peak value, mean $(\cdot)$ is the mean, and var $(\cdot)$ is the variance. The variable d_f measures the distance between the peak value of $X(f)$ to the average background in units of the standard deviation of $X(f)$.

3. Alternatives for Frequency Estimation

Given the correct hop start/stop times, the hop frequency may also be estimated directly from the time signal or from the ICF surface. To extract the frequency from the original time signal we use the FFT over the hop length. Recall that the FFT is a matched filter for sinusoidal signals in white Gaussian noise. Thus, a better performance is expected in comparison to the nonlinear processing of the signal through the ICF computation and the wavelet transformation. The performance of frequency estimation from the signal or from its ICF is evaluated using the already defined measures P_f and d_f. We note that P_{fs} and P_{fc} denote the success rate using the original time signal or using the ICF surface, respectively. Also, d_{fs} and d_{fc} denote the measure of the frequency estimation quality at the original signal or at the

ICF surface, respectively. The performance of P_{fs} and P_{fc} are evaluated and results will be given in Chapter VII.

G. EXTRACTION OF HOP TIMES

Hop timing extraction is obtained by estimating the hop start and stop points. We recall that ICF surface and wavelet surfaces have both a cellular structure consisting of diamonds, where each diamond is associated with a specific hop. The diamond edges define the start/stop point of the hops. The diamond width corresponds to the hop interval T_h. The sides (edges) of the diamonds of hops are mutually parallel and spaced by the hop interval T_h. Therefore, we obtain the distance between two sequential intersections of the diamonds and the time axis, to determine the hop start (or stop) point. This tends to transform the transition point detection into an edge detection problem. There are many approaches to tackle the problem of hop timing extraction; in the following section we address one technique based on an edge detection operator.

Compass Operator

Edge detection is a fundamental problem in image analysis since edges help to identify objects. Edges are characterized by an abrupt change in gray level, therefore, edges can be detected using the derivative (gradient) operators which will be maximum in the direction of the edges. There are two types of edge operators, the gradient operators and the compass gradient operators (also called the compass operators) [Ref. 62]. The gradient operator measures the gradient of the two-dimensional image in two orthogonal directions. It is usually applied to detect edges with unknown directions. The compass operator measures the gradient of the two-dimensional image in a specific direction. It is used to detect edges with pre-determined directions. Since the wavelet surface has edges at angles of $\frac{\pi}{4}$ and $\frac{3\pi}{4}$ radians, a specific compass operator can be used to detect the edge in these directions. There is a variety of compass operators. They differ in form, depending on the direction of the edge

to be found. An example of the compass operator is the NE compass (NE stands for North-East). It has a 3×3 matrix NE $= [0, 1, 1; -1, 0, 1; -1, -1, 0]$. Another example is the NW compass (NW stands for North-West) with the 3×3 matrix NW $= [1, 1, 0; 1, 0, -1, 0, -1, -1]$. The compass operator is applied to the upper half of the wavelet surfaces to potentially detect the diamond edges. An array of the NE compass operator is shown in Figure 21. The compass array is used to scan the surface from left to right. All of the contributions are summed according to the weights of the 3×3 matrix. The maximum value is extracted to define the point where the compass array matches an edge. To make our data applicable to compass operations we need to take care of the negative portions of the surfaces, which is done by adding in a positive number equals in magnitude to the smallest (i.e., the most negative) surface value. Results are presented in Chapter VII.

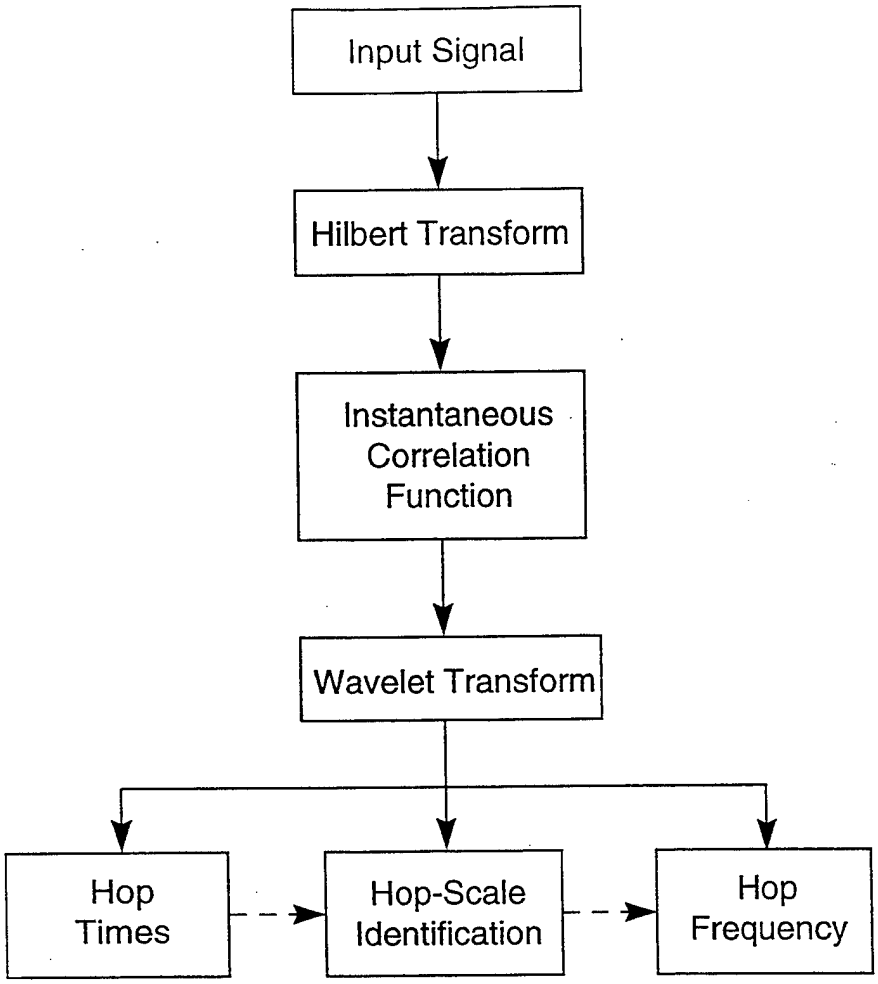

Figure 14. Functional description of the processing scheme.

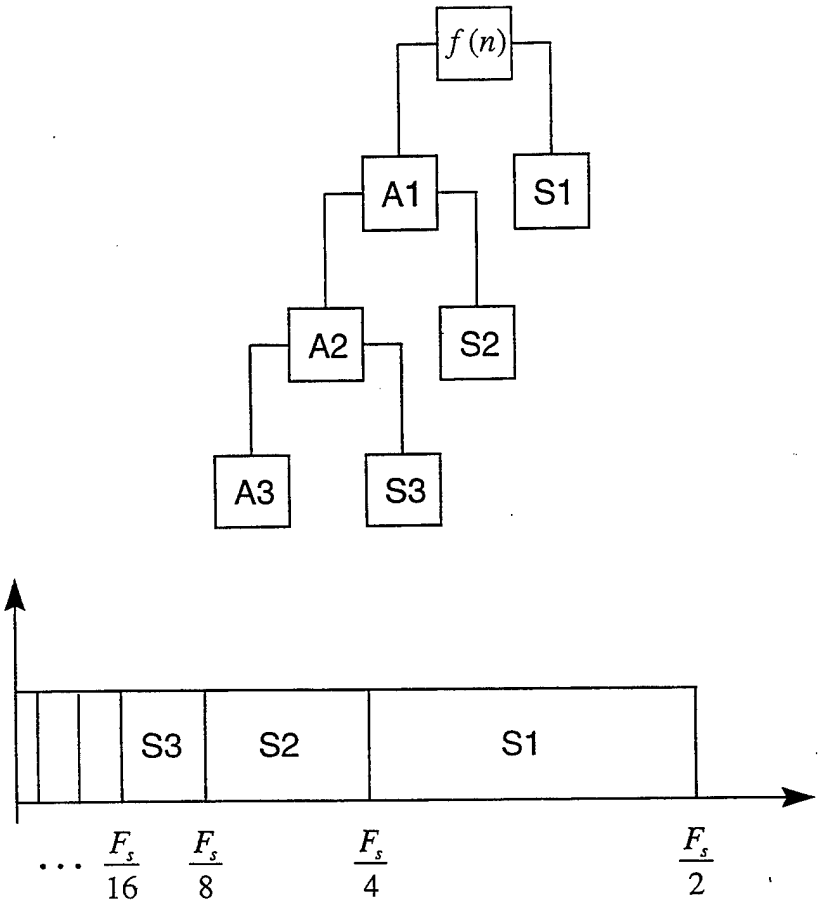

Figure 15. MATLAB wavelet scale designation and computation tree.

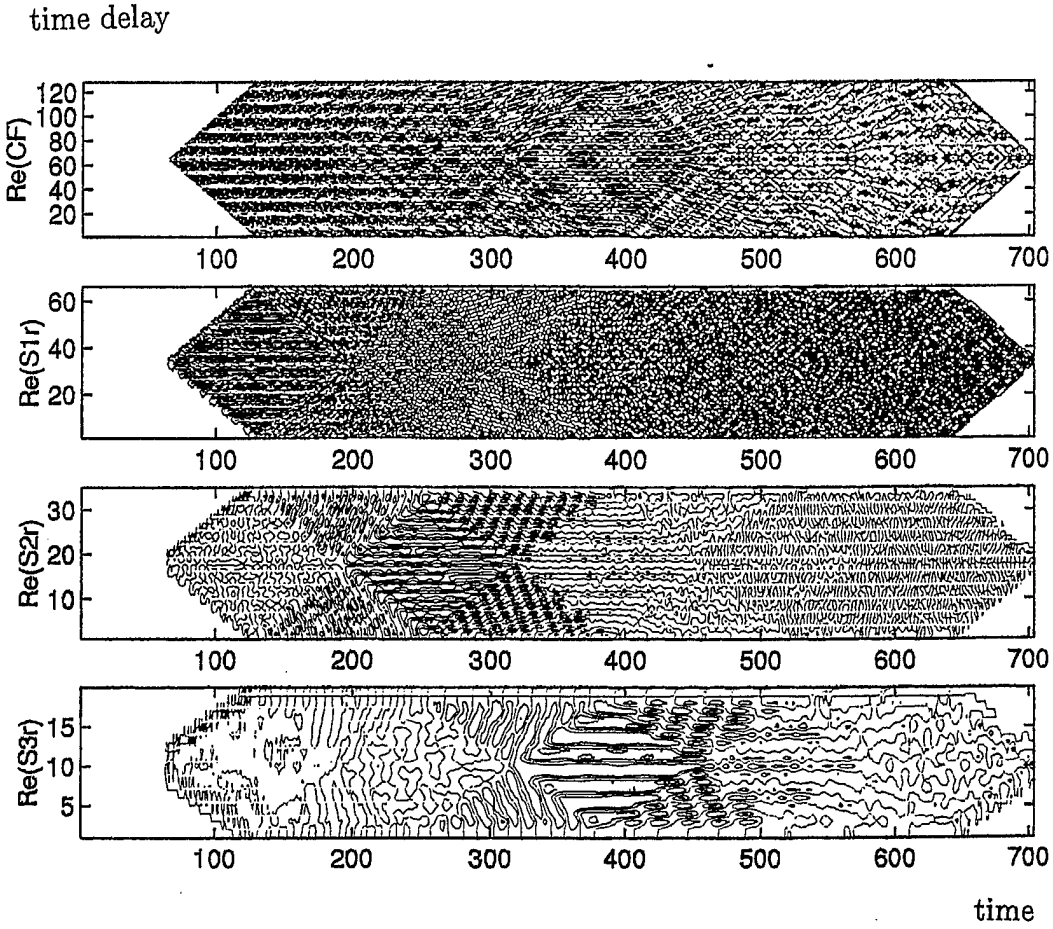

Figure 16. Wavelet surfaces of FH signals using Daub-3 at 10 dB (scale 1, 2, and 3).

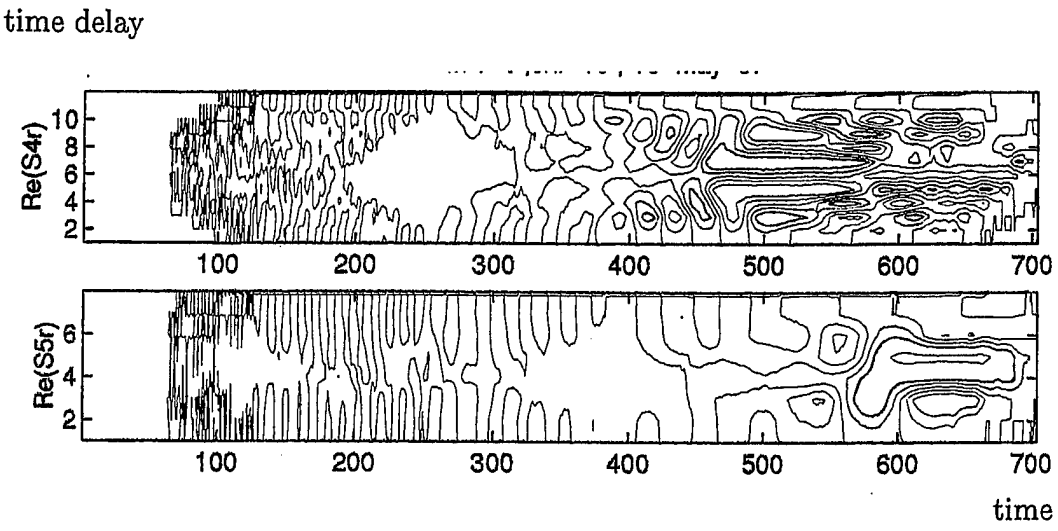

Figure 17. Wavelet surfaces of FH signals using Daub-3 at 10 dB (scale 4 and 5).

time delay

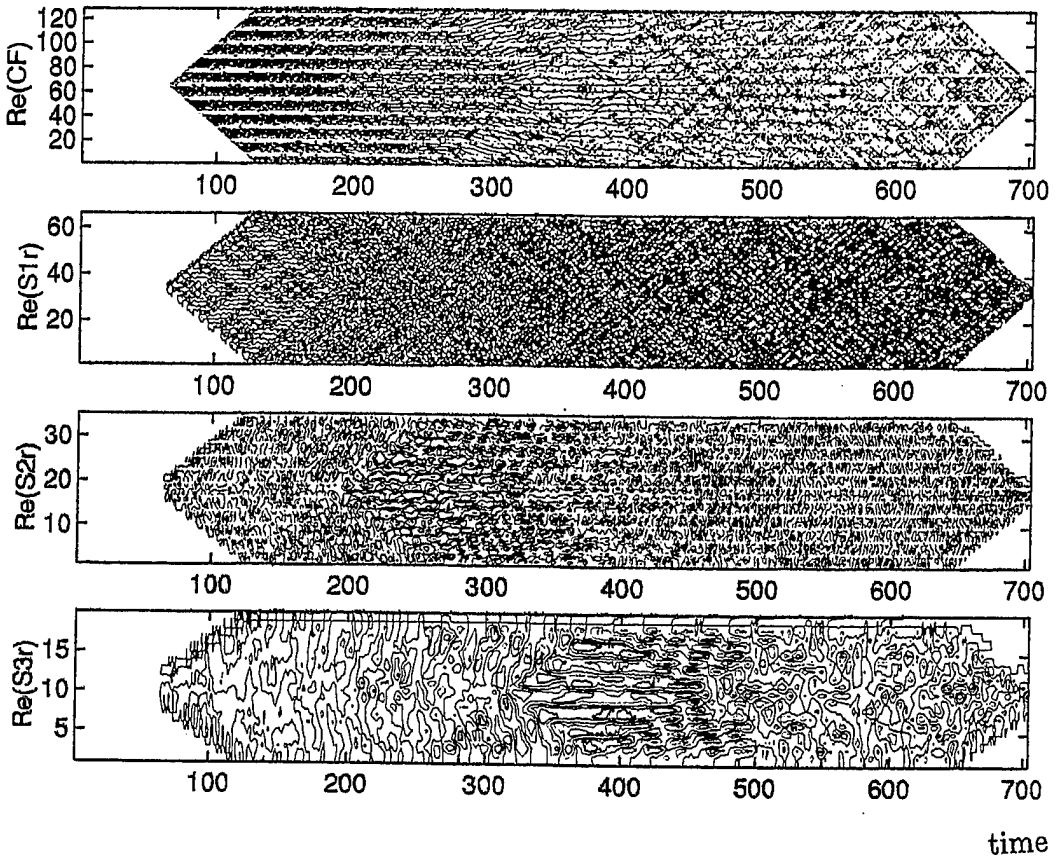

Figure 18. Wavelet surfaces of FH signals using Daub-3 at 3 dB (scale 1,2,and 3).

time delay

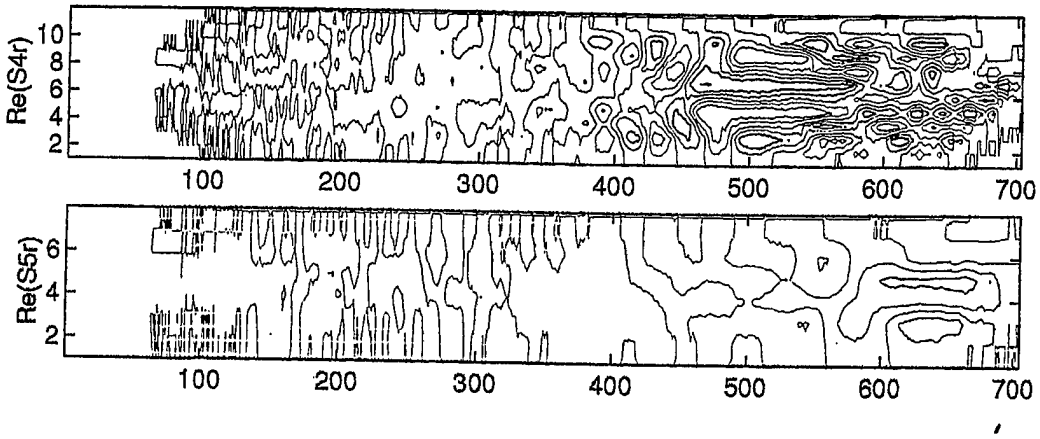

Figure 19. Wavelet surfaces of FH signals using Daub-3 at 3 dB (scale 4 and 5).

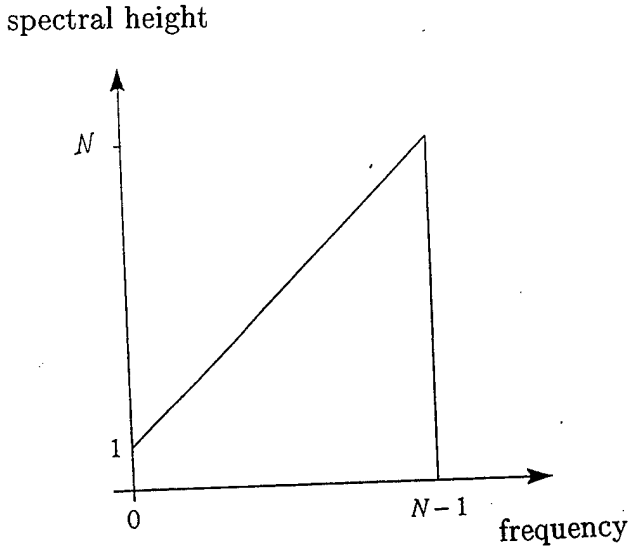

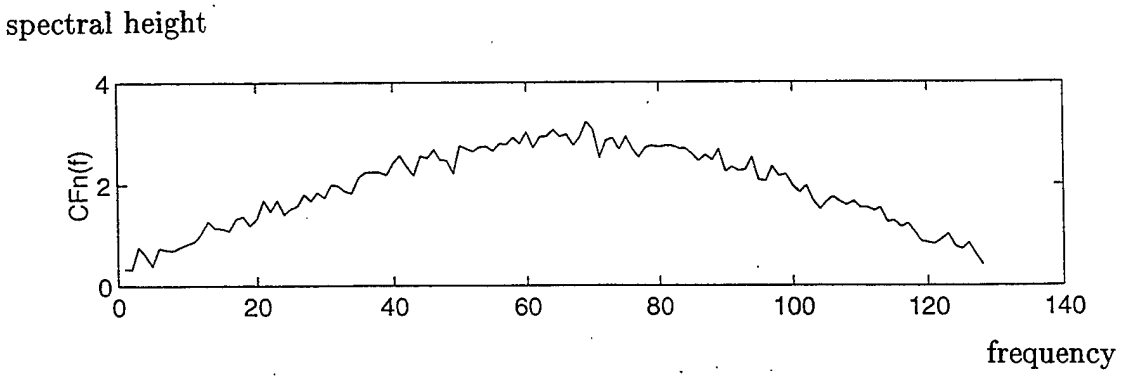

Figure 20. Theoretical and simulated spectrum of the ICF of white noise.

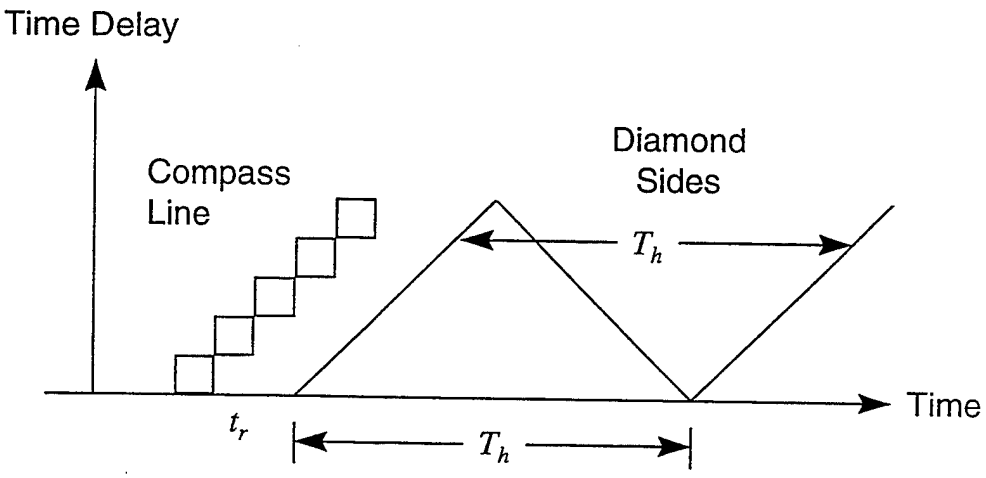

Figure 21. The compass line over the upper half of the wavelet surface.

VII. SIMULATIONS AND RESULTS

A. INTRODUCTION

In this chapter, we will provide experimental results of the processing scheme introduced in Chapter VI. Section VII.B shows the results obtained by visual inspection of wavelet surfaces as they pertain to the identification of FH signals. Wavelet surfaces from other digital modulation schemes are compared with those resulting from the FH signals. Section VII.C provides results of hop-scale identification. Section VII.D provides results of hop frequency extraction and compares results obtained using frequency estimation from wavelet surfaces and from the original time signal. Section VII.E provides the results of hop start/stop times estimation obtained by using the compass operator over the wavelet surface.

B. VISUAL INSPECTION

We carried out an opinion test to identify the FH scheme by examining the wavelet surfaces. Ten participants were involved, each one was asked to identify the diamond structure of the FH signal over the wavelet surfaces at all pertinent scales and for all hops. Two types of wavelet were used; the Morlet wavelet and the Daubechies wavelet of order 3. Both wavelets were used in their real and complex form. Four SNR values were used; 10, 6, 3 and 0 dB. Four different surface representations were used; the real part, imaginary part, magnitude, and phase. To avoid biasing and preconception all participants started to identify the surfaces resulting from the lowest SNR value and then the higher SNR values consequently. Detailed scoring tables and the scoring code are given in Appendix B. Only scoring tables belonging to 10 and 3 dB are given in this section because of their significance to the final conclusion of the opinion test. 10 dB is the highest tested SNR value while 3 dB is the minimum SNR which provided the minimum acceptable identification score of 2 (according to the scoring code). In Appendix B, each scoring table is dedicated

for a specific wavelet type at a specific SNR value and contains the scores given for different representations at different wavelet scales. "Real" stands for representing the wavelet surface by the contour plot of its real part, while "Imag." , "Abs." and "Angle" stand for representing the surface using the contour plots of imaginary part, magnitude and phase, respectively. The fractions in numbers listed in the tables came from averaging the ten scores given by the ten participants.

Table 3 shows the summary of scores obtained from different wavelet types at SNR values of 10 and 3 dB when representing the wavelet surfaces by their real part. Eventually, the real part and the imaginary part outperformed other representations. The ratings in Table 3 ranges from 0.2 to 1, where 1 represents perfect identification of the hop diamonds at their proper positions and 0.2 represents just distinction of the hop diamonds from the background noise. Test signals were designed to reside within the five wavelet scales given in the table. Comparing different scoring tables in Appendix B, it becomes apparent that the real part or imaginary part provided the best surface representation for the purpose of visual inspection. The magnitude or phase provided a very poor representation. We noted that real valued wavelets did a slightly better job than the complex valued wavelets (at least for the wavelet types used in the simulations).

Thus, this visual opinion test indicates that:

(1) The FH signal can be identified over the wavelet surfaces by its cellular structure which is dominant at the proper scale. That is, each scale will emphasize the hops which belong to the scale and attenuate other hops. The (diamond) cellular structure provides an estimate for the hop start/stop times.

(2) The FH signal can be well identified at 3 dB SNR and above.

(3) The real part or imaginary part provides the best surface representation for the purpose of visual inspection.

(4) The real form of the wavelet function provides better surface representation than the complex form for the wavelets used in simulations. However, other types of wavelets may perform differently.

(5) The Morlet wavelet has better performance than the Daubechies wavelet especially at higher scales. This is because our Morlet wavelet has a narrower bandwidth than that obtained with Daubechies wavelet, and the Daubechies wavelet results in a decimated transform which reduces the number of coefficients at higher scales.

(6) Other modulation schemes such as ASK, PSK, and MFSK will have wavelet surfaces residing only at one scale. Plots of these wavelet surfaces are given in Appendix C.

Table 3: Summary of identification scores for real part representation.

Wavelet Type	SNR [dB]	Scales				
		S1	S2	S3	S4	S5
Real Morlet	10	1.0	1.0	1.0	0.95	0.95
	3	1.0	1.0	1.0	0.95	0.9
Complex Morlet	10	1.0	1.0	1.0	0.9	0.75
	3	0.7	0.8	0.9	0.5	0.4
Real Daub-3	10	1.0	1.0	0.8	0.2	0.2
	3	0.8	0.7	0.5	0.2	0.2
Complex Daub-3	10	1.0	1.0	1.0	0.3	0.2
	3	0.6	0.5	0.7	0.4	0.2

- Scores vary between 0.2 and 1, where
- 1: perfect identification of hop diamonds.
- 0.2: just distinction of hops from background noise.

C. SCALE IDENTIFICATION

The proposed processing scheme is used to extract hop start/stop times, the hop-scale pattern, and the hop frequency. First, we investigate scale identification and hop frequency extraction assuming correct hop timing is available. Extraction of hop start/stop times will be considered later. For scale identification performance we carried out simulations using the following data:

(1) Signal pattern length: 5 hops.

(2) Wavelet scales: S1, S2, S3, and S4.

(3) Wavelet types: Daub-2, 4, and 8.

(4) SNR: from 10 to -10 dB.

(5) Number of experiments: 250 per wavelet per SNR value.

The hop frequencies of FH signals are selected to generate the hops according to a known scale pattern taking in consideration the doubling effect of frequencies by computing the ICF surface. The test pattern is selected of four scales; S1, S2, S3 and S4. The wavelet surfaces are generated from the ICF surfaces at those relevant scales. The total energy of each hop at each scales are computed and the energy per samples are obtained by dividing the total energy by the number of wavelet coefficients at each scale. Over each hop, the scale with the greatest energy per sample is estimated as the proper scale. The resultant estimated hop pattern is compared to the known hop pattern and the probability of correct identification is computed. We compute the energy contained in each hop over the diamond corresponding to that hop. We disregard energy contained outside the diamond since it is contributed by different hops. To avoid bias from the colored noise of the ICF surfaces an equalization must be performed to the resultant energy per samples at all pertinent scales before using them in deciding upon the proper hop scale. Although, the equalization process is based on the theoretical spectral shape given in Figure 20, the resultant equalized energy per samples, for ideal input white Gaussian noise, do not have the same value

at all scales. Table 4 presents averages and variances obtained for the equalized energy per samples for Daubechies of order 2, 4, and 8. We note that the average values for Daub-2 and Daub-8 are monotonically increasing with the scale index. For Daub-4 they are monotonically increasing for the scales S1,S2 S3 and S5 while they have a dip at scale S4. These different trends suggest that different wavelets respond differently to the theoretical equalization of the spectral shape of the ICF. Therefore the correction weights of the energy per sample depend on the wavelet used. In these simulations, results are given for the proper scale identification after equalization and correction.

Figures 22 to 24 show the success rate, P_{id} obtained for Daubechies wavelets of order 2, 4, and 8 at scales S1, S2, S3, and S4. For the performance of scale identification we consider the minimum SNR at which P_{id} is 1 as the figure of merit. Over all tested scales the success rate, P_{id} assumes the value of 1 at different minimum input SNR values. This is a function of the order of the wavelet and the scale. Figure 22 shows that the performance of P_{id} obtained from Daub-2 has achieved the value of 1 at SNR equals -1 dB at most of the scales, hence , -1 dB is considered the minimum SNR value for Daub-2. The minimum SNR value for Daub-4 and Daub-8 is -2 dB at most of the scales as shown in Figures 23 and 24. We note also that for Daub-8, P_{id} assumes the value of 0.9 for most of the scales at an SNR of -3 dB. Results show that:

(1) For long wavelets (Daub-8) the probability of correct scale identification is 1.0 at SNR equals to -2 dB, while it is 0.9 at SNR equals -3 dB.

(2) Longer wavelets perform better than shorter ones.

(3) The performance at higher scales is mostly better than the performance at lower scales in terms of minimum SNR at which P_{id} is 1. The exception of that case is the performance at the scale S1 which can be justified by the imperfect equalization of the ICF spectral shape.

Table 4: Mean and standard deviation of energy per sample.

Mean	S1	S2	S3	S4	S5
Daub-2	1.5688	1.7557	1.9479	2.3165	2.6086
Daub-4	1.6303	1.8432	2.0218	2.5585	2.1149
Daub-8	1.7173	1.9979	2.2725	2.4776	2.7525

Standard Deviation	S1	S2	S3	S4	S5
Daub-2	0.3419	0.3763	0.6503	0.9542	1.3176
Daub-4	0.3507	0.4103	0.6891	1.1328	1.2776
Daub-8	0.3665	0.4520	0.7874	1.1063	1.5845

Theoretically, wavelet surfaces at higher scales have higher SNR values than those at lower scales due to the higher processing gain at higher scales. Consequently, the decay in the P_{id} performance, at low input SNR, is slower at higher scales than the decay at lower scales. But, we noted that the decay in P_{id} is not consistent at different scales, especially at scale S1, which shows, mostly, the slowest decay compared to other scales. This anomaly may come from many interacting effects due to the imperfect equalization and the non-ideal wavelet filters at different scales.

D. FREQUENCY EXTRACTION

We carried out simulations to evaluate the performance of frequency estimation using the data from Section VII.C.

The hop frequencies are estimated by taking the FT of the vector of wavelet coefficients located at the center of the diamond in the direction of the time delay. The bin corresponding to the peak value represents the estimated hop frequency. The estimated hop frequency is then compared to the true hop frequency and the probability of correct frequency extraction (the success rate) is computed. The estimated frequency is considered correct if the estimation error is less, in percentage of the true frequency, than $\frac{1}{N}$, where N is the length of the vector of the wavelet coefficients.

Figures 25 to 27 plot the success rate P_f obtained for different wavelets at different scales. Figures 28 to 30 display the corresponding values of the distance d_f.

We consider the minimum SNR, at which P_f is 1, as the figure of merit for the performance of frequency extraction. Over all tested scales the success rate of frequency estimation, P_f, assumes the value of 1 at different minimum input SNR values.

Figure 25 shows that the P_f value for Daub-2 is 1 at SNR equals 0 dB at most of the scales, hence, 0 dB is considered the minimum SNR value for Daub-2. The minimum SNR value for Daub-4 and Daub-8 is also 0 dB at most of the scales, as shown in Figures 26 and 27.

For Daub-2, Daub-4 and Daub-8 the minimum input SNR is 0 dB at scales S1, S2, and S3. At a success rate P_f of 0.9, the minimum SNR equals -2 dB over most scales. The distance d_f is about 4 times the standard deviation of the wavelet surface data for all tested scales as shown in Figures 28 to 30. Values of the success rate P_f and the distance d_f shows that the hop frequency can be reliably extracted from the wavelet surfaces at an SNR equals 0 dB or better using only one FT at the center of the hop diamond area in the direction of the time delay.

Alternatives for frequency estimation

Hopping frequencies may also be estimated from the original signal or from the ICF. Figure 31 plots the performance P_{fs} and P_{fc} obtained from the time signal and from the ICF, respectively, at different SNR values, assuming exact estimates of hopping

start/stop times are available. Figure 32 plots the distance d_{fs} and d_{fc} obtained from the time signal and from the ICF, respectively, at different SNR values. The frequency estimation success rate from the time signal, P_{fs}, is 1 at SNR value of -5 dB. The frequency estimation success rate from the ICF, P_{fc}, is 1 at SNR value of 0 dB. The distances d_{fs} and d_{fc}, obtained from the original signal and from the ICF are 6 and 7, respectively. This shows that, assuming exact estimates of hopping start/stop times are available, hop frequencies may be estimated by processing the original signal at lower SNR values than can be achieved using the wavelet surfaces. The benefit obtained by analyzing the ICF surface by wavelet analysis is significant in case of unknown hop start/stop times. Also, less computations are needed, in case of estimating the frequency from wavelet surfaces, due to applying one FT per hop, using few coefficients.

E. EXTRACTION OF HOP TIMES

This section presents hopping time extraction results obtained using the compass operator discussed earlier in section VI.G. The wavelet surface is represented by its upper half plane resulting in a triangular shape instead of the familiar hop diamond shape. The line compass operator is used over the surface from left to right and the peak value of the resultant contribution is located over the time axis. The location of the peak value points to the estimated hop starting time. The difference between the true and the estimated starting time is considered the estimation error and is evaluated in terms of points over the time axis. Each SNR value is used in 20 trials. Figures 33-35 show the results of the estimation error (Er) at different SNR values for different Daubechies wavelet lengthes. The mean-square error (MSE) and standard deviation (SD) of the estimation error are also given. Results show that the hop start/stop times can be extracted within accuracy of ± 7 points (out of the 128-point hop interval) at SNR values of 6 dB or better.

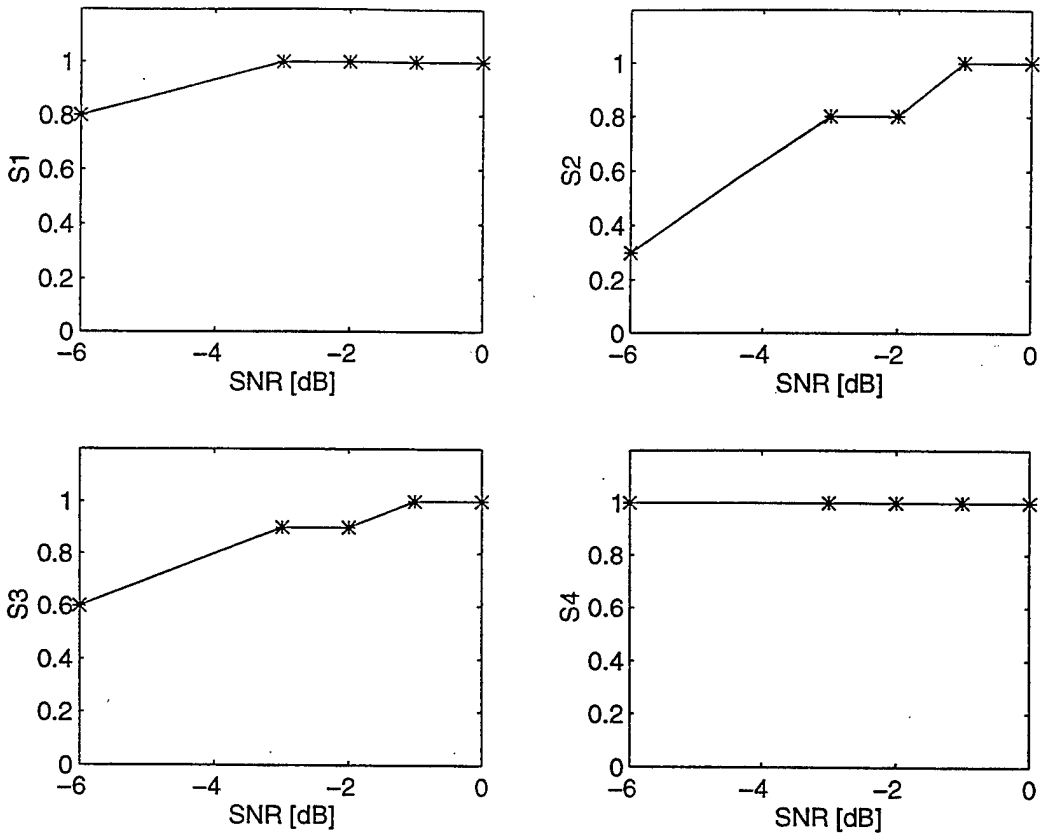

Figure 22. P_{id} for Daub-2.

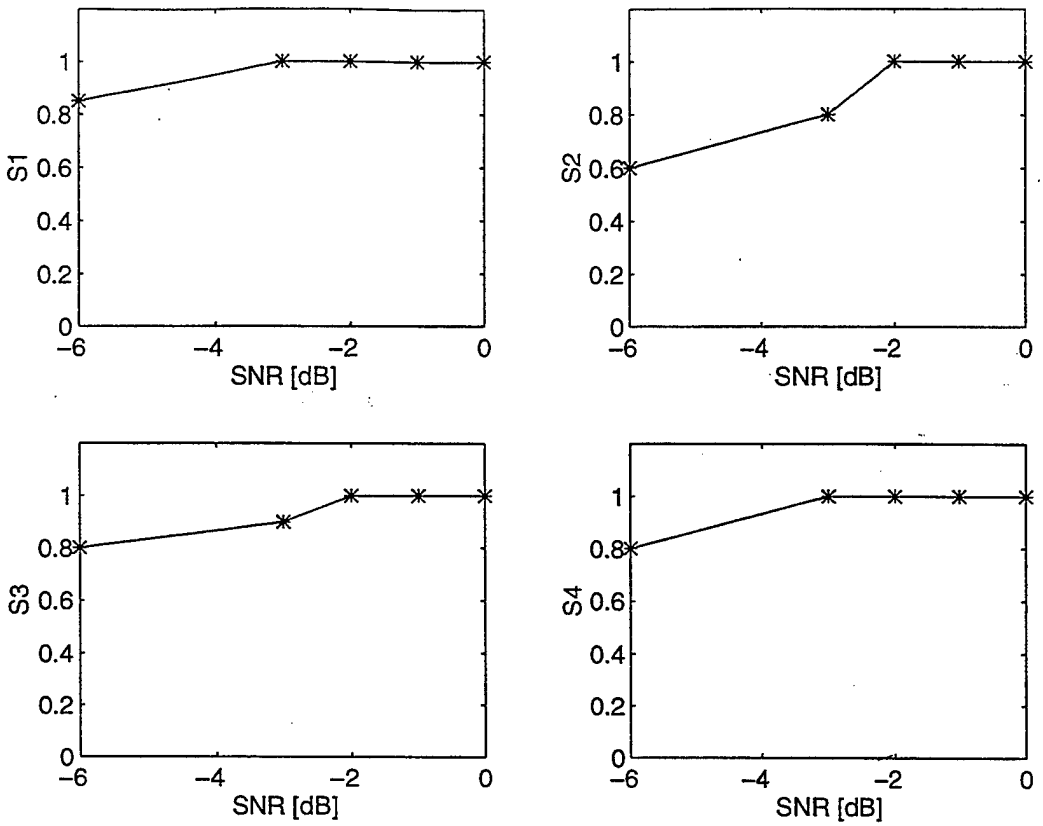

Figure 23. P_{id} for Daub-4.

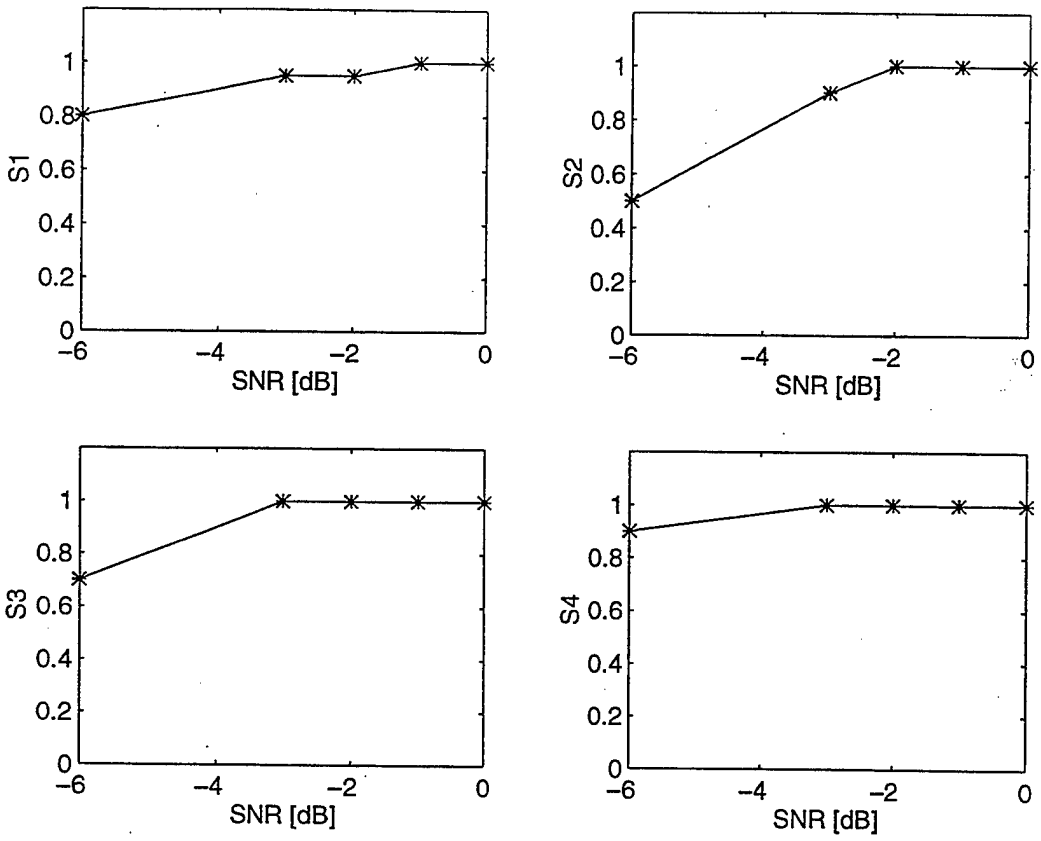

Figure 24. P_{id} for Daub-8.

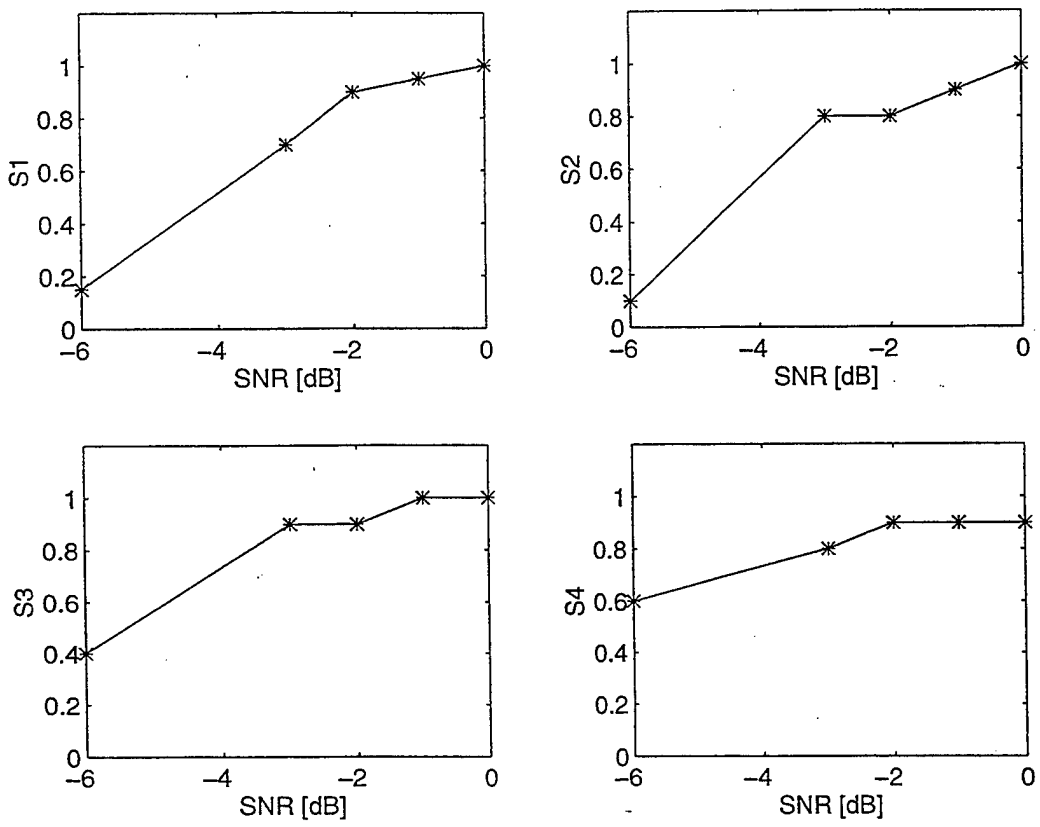

Figure 25. P_f for Daub-2.

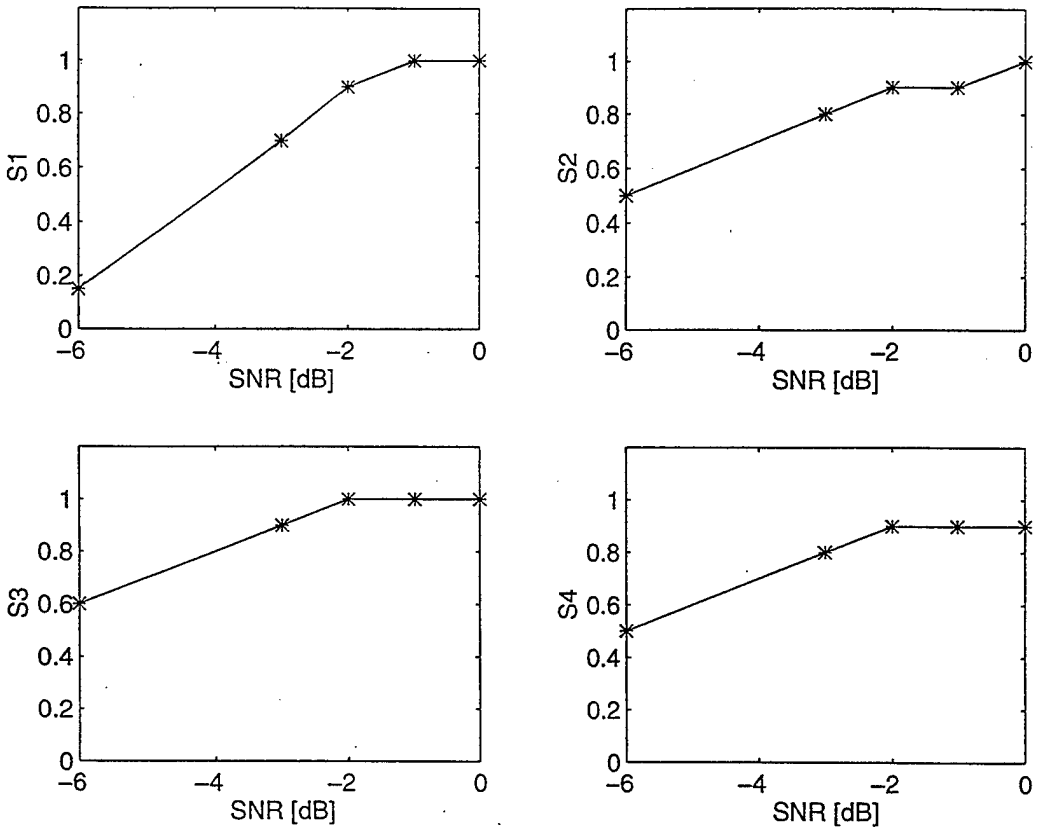

Figure 26. P_f for Daub-4.

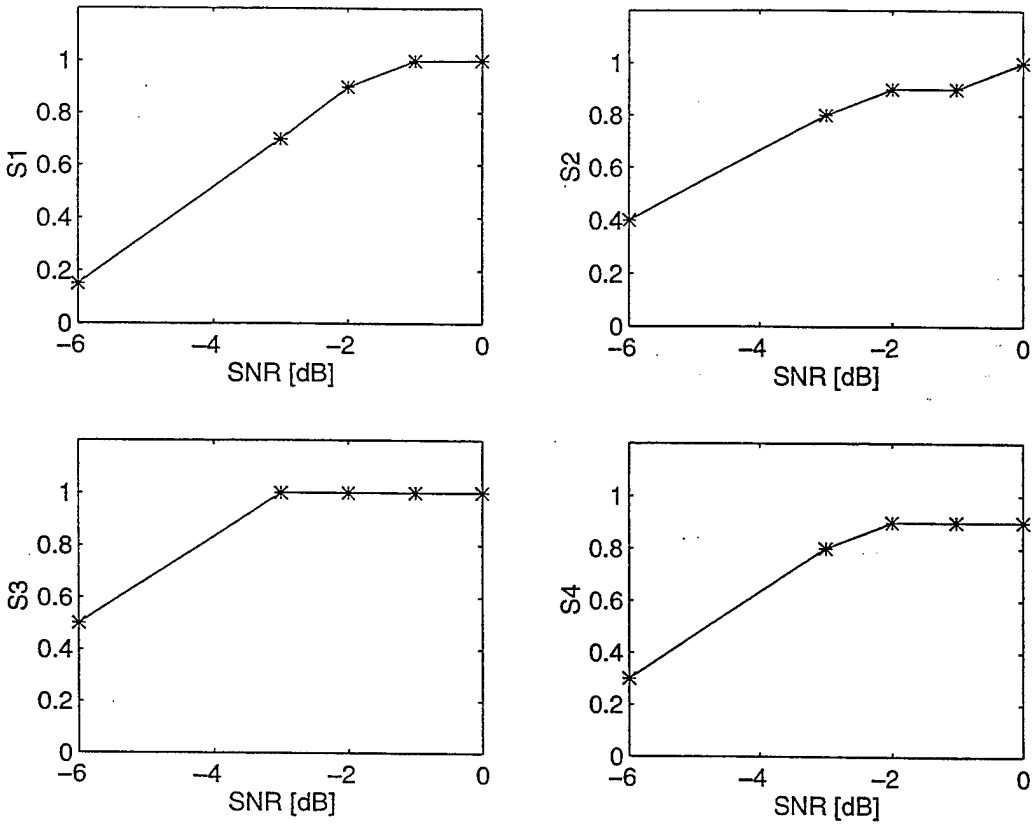

Figure 27. P_f for Daub-8.

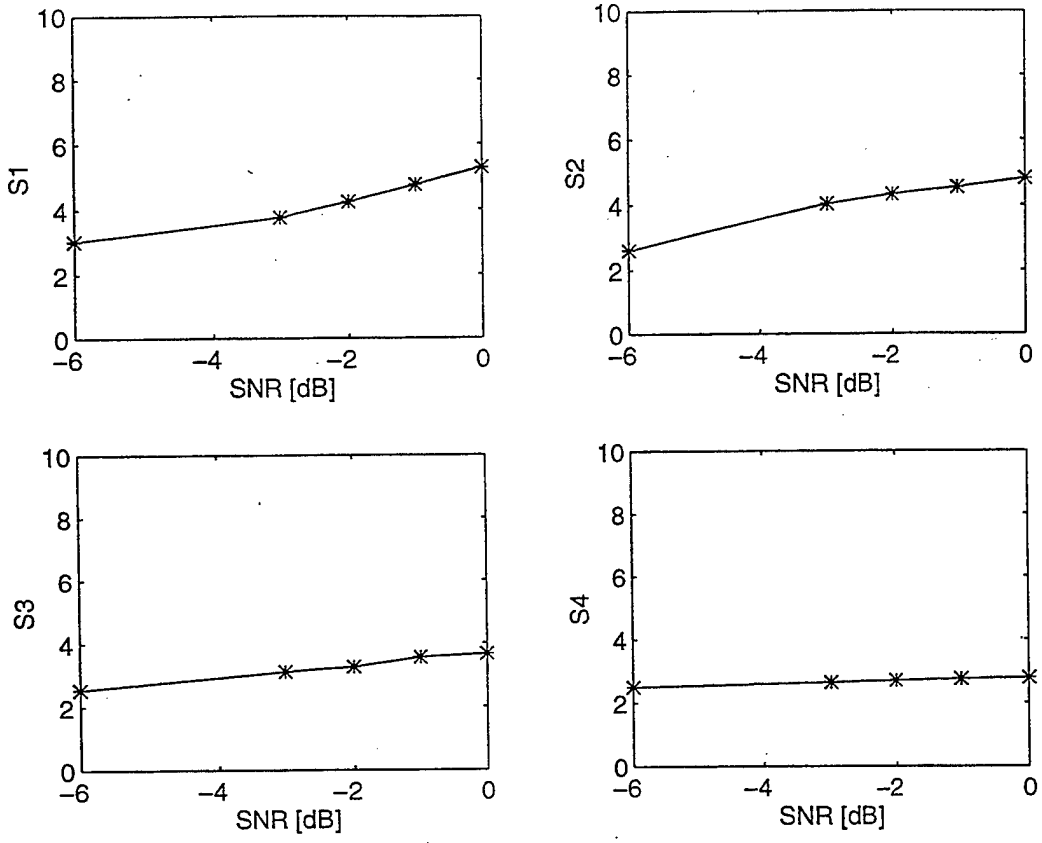

Figure 28. The spectral distance d_f for Daub-2.

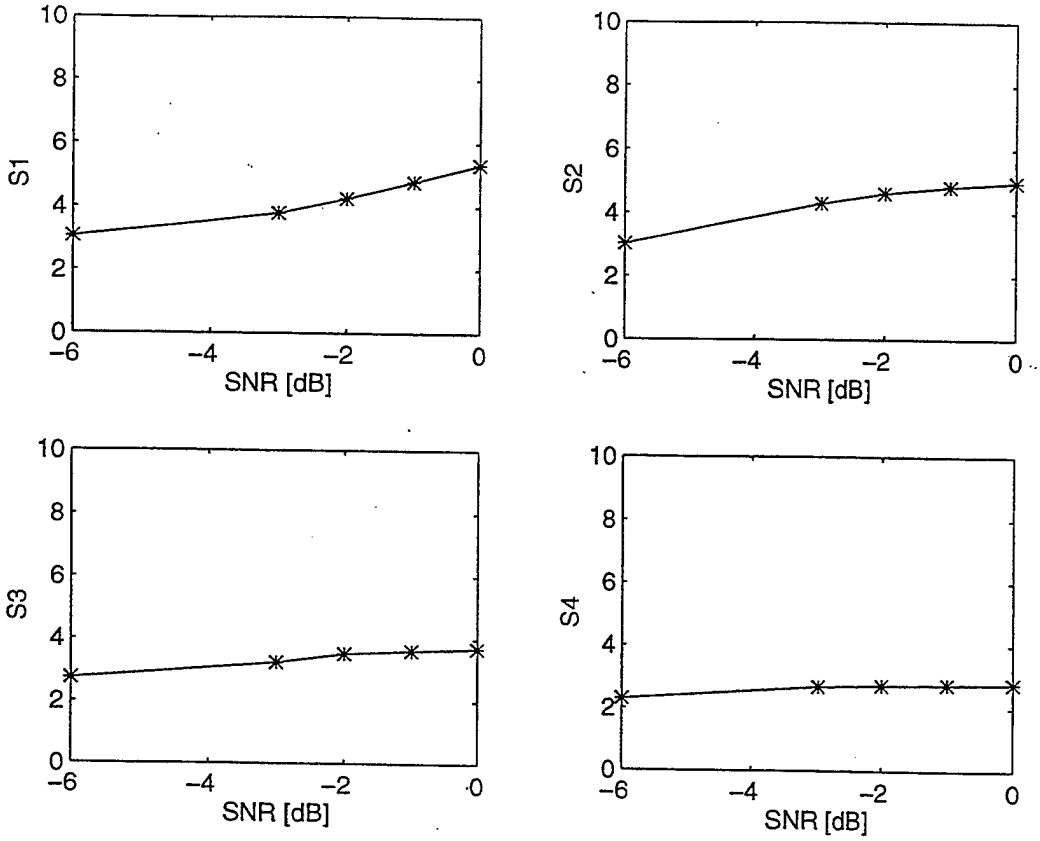

Figure 29. The spectral distance d_f for Daub-4.

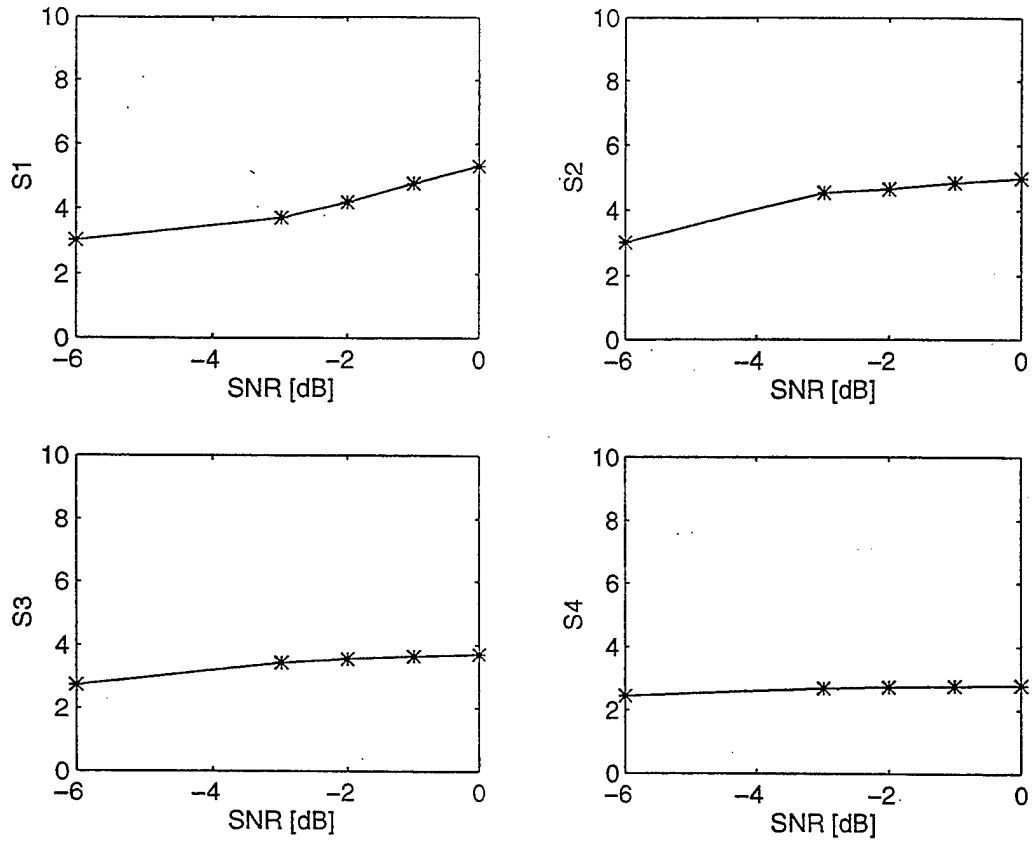

Figure 30. The spectral distance d_f for Daub-8.

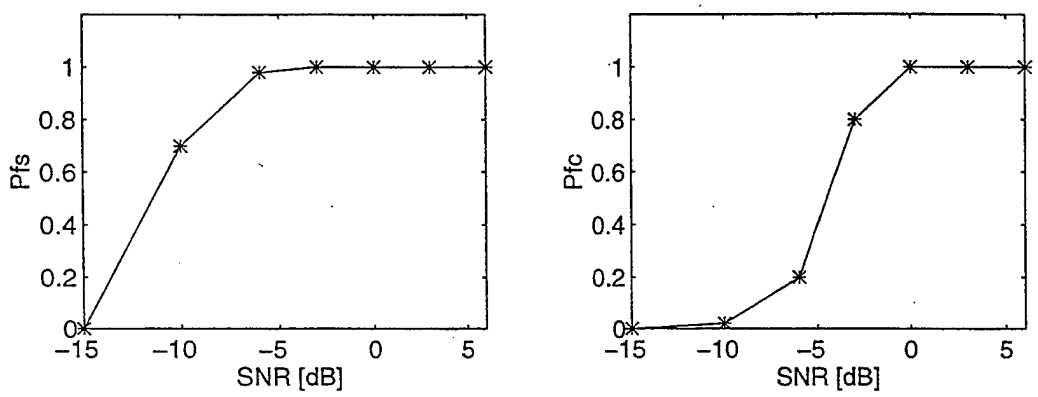

Figure 31. P_{fs} using the signal and P_{fc} using the ICF.

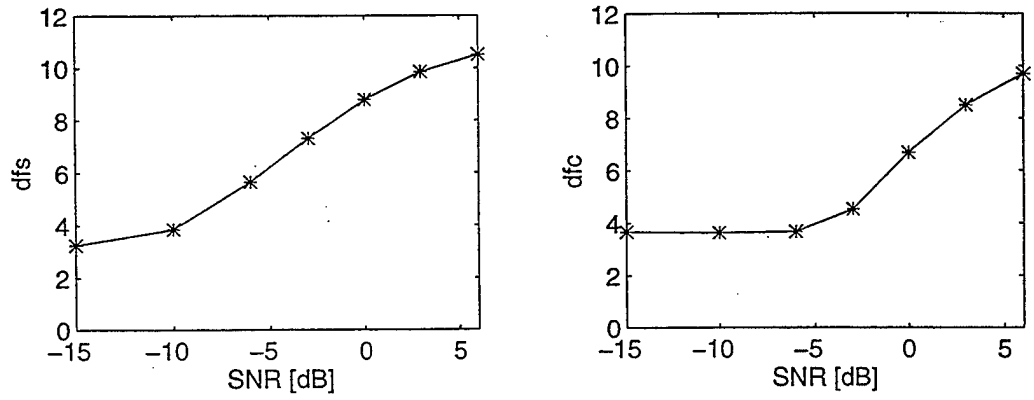

Figure 32. d_{fs} using the signal and d_{fc} using the ICF.

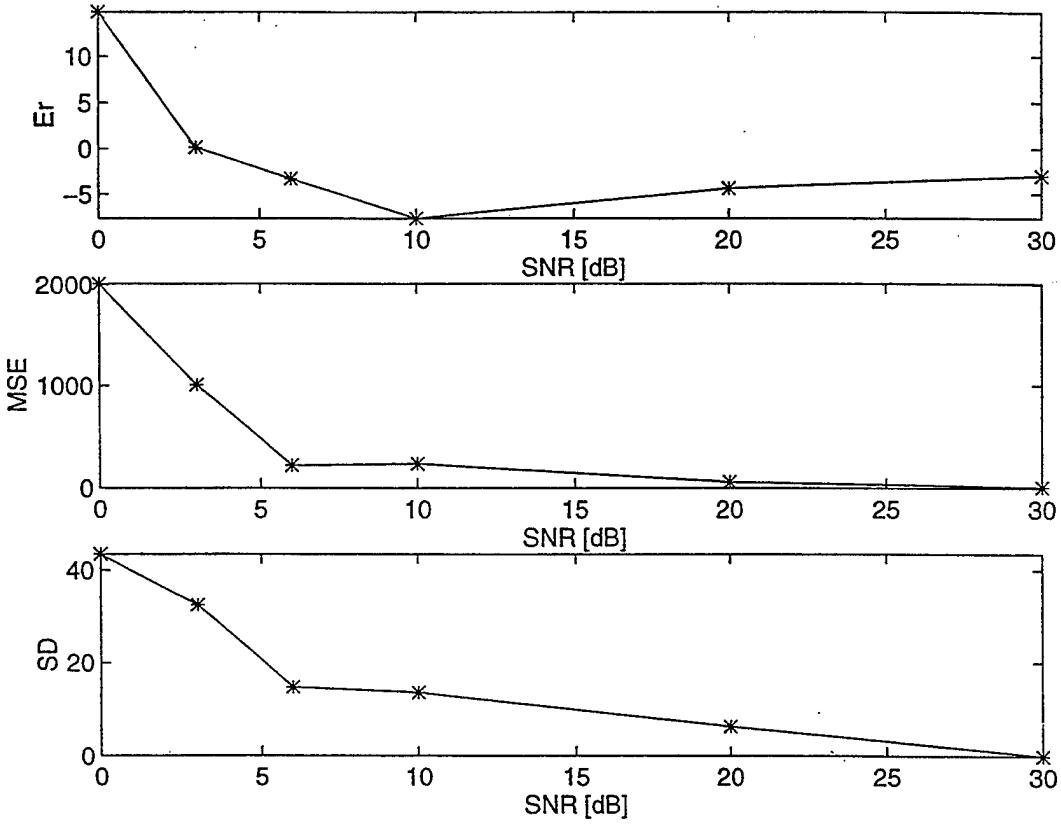

Figure 33. Hop timing estimation error for Daub-2.

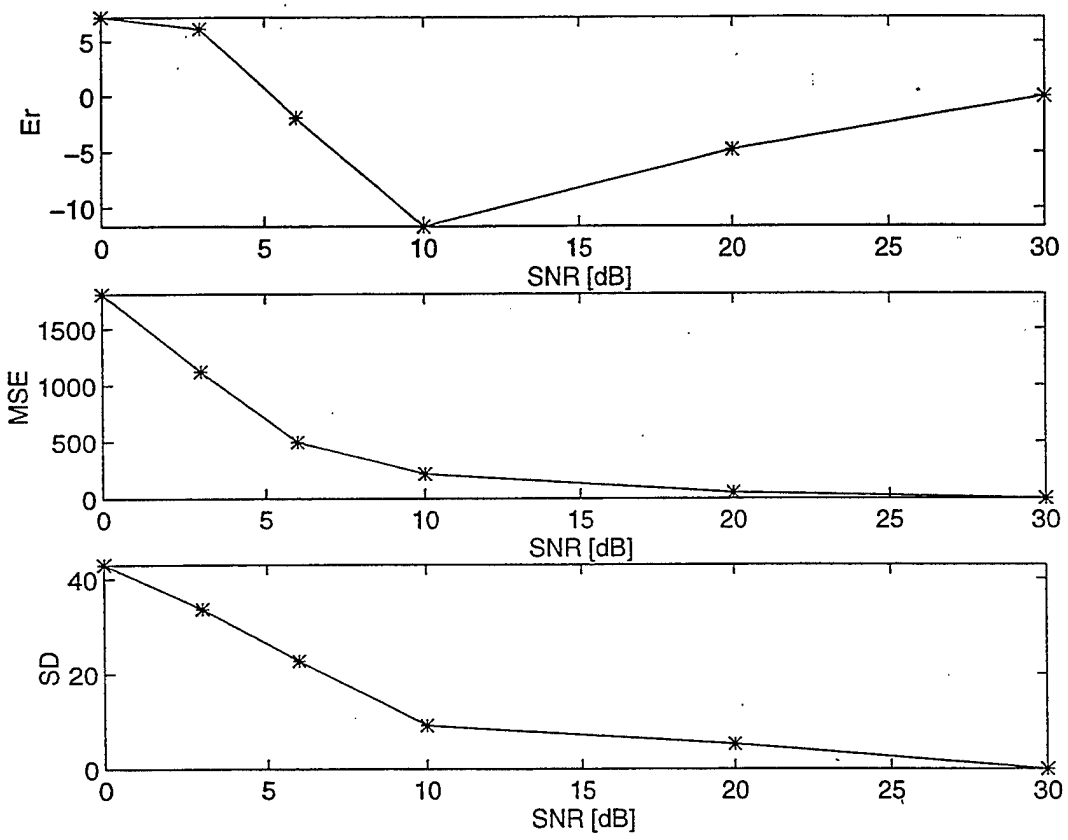

Figure 34. Hop timing estimation error for Daub-4.

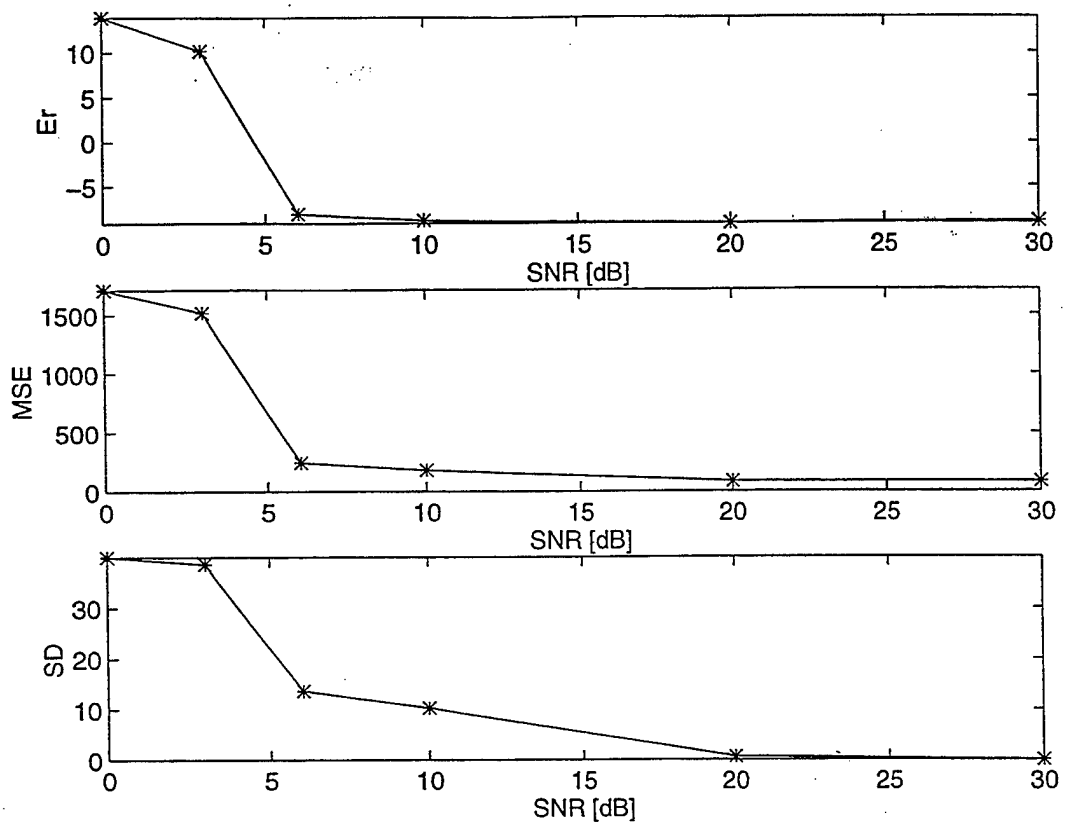

Figure 35. Hop timing estimation error for Daub-8.

VIII. CONCLUSIONS AND RECOMMENDATIONS FOR FUTURE WORK

A. CONCLUSIONS

Wavelet analysis of correlation functions is a new area which can be used to intercept communication signals embedded in noise. This work aimed at applying wavelet analysis to the instantaneous correlation function to identify frequency hopped signals.

The pure FH is the most popular scheme for frequency hopped signals. The instantaneous correlation function (ICF) of the complex-valued pure FH signal was shown to have a cellular (diamond) structure, where each hop contributes to one main diamond. Inside this diamond, the ICF has a single complex exponential component representing the hop frequency in the delay direction. We showed that the diamond intersections with the time axis are the hop start/stop times while the width of the diamond is the hop interval.

The wavelet transform of the ICF surface results into a number of surfaces each at a specific wavelet scale (called the wavelet surface). The wavelet surface at any scale emphasizes the hops which reside in it and attenuates other hops.

We addressed the interception problem using two possible approaches. In the first approach, we visually inspected the wavelet surfaces to identify and classify the structure of the FH signal and to obtain a rough estimate for the hop time interval. In the second approach, we applied the processing scheme which can also be used to automate the interception task. The proposed processing scheme estimates the hop start/stop times, the hop-scale pattern, and the hop frequency. The extraction of the hop start/stop times was addressed using an edge detection approach, by applying a compass operator, which is a well known technique in the image processing area. The hop-scale pattern is obtained by applying an energy analysis.

The frequency of each hop can be extracted from the wavelet surface at the

proper scale, or as an alternative, from the original time data using the time parameters.

Visual inspection of the wavelet surfaces showed that the FH signal can be identified from the wavelet surfaces for an input SNR of 3 dB and above. Other modulation schemes such as ASK, PSK, and MFSK will have significant wavelet surfaces at one scale only since their frequency bandwidth does not span more than one wavelet scale. Hop timing extraction showed that the hop start/stop times can be extracted within accuracy of $\pm 5\%$ for short wavelets (Daub-2) at SNR of 6 dB or better.

For the hop-scale identification, we adopted the energy per sample as a measure for the proper scale, assuming exact estimates of hop start/stop times are available. Results showed that the probability of correct scale identification is 1.0 at an input SNR of -2 dB for long wavelets (Daub-8), and it is 0.90 at an input SNR of -3 dB. The performance of longer wavelets is better than that of shorter ones since longer wavelets have better spectral energy concentration than shorter ones. For hop frequency extraction, the success rate of frequency estimation from the wavelet surfaces showed that the probability of correct frequency extraction is 1.0 at an input SNR of 0 dB and above.

Results showed that the minimum SNR required for automating the interception task is 6 dB. However, a better performance of frequency estimation is obtained at lower SNR value (-5 dB) by processing the original time signal, using the hop time information.

B. RECOMMENDATIONS FOR FUTURE WORK

For future extension of this work we recommend the following:

(1) Addressing the automatic recognition of the cellular structure of the FH signal over the wavelet surfaces. There are two topics in the image processing area which may be helpful in this task; the automatic recognition of regions of interest, and automatic target recognition [Ref. 63].

(2) Improving the performance of the hop-scale identification at lower SNR levels. In addition, it is suggested to readdress the equalization of the spectrum of the ICF surfaces.

(3) Investigating other wavelet types, and the use of other definitions for the instantaneous correlation function.

(4) Combining information from different wavelet surfaces to improve parameter estimation.

LIST OF REFERENCES

[1] Gardner, W. A., "Signal Interception: A Unifying Theoretical Framework for Feature Detection," *IEEE Trans. on Communication*, Vol. 36, No. 8, pp. 897-906, Aug. 1988.

[2] Gardner, W. A., "Spectral Correlation of Modulated Signals: Part II- Digital Modulation," *IEEE Trans. on Communications*, Vol. Com-35, No. 6, June 1987.

[3] Reichert, J., "Automatic Classification of Communication Signals Using Higher Order Statistics," *ICASSP-92.*, Vol. 5, pp. 221-224, San Francisco, Mar. 1992.

[4] Goh, T. T., Liu, J., and Soong, B. H., "Deterministic Signal Detection:A Hybrid Approach," *Communication on the Move, Singapore, ICCS/ISITA* , Vol. 1, pp. 385-389, 1992.

[5] Hippenstiel, R. D., and Fargues, M. P., "Feature Extraction from Digital Communication Signals Using Wavelet Transform," Naval Postgraduate School Technical Report No. NPS-EC-95-001, Feb. 1995.

[6] Wei, W., and Mendel, J. M., "A New Maximum Likelihood Method for Modulation Classification," *Asilomar-95, IEEE Conf. on Signals, Systems and Computers*, Vol. 2, pp. 1132-1136, 1995.

[7] Fonollosa, J. R., and Nikias, C. L., "Analysis of QAM Signals Using Higher-Order Spectra Based Time-Frequency Distributions," *IEEE Signal Processing Workshop on High-Order Statistics*, pp. 225-229, South Lake Tahoe, CA, 1993.

[8] Vergara, L., Borrallo, J. M., Garcia, J. P., and Mezcua, B. R., "A General Approach to the Automatic Classification of Radio Communication Signals," *Signal Processing*, Vol. 22, pp. 239-250, 1991.

[9] Lin, Y., and Jay Kuo, C-C., "Sequential Modulation Classification of Dependent Samples," *ICASSP-96* , Vol. 5, pp. 2690-2693, Atlanta, 1996.

[10] Kim, K., and Polydoros, A., "Digital Modulation Classification: The BPSK versus QPSK case," *MILCOM 88*, pp. 431-436, 1988.

[11] Gardener, W., "The Role of Spectral Correlation in Design and Performance Analysis of Synchronizers," *IEEE Trans. on Communications*, Vol. Com-35, No. 11, Nov. 1987.

[12] Wickert, M. A., and Turcotte, R. L., "Rate-Line Detection Using Higher-Order Spectra," *MILCOM'92, Communication-Fusing Command, Control, and Intelligence*, Vol. 3, pp. 1221-1225, 1992.

[13] Chuan, Y., and Jay Kuo, C., "Modulation Classification Using Wavelet Transform," *Proc. of SPIE, Wavelet Application in Signal and Image Processing II*, Vol. 2303, pp. 260-271, 1994.

[14] Marinovich, N., Nelson, D., Cohen, L., and Umesh, S., "Classification of digital modulation types," *IEEE SPIE*, Vol. 2563, pp. 126-143, 1996.

[15] Roessgen, M., and Boashash, B., "Time-Frequency Peak Filtering Applied to FSK Signals," *Proc. of IEEE-SP International Symp. on Time-Frequency and Time-Scale Analysis*, Philadelphia, Oct. 1994.

[16] Garcia, F. M., and Lourtie, I. M., "A Wavelet Transform Frequency Classifier For Stochastic Transient Signals," *IEEE ICASSP-96*, Vol. 6, pp. 3057-3060, 1996.

[17] Hippenstiel, R., and Fargues, M., "Feature Extraction from Digital Communication Signals Using Wavelet Transform," *Asilomar-95, IEEE Conf. on Signals, Systems and Computers*, Vol. 1, pp. 285-289, 1995.

[18] Reappaport, S. S., and Grieco, D. M., "Spread Spectrum Signal Acquisition: Methods and Technology," *IEEE Communication Magazine*, Vol. 22, No. 6, June 1984.

[19] Simon, M., Omura, J., Scholtz, R, and Levitt, B, *Spread Spectrum Communication Systems*, Computer Science Press, Vol. III, Ch. 4, 1985.

[20] Krasner, N., "Optimal Detection of Digitally Modulated Signals," *IEEE Trans. on Communications*, Vol. Com-30, No. 5, May 1982.

[21] Polydoros, A., and Weber, C.L., "Detection Performance Consideration for Direct-Sequence and Time-Hopping LPI Waveform," *IEEE J. on Selected Areas of Communications*, SAC-3, pp. 727-744, Sep. 1985.

[22] Beaulieu, N., Hopkins, W., and McLane, P., "Interception of Frequency-Hopped Spread Spectrum Signals," *IEEE J. on Selected Areas of Communications*, SAC-8, pp. 853-870, June 1990.

[23] Chung, C. D., "Generalized Likelihood-Ratio Detection of Multiple-Hop Frequency-Hoping Signals," *IEE Proc. Communications*, Vol. 141, Iss: 2, pp. 70-78, Apr. 1994.

[24] Dillard, R. A., and Dillard, G. M., "Likelihood-Ratio Detection of Frequency-Hopped Signals," *IEEE Trans. on Aerospace and Electronic Systems*, Vol. 32. pp. 543-553, Apr. 1996.

[25] Nemisick, L. W., and Geraniotis, E., "Adaptive Multichannel Detection of Frequency-Hopping Signals," *IEEE Trans. on Communications*, Vol. 40, No. 9, Sep. 1992.

[26] Nemisick, L. W., and Geraniotis, E., "Detection of Frequency Hopping Signals via Adaptive Multichannel Radiometry," *IEEE MILCOM-92, Communication, Fusing Command, Control and Intelligence*, Vol.3, pp. 1215-1220, 1992.

[27] Chung, C. D., and Polydoros, A., "Detection and Hop-Rate Estimation of Random FH Signals via Autocorrelation Technique," *IEEE MILCOM-91, Communication in a Changing World*, Vol. I, pp. 345-49, Nov. 1991.

[28] Aydin, L., and Polydoros, A., "Hop-Timing Estimation for FH Signals Using a Coarsely Channelized Receiver," *IEEE Trans. on Communications*, Vol. 44, pp. 516-5226, April 1996.

[29] Mauck, K. D., and Betz, J. W., "Quadratic Extraction of Feature from Direct Sequence Signals," Mitre Technical Report, Bedford, MA, 1991.

[30] Kuehls, J. F., and Geraniotis, E., "Presence Detection Of Binary-Phase-Shift-Keyed and Direct-Sequence Spread Spectrum Signals Using a Prefilter-Delay-and-Multiply Device," *IEEE J. on Selected Areas in Communication*, Vol. 8. No. 5. June 1990.

[31] Mammone, R. J., Rothaker, R. J., Podilchuk, C. I., Davidvici, S., and Schilling, D. L.,"Estimation of Carrier Frequency, Modulation Type and Bit Rate of an Unknown Modulated Signal," *IEEE International Conf. on Communications 87*, Vol.2, pp. 1006-1012, Seattle, WA, June 7-10, 1987.

[32] Ho, K. C., Prokopiw, W., and Chan, Y. T.,"Modulation Identification by the Wavelet Transform ," *MILCOM-95*, Vol. 2, No. 2/3/4, pp. 886-890, Nov. 1995.

[33] Chung, C. D., and Polydoros, A., "Parameter Estimation of Random FH Signals Using Autocorrelation Techniques," *IEEE Trans. on Communications*, Vol. 43, No.2/3/4, pp. 1097-1106, Feb./Mar./Apr. 1995.

[34] Kimble, K. R., and Tibbals, T. F., "Spectral Analysis Techniques Using Wavelets as an Alternative to Fourier Analysis For Transient Dynamic Data," Arnold Engineering Development Center Final Technical Report, AEDC-TR-94-17, Jan. 1995.

[35] Cochran, D., "Application of Wavelet Transform Techniques to Spread Spectrum Demodulation and Jamming," Air Force Office of Scientific Research Final Technical Report, TRC DC-9302, Feb. 1993.

[36] Proakis, J. D., and Manolakis, D. G., *Digital Signal Processing, Principles, Algorithms, and Applications*, Prentice Hall, Inc., Englewood Cliffs, NJ, 1996.

[37] Akansu, A. N., and Haddad, R. A., "Multiresolution Signal Decomposition," *Academic Press Inc.*, 1992.

[38] Cohen, L., *Time-Frequency Analysis*, Prentice-Hall Inc., Inglewood Cliffs, NJ, 1995.

[39] Classen, T., and Mecklenbrauker, W., "The Wigner Distribution: A Tool for Time-Frequency Signal Analysis, Part I: Continuous-Time Signal," *Philips J. of Research*, Vol. 35, pp. 271–250, 1980.

[40] Classen, T., and Mecklenbrauker, W., "The Wigner Distribution: A Tool for Time-Frequency Signal Analysis, Part II: Discrete-Time Signal," *Philips Journal of Research*, Vol. 35, pp. 276–300, 1980.

[41] Hill, R. O., *Elementary Linear Algebra with Applications*, Harrcourt Brace Jovanovich Press, 1991.

[42] Daubechies, I., *Ten Lectures on Wavelet*, SIAM, 1992.

[43] Kaiser, G., *A Friendly Guide to Wavelets*, Birkhauser, 1995.

[44] Rioul, O. L., and Vetterli, M., " Wavelets and Signal Processing," *IEEE Signal Processing Magazine*, Oct. 1991.

[45] Vetterli, M., and Herley, C., "Wavelet and Filter Banks: Theory and Design", *IEEE Trans. on Signal Processing*, Vol. 40, No. 9, Sep. 1992.

[46] Strang, G. and Nguyen, T., *Wavelet and Filter Banks*, Wellesly-Cambridge Press, 1996.

[47] Burrus, C. S., Gopinath, R. A., and Guo, H., *Introduction to Wavelets and Wavelet Transforms*, Prentice-Hall, Englewood Cliffs, NJ, 1998.

[48] Drumheller," Theory and Application of the Wavelet Analysis to Signal Processing," Naval Research Laboratory Technical Report, No.9316, July 1991.

[49] Friedlander, B., and Marple, L., Jr., "High Performance Spectral Analysis Techniques for Non-Stationary Signals," Signal Processing Technology Ltd. Technical Report, June 1995.

[50] Peterson, R., Ziemer, R., and Borth, D., *Introduction to Spread Spectrum Communications*, Prentice-Hall, Inc., Englewood Cliffs, NJ, 1995.

[51] Couch, L. W., *Digital and Analog Communication Systems*, Macmillan Publishing Company, 1990.

[52] Papoulis, A., *Probability, Random Variables and Stochastic Processes*, 3rd ed., McGraw-Hill, Inc., New York, 1991.

[53] Whalen, A. D., *Detection of Signals in Noise*, Academic Press Inc., 1970.

[54] Abramowitz, M, and Stegun, I. A., *Handbook of Mathematical Functions*, Dover Publications, Inc., 1970.

[55] Gradshteyn, I.S., and Ryzhik, I.M., *Table of Integrals, Series, and Products*, 5th ed., Academic Press Inc., 1994.

[56] Gautschi, W., "Efficient Computation of the Complex Error Function," *SIAM J. Number Anal.*, Vol. 7, No. 1, Mar. 1970.

[57] Helstrom, C. W., *Probability and Stochastic Processes for Engineers*, Macmillan, New York, 1991.

[58] Spiegel, M. R., *Mathematical Handbook of Formulas and Tables*, 32nd ed., McGraw-Hill, Inc., 1994.

[59] Misiti, M., Misiti, Y., Oppenheim, G., and Poggi, J., *Wavelet Toolbox User's Guide*, The Mathworks Inc., 1996.

[60] Lina, J., and Mayrand, M., " Complex Daubechies Wavelets", *UdeM-Physnum-ANS-15*, Dec. 1993.

[61] Kay, S. M., *Modern Spectral Estimation Theory and Application*, Prentice-Hall, Englewood Cliffs, NJ, 1988.

[62] Jain, A. K., *Fundamentals of Digital Image Processing* , Prentice-Hall, Inc. Englewood Cliffs, NJ, 1990.

[63] Marchette D., Solka, j., Guidry, and Green, J. "Advanced Distributed Region of Interest Tool", *Advanced Computaion Technology Group, Space Systems Applications Branch. Dahlgren Division of Naval Surface Warfare Center,* 1997.

APPENDIX A. THE INSTANTANEOUS CORRELATION FUNCTION (ANALYTIC APPROACH)

Let the complex FH signal be defined as:

$$s(t) = \exp\left(j \sum_{n=1}^{N} (\omega_n t + \theta_n)\Big|_{t\in\{n\}} \right), \tag{A.1}$$

where ω_n is the hopping frequency (in radians) and θ_n is the carrier phase chip of the n^{th} hop. N is the total number of observed hops. The shorthand notation $t \in \{n\}$ stands for the condition:

$$t_0 + (n-1)T_h \le t \le t_0 + nT_h\,, \tag{A.2}$$

i.e., it confines the value of the time t corresponding to the n^{th} hop duration. T_h denotes the hop interval and t_0 denotes an initial misalignment. The resulting instantaneous correlation function(ICF) is defined in terms of the signal values at time $(t+\tau/2)$ and $(t-\tau/2)$.

If "t" is restricted over the n^{th} hop, the sum term $(t \pm \tau/2)$ may stay over the n^{th} hop or may extend to $(n \pm 1)$ hop. Consider a positive "τ", i.e., $0 \le \tau \le T_h$, and let t be restricted to the first half of the n^{th} hop and let $t_0 = 0$, then, t will be restricted to

$$(n-1)T_h \le t \le \left(n - \frac{1}{2}\right) T_h\,, \tag{A.3}$$

and this is denoted as:

$$t \in \left\{\frac{1}{2}n\right\}, \tag{A.4}$$

and implies that if t is restricted to the 1^{st} half of the n^{th} hop $s(t+\tau/2)$ will remain within the n^{th} hop since $0 \le \tau < T_h$. Therefore,

$$s\left(t+\frac{\tau}{2}\right) = \exp\left(j \sum_{n=1}^{N} \left\{ \omega_n \left(t+\frac{\tau}{2}\right)\Big|_{t+(\tau/2)\in\{n\},\ t\in\{(1/2)n\}} \right\} \right). \tag{A.5}$$

If $(t-\tau/2)$ stays within the n^{th} hop or the $(n-1)^{\text{st}}$ hop, then,

$$s\left(t-\frac{\tau}{2}\right) = \exp\left(\sum_{n=1}^{N}\left\{\omega_n\left(t-\frac{\tau}{2}\right)\Big|_{t-(\tau/2)\in\{n\},\ t\in\{(1/2)n\}}\right.\right.$$
$$\left.\left.+\omega_{n-1}\left(t-\frac{\tau}{2}\right)\Big|_{t-(\tau/2)\in\{n-1\},\ t\in\{(1/2)n\}}\right\}\right). \qquad \text{(A.6)}$$

The condition $t\in\{1/2n\}$ is common for Equations A.5 and A.6. Therefore we take it from the equation body and place it aside as follows:

$$R^{\mathrm{i}}(t,\tau) \triangleq s\left(t+\frac{\tau}{2}\right)s^*\left(t-\frac{\tau}{2}\right)$$
$$R^{\mathrm{i}}(t,\tau) = \exp j\left(\sum_{n=1}^{N}\left\{\omega_n\left(t+\frac{\tau}{2}\right)\Big|_{t+(\tau/2)\in\{n\}}-\omega_n\left(t-\frac{\tau}{2}\right)\Big|_{t-(\tau/2)\in\{n\}}\right.\right.$$
$$\left.\left.-\omega_{n-1}\left(t-\frac{\tau}{2}\right)\Big|_{t-(\tau/2)\in\{n-1\}}\right\}\right), \qquad t\in\left\{\frac{1}{2}n\right\}. \qquad \text{(A.7)}$$

The resultant terms of this summation depend on the validity of the indicator functions, i.e., terms to be combined together must have common (intersection) regions of their indicator functions. Thus,

$$R^{\mathrm{i}}(t,\tau) = \exp j\left(\sum_{n-1}^{N}\left\{\omega_n\left(t+\frac{\tau}{2}\right)-\omega_n\left(t-\frac{\tau}{2}\right)\Big|_{t+(\tau/2)\in\{n\},\ t-(\tau/2)\in\{n\}}\right.\right.$$
$$\left.\left.+\omega_n\left(t+\frac{\tau}{2}\right)-\omega_{n-1}\left(t-\frac{\tau}{2}\right)\Big|_{t+(\tau/2)\in\{n\},\ t-(\tau/2)\in\{n-1\}}\right\}\right),$$
$$t\in\left\{\frac{1}{2}n\right\}. \qquad \text{(A.8)}$$

Let us examine the regions satisfying the following conditions:

$$\text{Condition 1}: \quad t+\frac{\tau}{2}\in\{n\},\ t-\frac{\tau}{2}\in\{n\},$$
$$\text{Condition 2}: \quad t+\frac{\tau}{2}\in\{n\},\ t-\frac{\tau}{2}\in\{n-1\},$$
$$\text{for} \quad t\in\left\{\frac{1}{2}n\right\} \quad ,\tau\geq 0. \qquad \text{(A.9)}$$

The region where Condition 1 is valid can be defined from Equations A.2 and A.10 for $(t_o=0)$ as:

$$(n-1)T_h\leq t+\frac{\tau}{2}\leq T_h \quad \text{and} \quad (n-1)T_h\leq t-\frac{\tau}{2}\leq nT_h\,, \qquad \text{(A.10)}$$

where

$$(n-1)T_h \leq t < \left(n-\frac{1}{2}\right)T_h \quad \text{and} \quad T_h > \tau \geq 0. \tag{A.11}$$

Equation A.10 and A.11 can be plotted according to the following set of inequalities (take, e.g., $n=1$):

$$\begin{aligned} &t+\frac{\tau}{2} \leq T_h,\ t+\frac{\tau}{2} \geq 0, \\ &t-\frac{\tau}{2} \leq T_h,\ t-\frac{\tau}{2} \geq 0, \\ &t \geq 0,\ t \leq \left(\frac{1}{2}\right)T_h, \\ &0 \leq\ \tau < T_h. \end{aligned} \tag{A.12}$$

An illustration of the corresponding set of equalities is shown in Figure 36.

Therefore, condition 1 is valid over the triangle ABC. Similarly, condition 2 is defined by the following set of inequalities:

$$t+\frac{\tau}{2} \leq T_h,\ t+\frac{\tau}{2} \geq 0,\ t-\frac{\tau}{2} \geq -T_h,\ t-\frac{\tau}{2} \leq 0, \tag{A.13}$$

and $0 < t(T_h/2)$, $0 \leq \tau \leq T_h$. Condition 2 is valid over the triangle ADC, therefore

$$\begin{aligned} R^{\mathrm{i}}(t,\tau) \;=\; &\exp j\left(\sum_{n=1}^{N}\omega_n\left(t+\frac{\tau}{2}\right)-\omega_n\left(t-\frac{\tau}{2}\right)\Big|_{\text{Condition 1}}\right. \\ &\left.+\omega_n\left(t+\frac{\tau}{2}\right)-\omega_{n-1}\left(t-\frac{\tau}{2}\right)\Big|_{\text{Condition 2}}\right), \end{aligned}$$

or

$$R^{\mathrm{i}}(t,\tau) = \exp j\left(\sum_{n=1}^{N}\omega_n\tau\Big|_{\text{Condition 1}} + \left[(\omega_n-\omega_{n-1})t+(\omega_n+\omega_{n-1})\frac{\tau}{2}\right]\Big|_{\text{Condition 2}}\right), \tag{A.14}$$

where $0 \leq \tau,\ t \in \{(1/2)n\}$.

Note for all hops, condition 1 and condition 2 valid areas will be as shown in Fig. 37 where the areas of valid condition 1 are denoted by 1 and the areas of valid condition 2 are denoted by 2.

For the case of negativ τ, while t is still in the 1st half of the n^{th} hop, we make use of the conjugate symmetry property of the ICF, this will conclude Condition 3 and Condition 4 as shown in Figure 38. When t is within the second half of the n^{th} hop, similar procedure will lead to the other 4 conditions (i.e., Condition 5, 6, 7, 8). These areas are shown in Figure 39.

Let us now summarize our observations from the derived formulai of the ICF by introducing the doubly indexed function $R_{\text{m,n}}(t,\tau)$. $R_{\text{m,n}}(t,\tau)$ will represent the ICF of the FH signal over the $t-\tau$ plane inside and outside the diamond of each hop. $R_{\text{m,n}}(t,\tau)$ will give the ICF expression once we assign its indices (m, n). The indices are shown in Figure 9. $R_{\text{m,n}}(t,\tau)$ is given by

$$R_{\text{m,n}}(t,\tau) = \exp j\left\{(\omega_m - \omega_n)t + (\omega_m + \omega_n)\frac{\tau}{2}\right\}, \tag{A.15}$$

where m and n are the indices of the two hops.

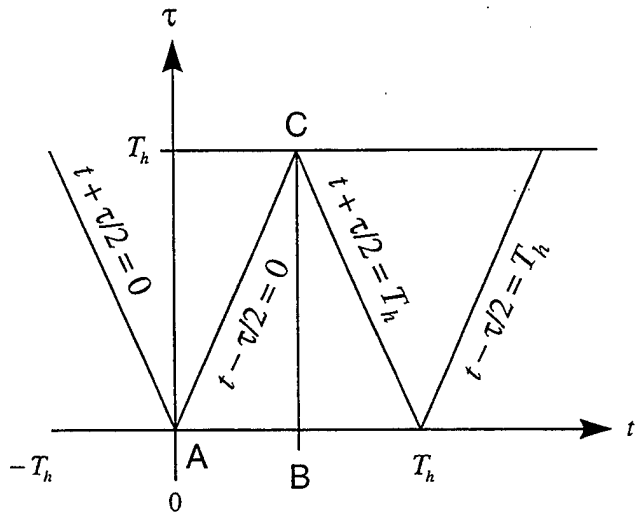

Figure 36. Geometric definition of Condition 1 and Condition 2.

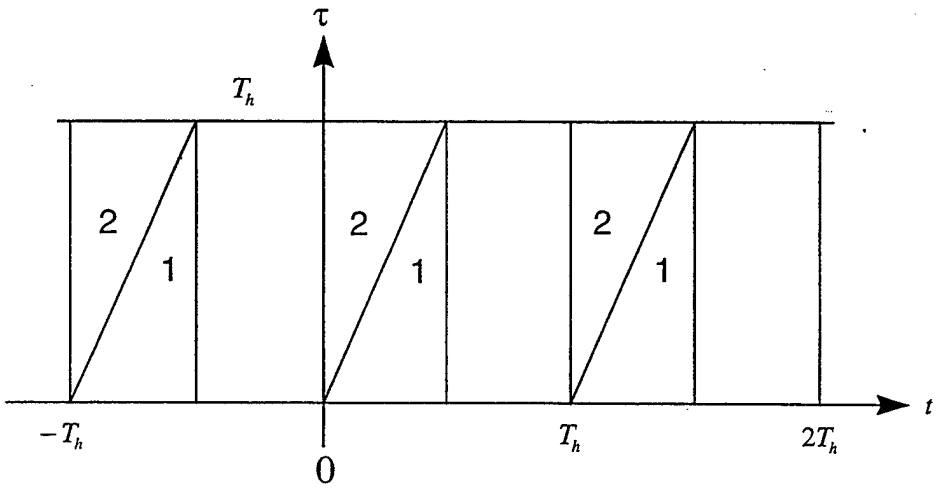

Figure 37. Areas of Condition 1 and Condition 2.

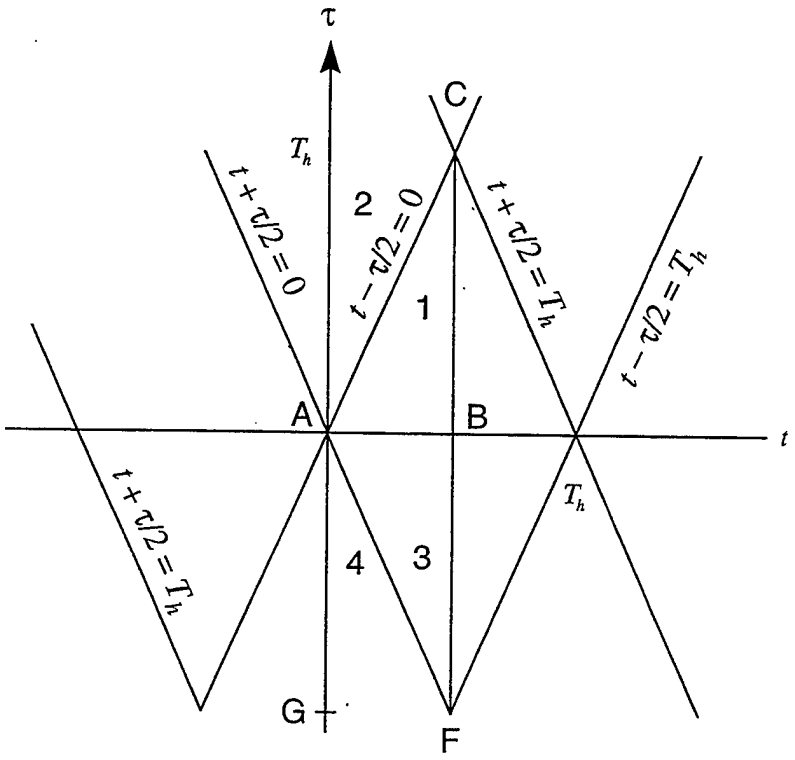

Figure 38. Areas of Condition 3 and Condition 4.

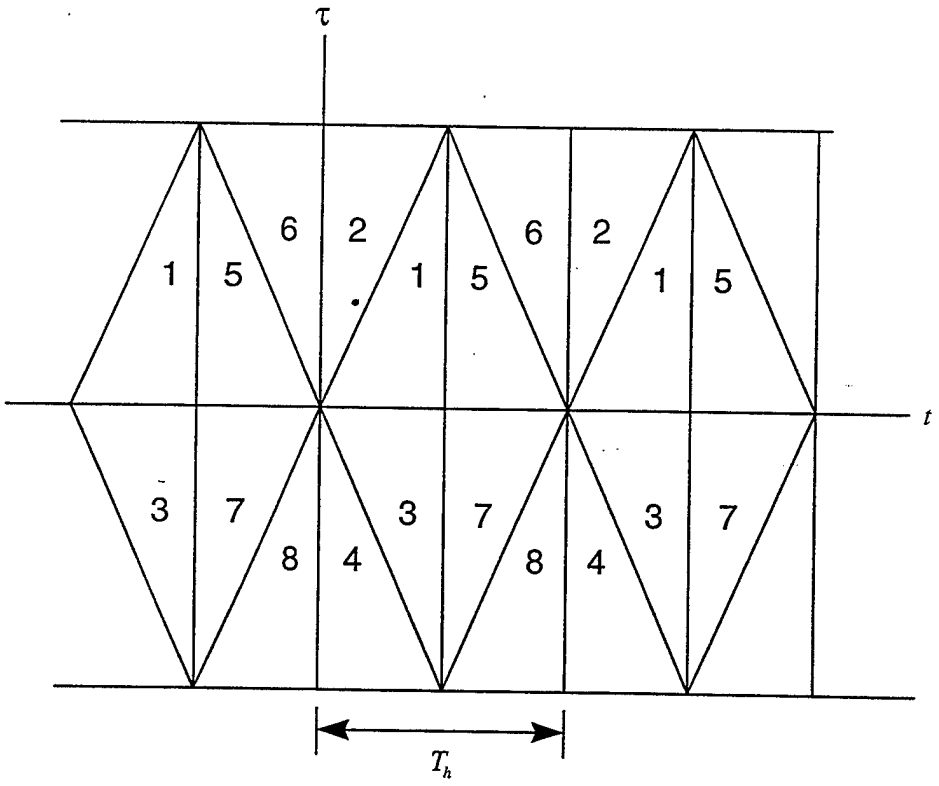

Figure 39. Areas of Condition 1,2,...,8.

APPENDIX B. SCORES OF OPINION TEST

This appendix includes the tables of scores of the opinion test carried out for visual inspection and identification of the FH signal. Only one table is shown for each wavelet type. Each table is the average of 10 corresponding tables originated from 10 experiments. This justifies the fractions in the tabulated scores.

Table B.1: Wavelet: Complex Daub-3, SNR:10 dB

S	Real	Imag.	Angle	Abs.
1	5	5	4.25	1.25
2	5	5	4.75	1
3	4	5	2	1
4	1	1.5	1	1
5	1	1	1	1.25

Table B.2: Wavelet: Real Daub-3, SNR:10 dB

S	Real	Imag.	Angle	Abs.
1	5	5	2.75	1
2	5	5	5	1
3	5	5	2	1.25
4	1.5	1	1	2.5
5	1	1	1	1.5

5 — sharply obvious with sharp boundaries.
4 — obvious.
3 — fair.
2 — distinguishable from background noise.
1 — not distinguishable from background noise.

Table B.3: Wavelet: Complex Morlet, SNR:10 dB

S	Real	Imag.	Angle	Abs.
1	5	5	4.5	1
2	5	5	4.5	1
3	5	5	4.5	1
4	4.25	4.75	1	3.5
5	3.75	3.75	1	2.75

Table B.4: Wavelet: Real Morlet, SNR:10 dB

S	Real	Imag.	Angle	Abs.
1	5	5	4.5	4.5
2	5	5	4.5	4.5
3	5	5	4.5	4.75
4	4.75	4.75	1	3.5
5	4.75	3.75	1	3.75

5 — sharply obvious with sharp boundaries.
4 — obvious.
3 — fair.
2 — distinguishable from background noise.
1 — not distinguishable from background noise.

Table B.5: Wavelet: Complex Morlet, SNR:3 dB

S	Real	Imag.	Angle	Abs.
1	3.5	3.25	3.5	4
2	4	3.5	4	3.5
3	4.5	4.5	3.5	3.5
4	2.5	1.75	1	3
5	2	2.25	1	3

Table B.6: Wavelet: Real Morlet, SNR:3 dB

S	Real	Imag.	Angle	Abs.
1	3	1.75	1	3.75
2	4.5	4	2.75	3.75
3	4.5	4.5	3	4
4	2.75	2.75	1	2
5	2.75	2.75	1	1.5

5 — sharply obvious with sharp boundaries.
4 — obvious.
3 — fair.
2 — distinguishable from background noise.
1 — not distinguishable from background noise.

Table B.7: Wavelet: Complex Daub-3, SNR:3 dB

S	Real	Imag.	Angle	Abs.
1	2.8	3.6	2.2	1
2	2.4	3.6	4.25	2.8
3	3.4	4.25	1.4	1
4	1.8	1	1	1
5	1	1	1	1

Table B.8: Wavelet: Real Daub-3, SNR:3 dB

S	Real	Imag.	Angle	Abs.
1	3.8	1.4	2.4	1.6
2	3.6	3.2	4.4	3.4
3	2.6	3.2	2.2	1.2
4	1	1	1	1
5	1	1	1	1

5 — sharply obvious with sharp boundaries.
4 — obvious.
3 — fair.
2 — distinguishable from background noise.
1 — not distinguishable from background noise.

APPENDIX C. WAVELET SURFACES OF OTHER SIGNALS

This appendix includes the wavelet surfaces obtained by processing noise only, ASK, PSK and FSK signals. Figures 40 and 41 show no identifiable diamond structure pattern for the noise only case. Each pair of successive figures (Figure 42 and 43, Figure 44 and 45, and Figure 46 and 47) show a diamond structure residing only in one scale .

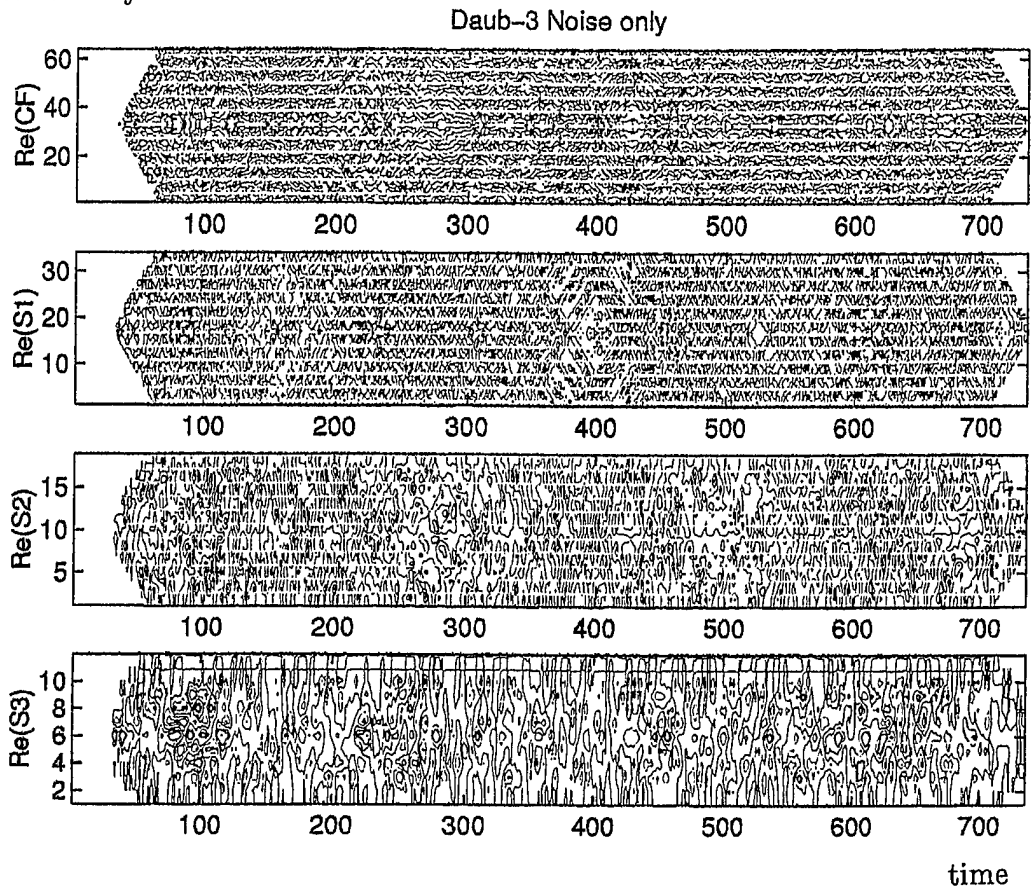

Figure 40. Wavelet surfaces obtained from noise only, scale 1, 2 and 3.

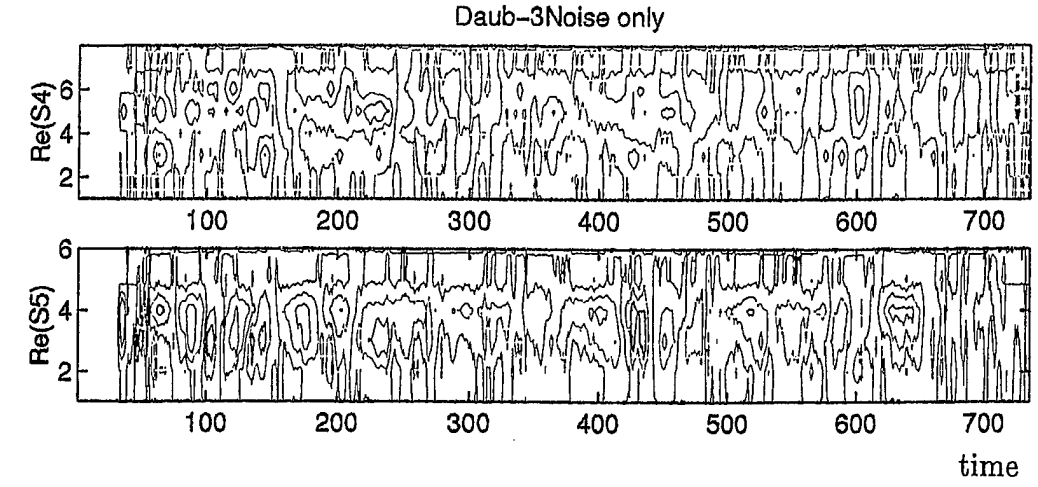

Figure 41. Wavelet surfaces obtained from noise only, scale 4 and 5.

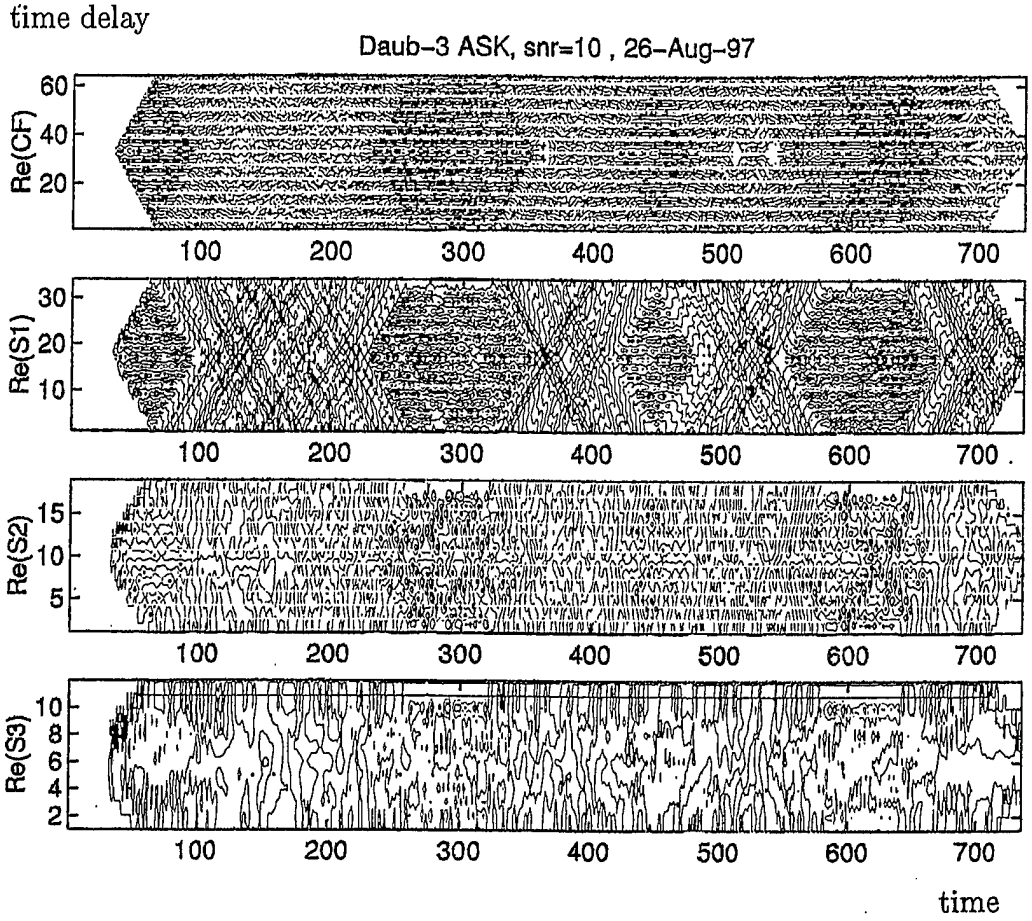

Figure 42. Wavelet surfaces obtained from ASK signal, scale 1, 2, and 3.

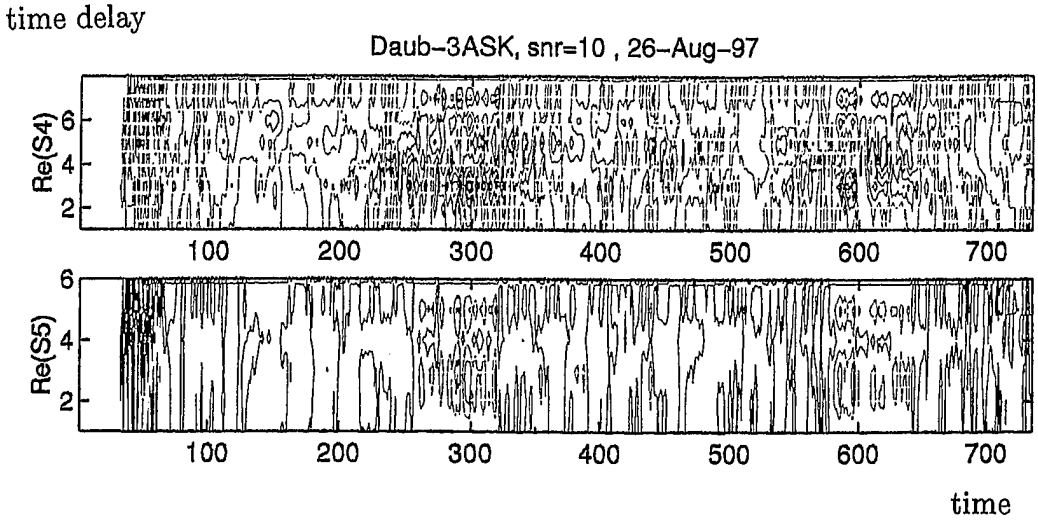

Figure 43. Wavelet surfaces obtained from ASK signal, scale 4 and 5.

time delay

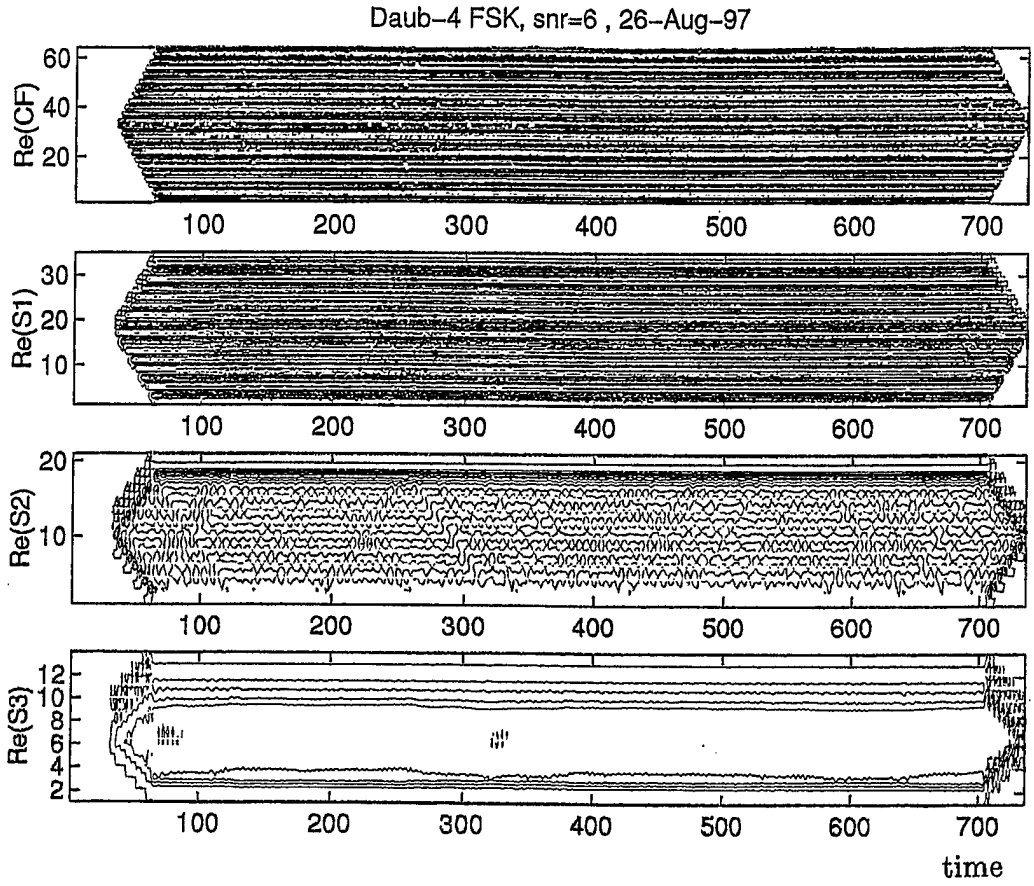

Figure 44. Wavelet surfaces obtained from FSK signal, scale 1, 2 and 3.

time delay

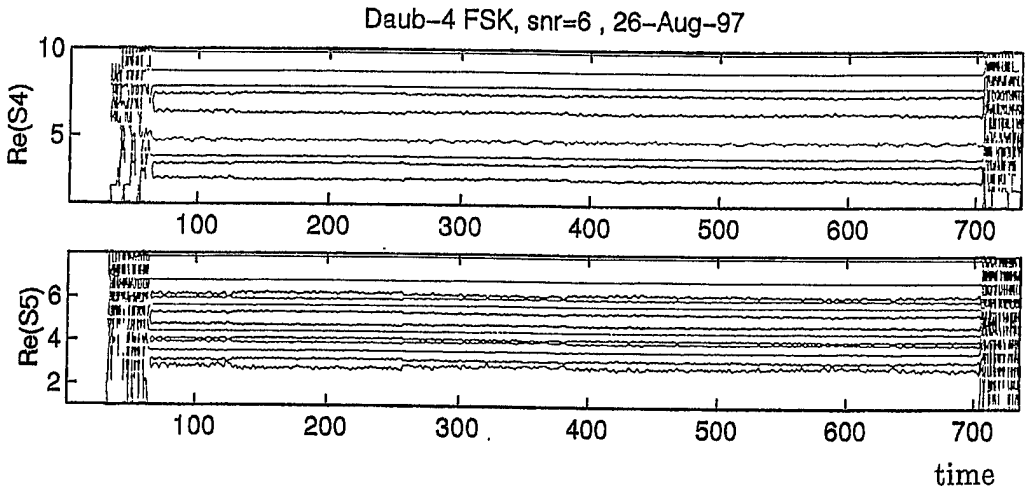

Figure 45. Wavelet surfaces obtained from FSK signal, scale 4 and 5.

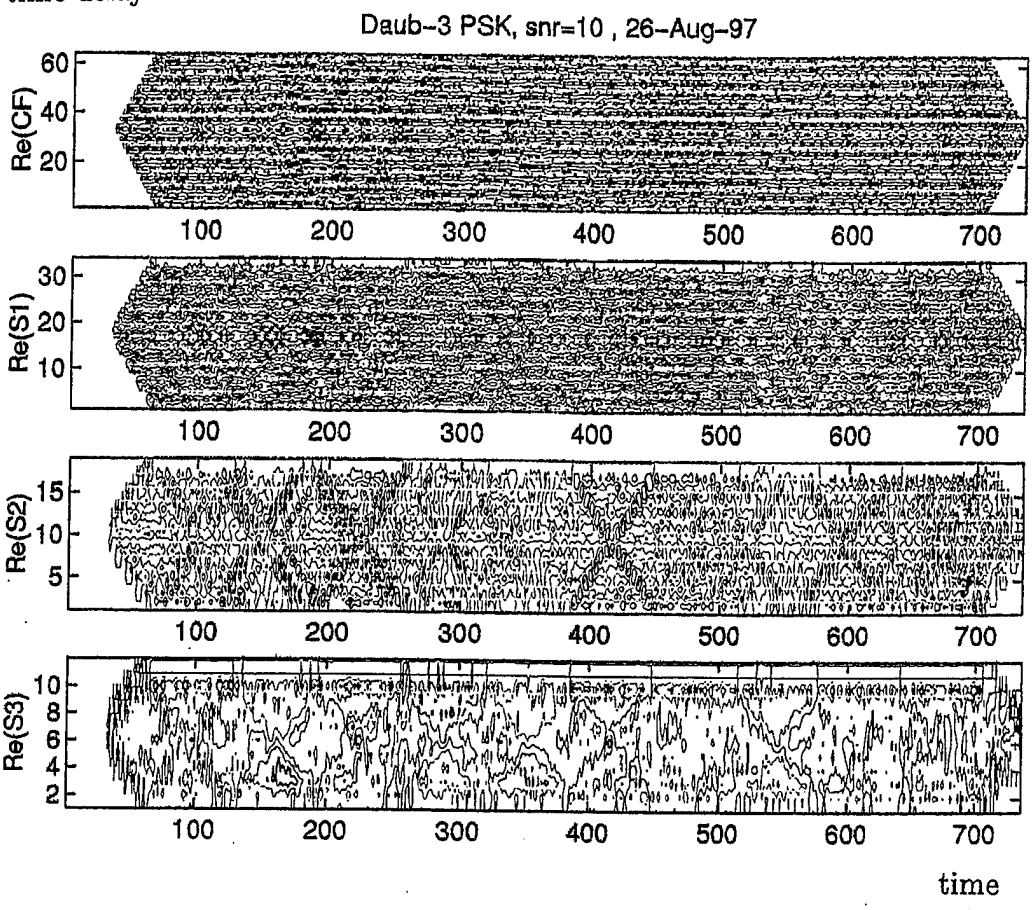

Figure 46. Wavelet surfaces obtained from PSK signal, scale 1, 2 and 3.

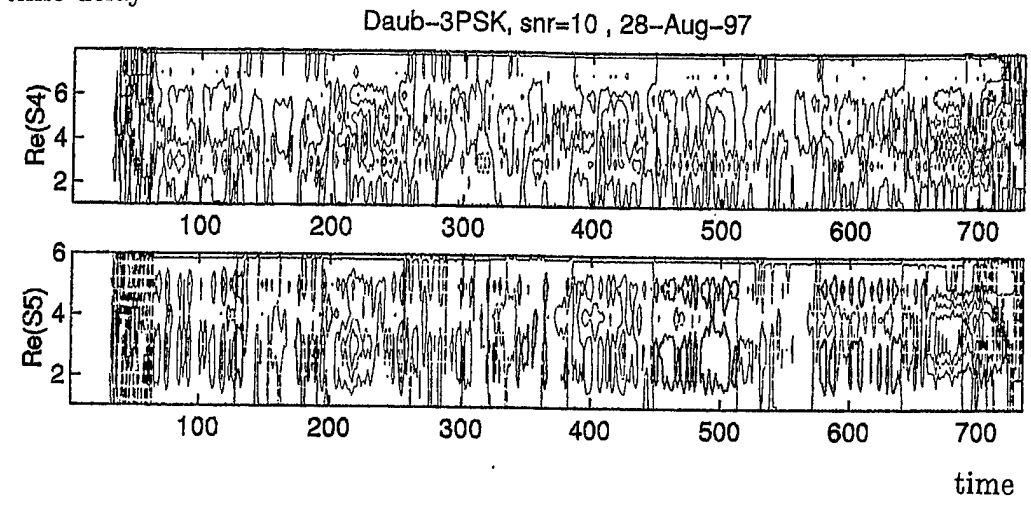

Figure 47. Wavelet surfaces obtained from PSK signal, scale 4 and 5.

INITIAL DISTRIBUTION LIST

1. Defense Technical Information Center 2
   8725 John J. Kingman Road., Ste 0944
   Ft. Belvoir, VA 22060-6218

2. Dudley Knox Library 2
   Naval Postgraduate School
   411 Dyer Rd.
   Monterey, CA 93943-5101

3. Chairman, Code EC 1
   Department of Electrical and Computer Engineering
   Naval Postgraduate School
   Monterey, CA 93943.

4. Prof. Ralph Hippenstiel, Code Ec/Hi 5
   Department of Electrical and Computer Engineering
   Naval Postgraduate School
   Monterey, CA 93943.

5. Prof. Monique Fargues, Code EC/Fa 1
   Department of Electrical and Computer Engineering
   Naval Postgraduate School
   Monterey, CA 93943.

6. Hesham Eldeeb 2
   Naval Postgraduate School, SGC 1824.
   Monterey, CA 93943.

7. Ashraf Aziz 2
   Naval Postgraduate School, SGC 1800.
   Monterey, CA 93943.

8. Egyptian Military Office 2
   2308 Tracy Place, NW
   Washington, DC 20008

9. Egyptian Armament Authority - Training Department 6
   c/o American Embassy, Cairo, EGYPT
   Office of military Co-operation
   Box 29 (TNG)
   FPO, NY 09527-0051